Aus dem Max-Planck-Institut für Polymerforschung in Mainz

Functionalization of Polyurethane Dispersions for Controlled Interactions with Different Substrates

Dissertation
zur Erlangung des Grades
“Doktor der Naturwissenschaften”
im Promotionsfach Chemie

am Fachbereich Chemie, Pharmazie und Geowissenschaften
der Johannes Gutenberg-Universität
in Mainz

Laura Breucker

geboren in Recklinghausen

Mainz, November 2015

Dekan:

1. Berichterstatter:
2. Berichterstatter:
3. Tag der mündlichen Prüfung: 24. November 2015

Die vorliegende Arbeit wurde im Zeitraum von September 2012 bis November 2015 im Rahmen eines Kooperationsprojekts bei der Henkel AG & Co. KGaA in Düsseldorf und am Max-Planck-Institut für Polymerforschung in Mainz im Arbeitskreis von Prof. Dr. Katharina Landfester angefertigt.

Use your gifts faithfully, and they shall be enlarged;
Practice what you know, and you shall attain to higher knowledge.
(-Matthew Arnold)

Table of Contents

1. Introduction and Motivation

In November of 2001, a group of Italian geologists made a monumental discovery during an excavation near Florence, Italy. Alongside elephant and rodent remains, they exposed pieces of stone partly covered by birch-bark tar which they were able to date back to the late Middle Pleistocene (ca. 781 – 126 000 years ago). This finding constitutes the most ancient record of the human use of adhesives ever discovered.[1]

Since the late Middle Pleistocene, adhesives have certainly come a long way. From plant-based polymers in water used to join materials such as wood, paper, or clothing, to synthetic polymers in organic solvents used to join metallic or polymeric materials, the structure and complexity of adhesives have evolved alongside society's needs. Congruently, adhesives have come to occupy a tremendously important role in today's developed world, touching virtually every aspect of it. Curiously, in the more recent past, adhesives may appear to have experienced a regression which is in fact not a regression at all: ecofriendly systems consisting of aqueous polymer dispersions or adhesives containing naturally occurring molecules such as peptides are attracting a great amount of attention from research scientists as well as from the industry. A general interest in such a topic is easy enough to understand in light of the above-named, prehistoric example of how mankind has always referred to nature for inspiration in the development of new skills and tools. However, one might wonder where the momentum for this reorientation is coming from. On the one hand, it can be attributed to an increase in global, environmental consciousness: the wish to limit the emission of volatile organic compounds, accompanied by the corresponding legislation. On the other hand, important advances have been made in the synthesis of polymeric nanoparticles and nanocapsules,[2, 3] peptides,[4] and in conjugation[5, 6] and functionalization techniques[7].

The present work is inscribed in this context and seeks to extend the reach of eco-friendly nanoparticle systems from adhesives to other areas of application. Polyurethane (PU) nanoparticles are chosen as the core component. PUs are a well-known class of polymers which are used for a wide variety of applications including construction materials, coatings, and particularly adhesives. The segmented block copolymer structure of PUs allows for a wide range of tailorable properties.[8] The aim of this work is to achieve particular surface functionalizations of ecofriendly, waterborne PU dispersions (PUDs) in order to introduce specific particle-substrate interactions and hence improve the affinity for three model substrates, namely hair, stainless steel, and hydroxyapatite. The substrates as well as the functionalization techniques chosen are intended to demonstrate the wide range of possibilities in the synthesis and application of functionalized PUDs.

The first project concerns the synthesis of peptide-functionalized PUDs using a hydrolyzed protein from wool in a simple, cost-efficient manner. Hydrolyzed proteins from natural resources are comparatively cheap, available in large quantities, and are well-known in the food and personal care industries. The goal of this project was to demonstrate that despite the challenge of functionalizing particles with a mixture of protein fragments, interesting hybrid properties such as peptide-stabilization, triggered coagulation, as well as complex film morphologies can be obtained. Furthermore, due to the nature of the hydrolyzed protein, a favorable interaction with the hair surface can be presumed and hence, the use of the resultant dispersions in hair care product applications is currently under investigation.

The second project concerns a related, alternative method of obtaining peptide-functionalized PUDs. In this case, both the peptide sequence as well as the method of coupling the peptide to the particles are well-defined. A thorough analysis of the functionalization reaction as well as of the resultant dispersion properties was intended. The peptide sequence used is known to show a strong adhesion to stainless steel surfaces and an application in paints, adhesives, or as protecting agent against corrosion is therefore intended.

The third project focuses on the synthesis of phosphonate-functionalized PUDs (P-PUDs) using an industrially scalable approach for a so-far little-investigated application. The functionalization is carried out in a single step and different analyses of the resultant interfacial and bulk compositions of the particles are provided. Functionalization with phosphorus-containing moieties is a well-known method for improving the adhesion of polymers to metallic surfaces[9] and the specific affinity of the P-PUDs for stainless steel is hence shown. However, phosphonate-functionalization has been much less investigated for ceramic substrates such as hydroxyapatite (HAP).[10, 11] Thus, here, we also examined the P-PUDs with regard to their affinity for HAP in order to allow for applications in *e.g.* dentistry and orthopedics. Furthermore, HAP also serves as model substrate for ceramic and pigment surfaces which are pertinent substrates for many technical applications.

In summary, the presented work was carried out to demonstrate the versatility of the possible functionalizations of PUDs for diverse areas of “adhesive” applications. We show that PUDs can be decorated with hydrolyzed peptides in a simple, one-step synthesis to yield a complex system useful for hair care applications, that a similar system may also be functionalized with a peptide of defined sequence to serve for metal adhesives, and that phosphonate moieties can be attached to PUDs to extend their reach to adhesives for dentistry and orthopedics, ceramics or pigments. We hereby hope to make a valuable contribution to the field of water-based coatings and adhesives in order to move further towards sustainable solutions for tomorrow’s society.

2. Theoretical Background

2.1. Particles at solid surfaces

2.1.1. Introduction

The interactions between small particles and solid surfaces play an important role in many areas of application. On the one hand, the adsorption of dust particles to glass and ceramic surfaces in the kitchen or the bathroom, and the attachment of tar to lung tissue are causes for concern. On the other hand, the adhesion of dust particles to a cleaning rag, the adhesion of paint particles to a car bumper, and the attraction of antimicrobial particles to door knobs are highly desirable interactions. It can therefore easily be imagined that controlling and directing the behavior of particles at solid surfaces is of importance for many applications. In order to achieve this, a general understanding of the governing factors is a prerequisite.

It should be noted that in the above-named examples, the dust or paint particles in question are colloidal particles (with dimensions in the nanometer to micrometer range). In this case, gravity is not the predominant factor.[12, 13] Instead, the observed macroscopic adhesion phenomena can be traced back to the other types of forces present at the microscopic level. These forces can be attractive or repulsive, large or small, short-range or long-range. They can be present between an individual particle and the surface in question or amongst the particles.

2.1.2. Surface tension or surface free energy[14, 15]

A first understanding of interactions in colloidal systems can be gathered based upon the notions of surface tension and surface free energy. To illustrate these concepts, we can consider the case of a liquid or a solid which is divided into two parts separated by vacuum, creating two surfaces from a bulk. Different, attractive interactions exist between the constitutive molecules of a liquid or a solid (see section 2.2-2.4 for details) which can be viewed as equal forces due to surrounding molecules, "pulling" every molecule in all directions (see ***Figure 2.1.1***). In the bulk, the net force acting upon every molecule is therefore zero. However, if an interface is created, the molecules present there will experience a net force directed inwards. Or, put in other terms, the creation of an interface always comes at an energetic cost because a certain energy barrier must be overcome in order to compensate for the attractive interactions between the molecules to be separated. We can therefore express the result in terms of an energy per unit area (in which case we speak of surface

free energy) or in terms of a force per distance (in which case we speak of surface tension). In case of liquids, it is common to speak of surface tension whereas solids are usually considered in terms of surface free energy. For liquid systems, due to the inwards-directed force, or again in order to minimize the energetic cost of the interface, the system will always have a tendency to minimize its surface area. This is commonly observed in water droplets which tend to adopt a spherical shape.

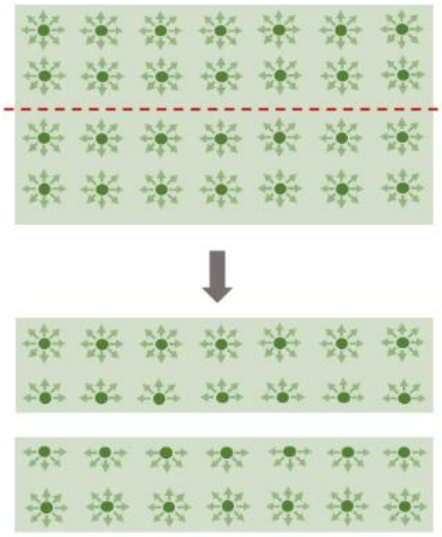

***Figure 2.1.1**: Illustration of the interactions among molecules in a liquid or solid and the evolution of the system due to the division of the bulk, creating two surfaces.*

A logical consequence is that the surface tension or surface free energy can be lowered due to the presence of other molecules at the surface which may compensate for the loss of attraction from neighboring molecules. The adsorption of particles to surfaces or the wetting of a liquid on a surface can be understood in those terms. Obviously, if the interactions are unfavorable, adsorption or wetting does not take place. This simple observation explains the immiscibility of hydrophobic and hydrophilic liquids and constitutes the central problem for the synthesis of emulsions and dispersions which display a specific adhesive behavior (see section 2.5 on aqueous polyurethane dispersions below). Prior to considering this particular case of particle-particle and particle-surface interactions which is of interest for this work, however, we will first present the basic types of interactions which may enter into play.

2.2. Long-range interactions in particle-surface and particle-particle systems

2.2.1. Van der Waals forces[14, 16]

Interactions between dipoles (permanent or temporary) cause an attractive force. The different contributions can be further differentiated into interactions between two permanent dipoles (Keesom forces), between a permanent and an induced dipole (Debye forces), and between two induced dipoles (London dispersion forces). The principles of temporary and induced dipoles are classically known for individual molecules, but can very well be extended to larger (colloidal) systems. In the case of a sphere-plate interaction, the energy of interaction is given by

$$V_{W\,sp} = -\frac{AR}{6H}$$

with *R* the radius of the spherical particle, *H* the distance of separation, and *A* the Hamaker constant. By convention, an attractive potential is negative whereas a repulsive one is positive. *A* is named after H.C. Hamaker[17] for his work on extending F. London's theory of the interactions between gas atoms[18] to solid surfaces by presupposing the additivity of molecular interactions. In this way, the interaction of two solid bodies of a given material *i* in a vacuum can be calculated with

$$A_{ii} = \frac{3}{4}\pi^2 N_i^2 \alpha^2 h v_0$$

with N_i^2 the density of atoms per volume, α the static polarizability of the atom *i*, h the Planck's constant, and v_0 the frequency of the electron in the ground state. In the case of two different bodies (*a* and *b*) interacting in a medium *c*, the Hamaker constant is given by

$$A_{abc} = \left(\sqrt{A_{aa}} - \sqrt{A_{cc}}\right)\left(\sqrt{A_{bb}} - \sqrt{A_{cc}}\right)$$

The value of the Hamaker constant for a given particle in practice is usually $k_B T \leq A \leq 10\, k_B T$ with k_B the Boltzmann constant and *T* the temperature.

It should be noted that in the case of two spheres, the expression for the Van der Waals potential of interaction is the same if the distance of separation is small with regard to the radii of the spheres (case of spheres in close proximity). However, if their distance of separation is very large with regard to their radii, we find $V_{W_{ss}} \propto \frac{1}{H^6}$ (which is the initial dependency for the interaction of two dipoles). It can further be observed that in the case of two identical particles *a* in a medium *b*, the Hamaker constant is given by

$$A_{aba} = \left(\sqrt{A_{aa}} - \sqrt{A_{bb}}\right)^2$$

Its value is thus strictly positive. The force acting between two identical particles in suspension is always attractive whereas the force between a particle and a surface of dissimilar nature may be attractive or repulsive. This deduction is pertinent for polyurethane dispersions (see section 2.5) because it summarizes the central problem in tuning the interactions of PUDs with substrates: we are facing the dual challenge of synthesizing particles which repel each other (to avoid coagulation), but have a high affinity for the substrate in question (to promote adhesion). This task is approached from different angles in the three projects (see chapter 4), with electrostatic forces playing an important role (see below).

2.2.2. Electrostatic forces[12, 14]

When immersed in an aqueous environment, all solid materials acquire a surface charge due to the preferential adsorption of ions from the aqueous phase or due to the dissociation of surface groups. This effect can be explained through the competition between the decrease in entropy and the increase in electrical energy due to the charges created. For ions with a valence of 1, the electrical energy is given by

$$E_{el} = \frac{e^2}{4\pi\varepsilon l}$$

With *e* the electron charge, ε the electrical permittivity of the medium, and *l* the distance between charges. Ionisation is favorable if $E_{el} < k_B T$ and thus the condition for ionization is $l > l_B = \frac{e^2}{4\pi\varepsilon k_B T}$. The characteristic length l_B is the Bjerrum length. In water, it is approximately equal to 6 Å and as a consequence, ionization is energetically favorable in water.

In practice, at neutral pH, most solid materials possess a net negative charge. Due to the presence of charged moieties in the aqueous medium, ions of opposite charge from the solution will be attracted to the solids whereas ions of equal charge will be repelled. In consequence, an electrical double-layer is created close to the solid's surface. For a charged surface, using the Debye-Hückel approximation ($\varphi \ll \frac{k_B T}{e}$), the electrostatic potential φ is given by

$$\varphi(H) = \varphi_o e^{-H/\lambda_D}$$

With φ_o the electrostatic surface potential which depends on the density of charges at the surface and λ_D the Debye length which describes the decrease in electrostatic potential with increasing distance from the surface. For an electrolyte with monovalent ions, λ_D is given by

$$\lambda_D = \sqrt{\frac{\varepsilon k_B T}{2 n_0 e^2}}$$

With n_0 the density of counter-ions. It is important to note that if the density of counter-ions decreases, the Debye length increases. λ_D can thus also be seen as the scope of the interaction due to the charges which is strongly dependent upon the ionic strength of the medium.

2.2.3. DLVO Theory[15]

Derjaguin[19] and Landau, and independently Verwey[20] and Overbeek proposed to consider the interaction between colloidal particles as resulting from the sum of the interactions due to the Van der Waals attraction and the electrostatic repulsion of equally charged bodies. This approach is now known as the DLVO-theory and can also be extended to the interactions present in a particle-surface system. As mentioned previously, the ionic strength of the surrounding medium is very important in determining which of the two contributions predominates. Three different cases of low, medium, and high ionic strength are illustrated in ***Figure 2.2.1***. In the case of low ionic strength, the electrostatic repulsion outweighs the Van der Waals attraction as the two bodies approach one another. An energy barrier exists which must be overcome in order to reach the primary minimum of infinite depth. In the case of intermediate ionic strength, a secondary minimum exists which corresponds to a reversible adhesion, for example. Brownian motion or external influences (such as agitation or rinsing) may still cause a separation of the interacting bodies.[21] If, however, the ionic strength is very high, the energy profile is entirely governed by the Van der Waals attraction. In the case of a dispersion of solid particles, this translates to an irreversible coagulation.

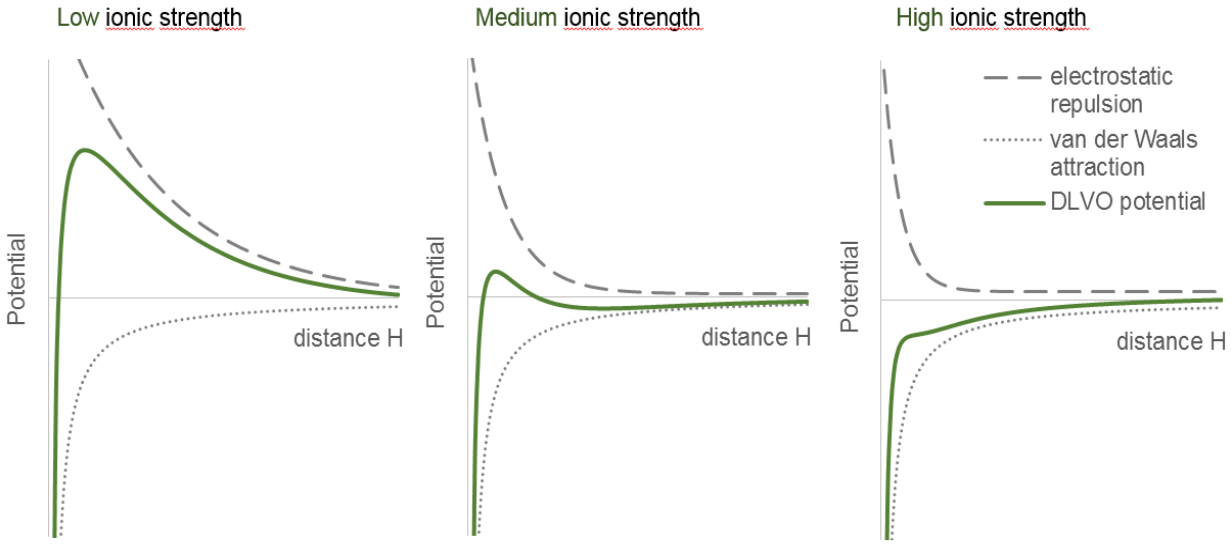

***Figure 2.2.1**: Illustration of the potential energy curve as predicted by the DLVO theory. From left to right, the three curves correspond to the cases of low, medium, and high ionic strength, respectively.*

2.3. Short-range interactions

2.3.1. Born repulsion

According to the DLVO theory, the adsorption of a particle to a surface should be an irreversible process due to the primary minimum of infinite depth (see ***Figure 2.2.1***). However, this is obviously not what is observed in nature. The reason for this is that the observed primary minimum is of finite, rather than of infinite depth due to the Born repulsion arising when non-deformable objects are brought into contact. The interpenetration of these objects contradicts the Born exclusion principle which leads to a minimum distance of approach, *i.e.* to a finite primary minimum. The corresponding expressions of the Born repulsion interaction for a sphere-plate system is

$$V_{BR_{sp}} = \frac{ARH_0^6}{168H^7}$$

With H_0 the equilibrium distance corresponding to the primary minimum.[22] The resulting potential of interaction is shown in ***Figure 2.3.1***.

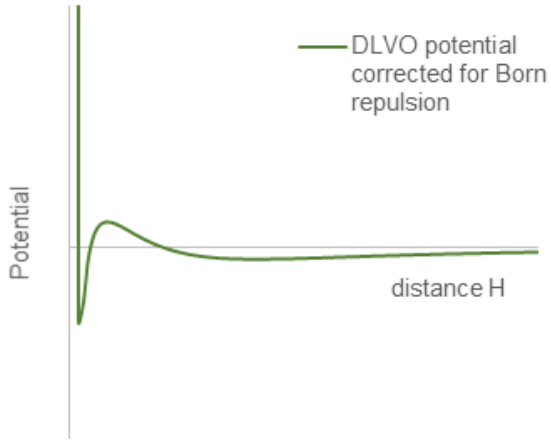

***Figure 2.3.1**: Curve of the potential of interaction according to the DLVO theory and corrected for the Born repulsion.*

2.3.2. Hydrophobic interactions[14]

Hydrophobic interactions are based on Lewis acid/base (electron donor-electron acceptor) interactions present in polar media such as water. Van Oss described those interactions which were thus-far neglected in the DLVO theory and which are often observed in systems in which proteins are present. The description is accomplished in terms of a surface tension for every substance consisting of two terms: the Lifshitz-van der Waals term and the term due to Lewis acid-base type interactions (including Hydrogen bonding)

$$\gamma = \gamma^{LW} + \gamma^{AB}$$

Where γ^{LW} is the Lifshitz-van der Waals term and γ^{AB} is the Lewis acid-base term of the surface tension.

2.3.3. Steric forces[15]

Steric forces may contribute to particle-particle or particle-surface interactions if the particles or the surface are coated with adsorbed or covalently attached polymers. If this polymer layer is very small with regard to the radius of the particles, the effect on the Van der Waals interactions can be neglected. However, if the size of the polymer corona is comparable to the dimensions of the particle, the interaction potential may be greatly altered and the situation is rather complex. Three effects must be taken into consideration which include a mixing effect due to the concentration of the polymer in the zone of interaction, an entropic effect due to restriction of the polymer to the interface, and a bridging effect which may arise if one chain is adsorbed/attached to more than one component of the system. The mixing largely depends on the quality of the solvent for the polymer in question. Also, non-adsorbed polymers may create depletion forces. If the dimensions of the freely moving polymer coils are large with regard to the dimensions of the particles, a resulting force will be created which will tend to bring the colloidal surfaces close in order to minimize the excluded volume.[23, 24]

2.3.4. Ion Bridging

Two species (either two particles or a particle and a surface) may be brought into contact through a mediator ion. This phenomenon has been observed for the adsorption of bacteria to metallic surfaces. Ions such as Ca^{2+} or Mg^{2+} can have a great effect on bacterial adhesion, even though the mechanism behind this may be complex.[25] The usefulness of ion bridges has also been shown in the

cohesion of clay platelets in which the distance between platelets was shown to depend upon the degree of hydration of the ion in question.[26]

2.4. Deformational effects[27]

If the particles and/or the surface in question are not rigid but deformable, when they enter in contact, the imposed stresses result in strains which may cause deformations of elastic, plastic, or viscoelastic nature. Historically, a number of different successive models were developed to treat this situation. The basis for all is the Hertzian indenter model[28] which describes the case of a rigid indenter applying a compressive load *P* onto a substrate and causing a plastic deformation of a certain radius *a*. If the indenter has a radius *d*, and the substrate has a Young's modulus *E* and a Poisson's ratio *v*, the radius of the deformation is given by

$$a^3 = \frac{3(1-\nu^2)dP}{4E}$$

This relation was taken as a basis by Derjaguin to explain adhesion-induced deformations for particle-substrate interactions.[29] Hamaker related the surface forces to the densities of atoms and the Hamaker constant to the London dispersion forces by

$$A = \pi^2 n_P n_S \lambda_{int}$$

With λ_{int} the interaction parameter of the particle-substrate interaction and with n_P and n_S the density of atoms in the particle and the substrate, respectively.[17]

The load *P* can then be calculated as follows

$$P = \frac{Ad}{6\, z_0^2}$$

With z_0 the separation distance between the two materials. Lifshitz further related the Van der Waals interactions to instantaneous dipole fluctuations which generate electromagnetic waves. He thereby showed that those forces are not contact forces, but rather forces acting over a range. Krupp showed that when all three approaches are combined, the contact radius is given by

$$a^3 = \frac{3\hbar\varpi(1-\nu^2)d^2}{32\pi z_0^2 E}$$

Adhesion can therefore induce stresses which may cause deformation of the materials.[30]

In this work, polyurethane particles are used which have a very low glass transition temperature and are therefore deformed easily at room temperature (see section 2.5). As a consequence, if

adsorption of the particles to a particular surface occurs, deformational effects are expected to enter into play.

2.4.1. Elastic deformations

Johnson and coworkers tried to apply the above-named theories on the study of adhesion-induced contact radii to the interaction of polyurethane spheres on gelatin. Strikingly, the measured radii were larger than predicted by the model and Johnson *et al.* attributed this to the existence of tensile forces along with compressive forces. In 1971, the Johnson, Kendall, and Roberts theory (JKR theory) was then published which explains that the total contact radius is due to two types of interactions: a tensile and a compressive component. This model presupposes that there are no long-range interactions and it is the basis for all subsequent studies on adhesion.[31]

An alternative model was proposed by Derjaguin, Muller, and Toporov (DMT model) in 1975. Supposing that the adhesion-induced deformations follow the Hertzian indenter model, the consequence is that half of the interactions take place in the region of adhesion and half take place outside.[32] This contradicts one of the assumptions of the JKR model and the predicted contact radii are therefore very different.

Muller, Yushchenko, and Derjaguin reconciled both the JKR and the DMT theories in defining areas of application in which each model is valid. They showed that the JKR model is applicable in the case of large particles and for materials of low modulus and high surface energy whereas the DMT model is applicable for cases of small particles, high modulus, and low surface energy.[33]

2.4.2. Plastic deformations

Another possibility which must be taken into account is that of plastic deformations. Maugis and Pollock proposed in the MP theory[34] that the force balance at the contact can be calculated from the work of adhesion, the hardness of the material and the radius of the area of contact. The model assumes a contact profile of the Hertzian intenter, but allows for the radius of curvature of the material to be changed due to the plastic deformation.

2.4.3. Interlocking

If coagulation or deposition has occurred, interlocking of materials due to surface roughness or partial interdiffusion may occur. This can create a mechanical obstacle to a separation of the two components.[27]

When studying the interactions in particle-surface systems, the nature of the interacting materials is obviously of prime importance for determining if the interactions present are favorable and if adhesion occurs. We will therefore go on to take a closer look at the particles of this study, *i.e.* aqueous polyurethane dispersions and the surfaces of study, *i.e.* hair, hydroxylapatite, and stainless steel.

2.5. Aqueous polyurethane dispersions

2.5.1. Polyurethanes: from discovery to application

Polyurethanes are a well-known class of polymers which find use in a wide range of different applications[35] and account for about 5% of the total plastic production worldwide (2011).[36] Since the discovery of PUs in 1937 by Otto Bayer (I.G. Farben, Germany), many uses for PUs were quickly discovered, including the use as adhesives between rubber, metal, and glass as one of the first in 1941 (see ***Figure 2.5.1***). Since then, the fields of application grew immensely, ranging from insulation (1948), shoe soles (1953), cushions (1954), spandex fibers for clothing (1958), lining for space suits (1959), car bumpers (1969), spray building insulation (1979), to catheters (1993). The wide variety of PU applications are on the one hand due to the strong inter- and intramolecular forces present among PU chains (see section 2.5.5) and consequent good shock absorbance, elasticity, and cohesion in the film. On the other hand, PUs show a very good adhesion to a range of substrates including metals, synthetic polymer films, textiles, paper, and wood.[37]

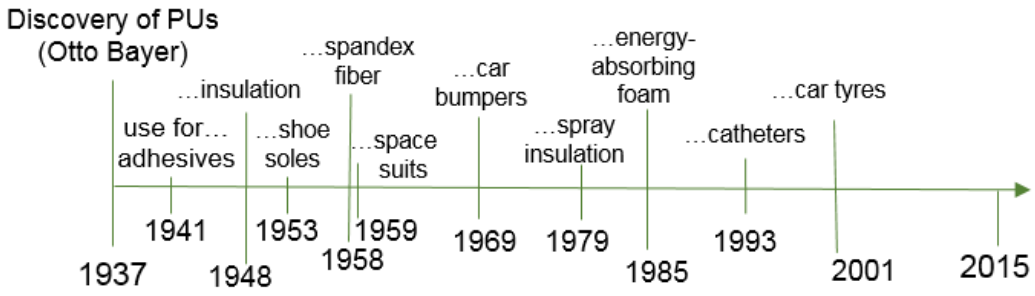

***Figure 2.5.1**: Timeline of PUs from their discovery to different applications, adopted from[38].*

2.5.2. Synthesis of PUs and raw materials

A PU polymer is most often synthesized through the polyaddition reaction between isocyanates and alcohols to form the characteristic urethane link RNH-COOR'. Commonly, the reaction of some

isocyanate groups with primary or secondary amines is also voluntarily included in the PU synthesis although the result is, strictly speaking, not a polyurethane, but a poly(urethane/urea).[8, 37, 39] Both reactions are shown in ***Figure 2.5.2***.

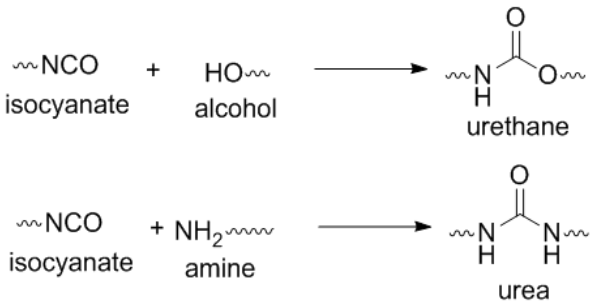

***Figure 2.5.2**: Reactions of isocyanates with alcohols or amines to yield urethane and urea groups, respectively.*

A polyaddition is a step-growth polymerization which is strongly exothermic, requiring cooling systems in commercial production plants. A commonly encountered side-reaction is the reaction of isocyanates with water which leads *via* a carbamic acid to the formation of a primary amine group. This group may, in turn, react with other isocyanate groups to form urea links (see ***Figure 2.5.3***).[40] Although this side-reaction is generally undesirable, it is largely utilized for the production of foams, the carbon dioxide generated serving as blowing agent.

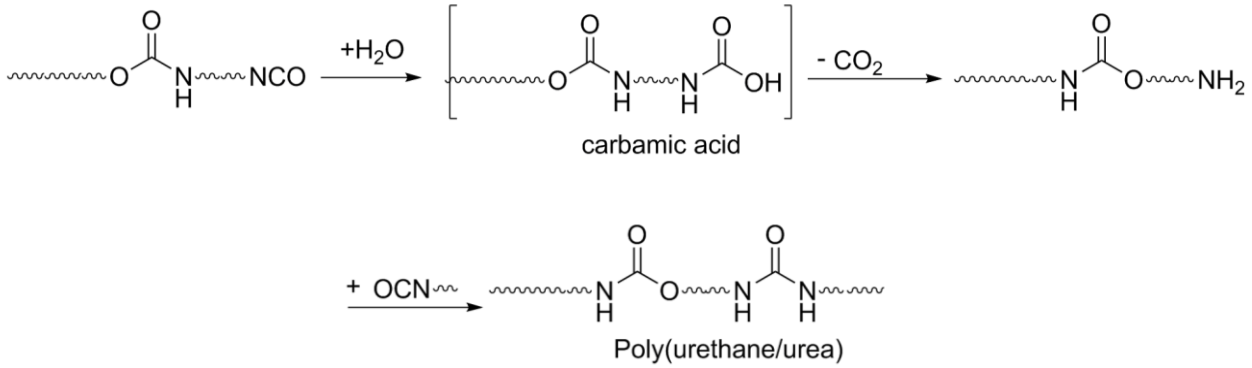

***Figure 2.5.3**: Side reaction of isocyanates with water. The reaction proceeds via an intermediary carbamic acid to the formation of an amine. This amine, in turn, may react with other isocyanates to form urea links.*

Batch polymerizations are usually carried out at moderate temperatures and with the addition of a catalyst, most often a metal-based one containing tin, zinc, bismuth, or titanium. If the presence

of metals is unwanted, tertiary amines may also be used.[41] If, however, the temperature increases above 120 °C during the polymerization, a significant degree of crosslinking reactions may occur which can result in the generation of allophanat or biuret groups (see ***Figure 2.5.4***).[40]

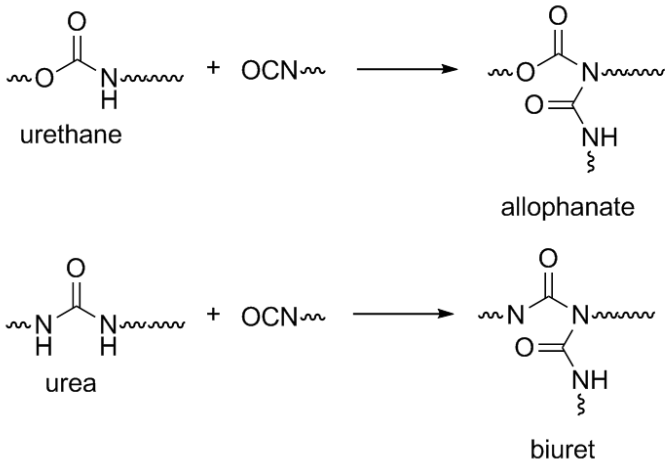

***Figure 2.5.4**: Crosslinking reactions of urethane and urea groups to form allophanate and biuret groups, respectively.*

The industrially synthesized PU structures are complex and diverse. However, only a handful of different isocyanate types are commonly employed in the synthesis which fall into two basic categories of aromatic and aliphatic diisocyanates. The aromatic ones are generally more reactive than the aliphatic ones. As a result, they are more prone to side reactions with water and are therefore less commonly used for the synthesis of water-based dispersions. Many diisocyanates are in fact isomeric mixtures, and ***Figure 2.5.5*** shows the predominant chemical structures of the aromatic methylene diphenyl diisocyanate (MDI) and toluene diisocyanate (TDI) and the aliphatic hexamethylene diisocyanate (HDI), fully hydrated MDI (H_{12}MDI), and isopohorone diisocyanate (IPDI).[39] Due to its lesser reactivity and hence to minimize side reactions with water, in this contribution, only IPDI will be used.

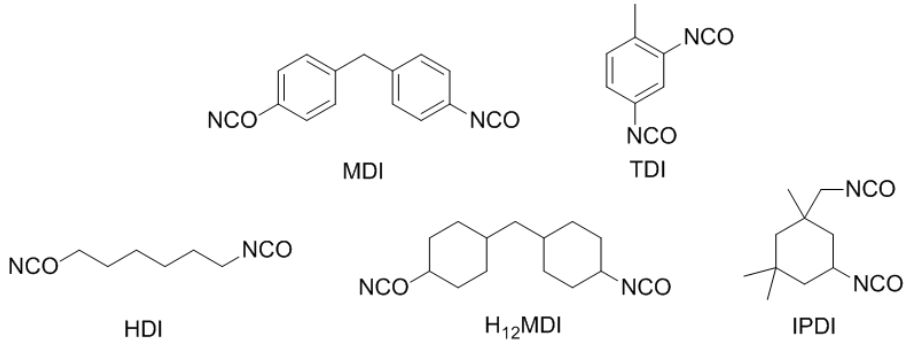

***Figure 2.5.5**: Chemical structures of the predominant isomers of the isocyanates MDI, TDI, HDI, H_{12}MDI, and IPDI.*

On the other hand, the alcohols used are numerous and often of high molecular weight. In this manner, the number of urethane links in the polymer chain can easily be modified which is decisive for the consequent film properties (see section 2.5.5).[42] The alcohols can stem from natural resources such as plant oils[43] or sugars,[44] possess interesting film properties through crystallization,[45] etc.. For PUDs in particular, alcohols may be used which contain water-swellable and charge moieties in order to stabilize the polymer chains upon emulsification and yield water-dispersible structures (see section 2.5.4).[46, 47]

2.5.3. Synthesis of PUDs

Like for most synthetic polymers, a high molecular weight and strong inter- and intramolecular interactions among PU chains lead to a bulk behavior resembling highly viscos liquids or even elastic solids at ambient temperature. For manufacturing processes, polymerization is thus either carried out *in situ* or, in the case of pre-synthesized polymers, high temperatures and/or organic solvents are used to facilitate handling. Of those options, only the use of an organic solvent is convenient and thus traditionally used for coating and adhesive applications in which a homogeneous surface coverage is crucial. However, due to a growing environmental awareness, much effort has been directed towards replacing PU solutions with their ecofriendly, water-based analogues, *i.e.* PUDs. Since the 1980s, PUDs have begun to substitute PUs for many applications, particularly coating and adhesive applications.[42, 46, 47]

PU nanocapsules or particles may be synthesized in dispersion directly. For instance, the miniemulsion process can be used to generate nanometer-size droplets of a water-soluble diol in an organic phase. An isocyanate may then be added *via* the continuous phase and the polyaddition

reaction then occurs at the interface.[48] However, this approach bears several drawbacks. Firstly, the side-reaction of isocyanates with water must be taken into account. Furthermore, a surfactant must be used in order to allow for dispersion formation. Also, the choice of diols and diisocyanates is very limited. For uses in which variable particle surface and film properties are important, this synthesis route is thus not well-suited.

To obtain nanoparticles with such specific interfacial and bulk properties, one might intuitively think of simply synthesizing the desired polymer structure, and then emulsifying it to obtain nanoparticles. However, due to the strong inter- and intramolecular interactions in PUs (see section 2.5.5), dispersing a high molecular weight PU is often not feasible. In order to reconcile the high viscosity of a presynthesized polymer with the low degree of compositional variability of a polymerization in dispersion, different, intermediate routes can be chosen.[49] One approach, the so-called "prepolymer mixing process" (see ***Figure 2.5.6***), consists of the synthesis of a reactive prepolymer of moderate molecular weight (commonly M_n = 2 000 – 15 000 g/mol) in bulk as the first step. The polymerization can be carried out at elevated temperatures and in nitrogen atmosphere, entailing a high degree of control over the polymerization, molecular weight, and composition of the prepolymer. Through the use of a slight excess of isocyanate groups with regard to alcohol groups, NCO chain termini can be obtained which may be used for further reactions. The relatively short polymer chains possess a rather low viscosity in the polymer melt and can therefore be dispersed in water. An auxiliary, low boiling point solvent like ethyl acetate or acetone (which is also used in the "acetone process" described below) may be added to further facilitate the process. The PU structures are usually chosen such that the resultant particles are self-stabilizing in water, *i.e.* an aqueous dispersion can be formed without the use of a surfactant. This can be accomplished through the use of hydrophilic and/or charged segments (see following section). Once the PUD is formed, di- or polyfunctional nucleophiles may be added in order to conduct a so-called "chain-extension" of the PU chains in the particles and to introduce crosslinks into the system. This is for instance described in chapter 4.1 where polyfunctional protein fragments are added to a PU prepolymer in order to achieve a peptide-decoration of the particles. Also, monofunctional nucleophiles can be used to complete a so-called "endcap" of the chains and/or to introduce specific functional groups. The chain extension or endcap of PUDs in dispersion is a complex process: the locus of the reaction can be the particle surface or its core, depending on the solubility of the reagent in question in the dispersed polymer solution,[50] and the amount of reagent added can strongly alter the particle size as well as the adhesive strength of the resultant polymer.[44] Primary or secondary amines are common choices for nucleophiles because they generally react much faster than the water molecules which they naturally compete with. This method was used for the synthesis of phosphonic acid functionalized PUDs (see chapter

4.3). In this manner, even in dispersion, a high degree of control over the polymeric structure and the particle surface can be maintained. The subsequent removal of the auxiliary solvent allows for the synthesis of a VOC-free adhesive or coating.[47]

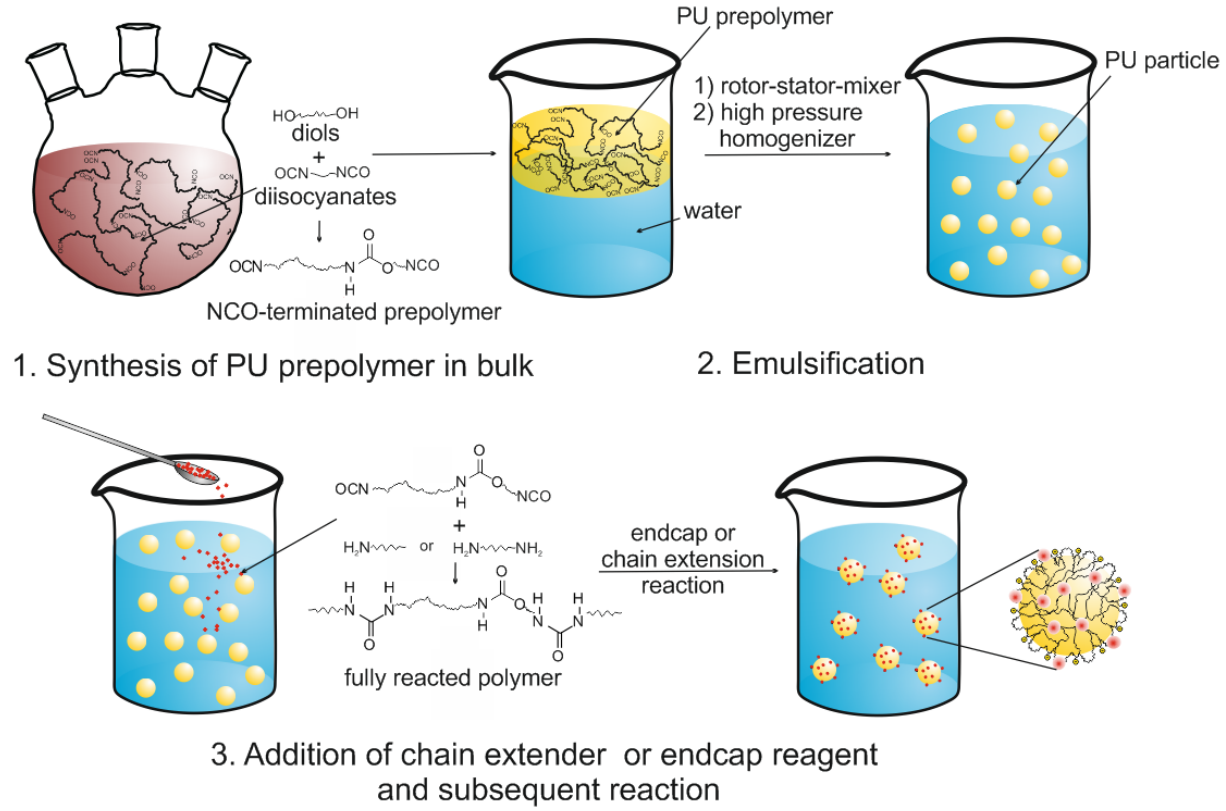

***Figure 2.5.6**: Illustration of the prepolymer mixing process. An NCO-terminated prepolymer is synthesized in bulk and dispersed in water. Endcapping or chain extension is the carried out via the aqueous phase.*

A closely related process is the so-called “acetone process” in which an isocyanate-terminated prepolymer is synthesized and dissolved in acetone. However, in this case, a partial chain extension using diamines is carried out prior to emulsification. This allows for a particularly tight control over the chain extension and ensures a high reproducibility.[51]

Another method is the “ketamine/ketazine process” in which the isocyanate-terminated polymer is blended with a blocked amine (ketamine) or a blocked hydrazine (ketazine). When the prepolymer is then dispersed in water, the amino group is deprotected and chain extension occurs directly inside the particle.[46, 47]

Many variations of the aforementioned, principal synthesis routes for PUDs exist. The type of method is usually chosen according to the desired PU structure. In this work, the basic, underlying approach is the prepolymer mixing process. However, slight alterations of the method were required in order to generate the desired film and surface structures.

2.5.4. Dispersion properties

When studying the interactions of PUDs with different substrates, a very important aspect is the surface of the particles. As explained in more detail before, the large surface area of polymeric nanoparticles as well as the numerous, strong inter- and intramolecular interactions between the chains and general incompatibility with the surrounding water lead to a high surface tension of the dispersions. As a consequence, a direct contact between the particles would lead to their coalescence. Section 2 of this chapter describes the DLVO theory and how steric and electrostatic contributions can provide long-range and medium-range repulsion, respectively.[19, 20] Both of these mechanisms can be exploited for nanoparticle stabilization.

In most cases, surface-active molecules (a.k.a. surfactants) are used which, due to their chemical composition, possess both hydrophilic and hydrophobic segments and thus spontaneously adsorb to the interface between a primarily hydrophobic particle and the surrounding water. Surfactants can be ionic or nonionic. Ionic surfactants consist of a hydrophobic tail and a charged, hydrophilic head group whereas nonionic surfactants also possess a hydrophobic tail, but an uncharged, hydrophilic head group. Whereas nonionic surfactants thus stabilize particles through steric repulsion, ionic surfactants provide stability through electrostatic interactions. Typical hydrophobic tails are aliphatic chains and typical hydrophilic head groups are sulfonate (anionic) or ammonium (cationic) groups or poly(ethylene oxide) chains of moderate length (uncharged).[52]

Surfactants may not only adsorb to the particle surface, but also be covalently attached to the polymeric chains, in which case they are termed monomeric surfactants (or “surfmers”).[53] For applications entailing elevated temperatures or high sheer forces, surfmers are particularly useful because desorption and hence coalescence can be avoided. However, depending on the nature of the particles, they may not be compatible with the polymer and hence segregate during film formation.[54]

In the case of PUDs, stabilization is commonly not due to any external, either adsorbed or covalently attached molecule. Instead, the PU structure is typically designed to comport water-swellable and/or charged groups.[8, 37, 46, 47, 55] In this way, an effective stabilization is achieved while maintaining a homogeneous polymeric structure. For steric stabilization, diols comporting

poly(ethylene oxide) or poly(ethylene oxide/propylene oxide) segments are often chosen. The hydrophilicity of the polymer can easily be adjusted by altering the relative amounts of ethylene oxide and propylene oxide segments. Anionic charge repulsion can be provided by diols comporting sulfonate groups or by dimethylolpropionic acid whereas cationic charge repulsion can be provided by diols containing quarternary amines.[46, 47, 56] Even though PUDs stabilized solely anionically,[55, 57] cationically,[58, 59] or nonionically[60] have all been described in the literature, the preferred route for stabilization is a combination of anionic and steric stabilization.[46, 47]

The method of stabilization is naturally very important for the interactions of PUDs with different substrates and a primary goal of the present work is therefore to modify the particle surface with different functional groups in order to tune the interactions with different substrates. The type of substrates and consequently the types of modifications to be conducted will be explained further in section 6 of this chapter.

2.5.5. Film properties

2.5.5.1. Film formation

An aspect of particle-surface interactions which should also be considered is what happens after particle deposition and evaporation of the solvent. In fact, the film formation process can have a great effect on the resultant film properties and will therefore be described here. Film formation can be described as a 3-step process (see ***Figure 2.5.7***).[61, 62] When the surrounding water evaporates, the polymer particle concentration increases until the particles come in contact with each other. In this first step, the particle identity and spherical morphology are maintained. In the second step, subsequent water evaporation leads to the creation of capillary forces. These will lead to a deformation of the particles to fill the interparticular voids if the particles are deformable, *i.e.* if the process takes place above the minimum film formation temperature of the polymer. Due to the weak plasticizing effect of the water, this temperature will be slightly lower than the glass transition temperature of the polymer. The third and last step then consists of the interdiffusion of the polymer chains to form a continuous film if the chains are sufficiently mobile (see section 2.5.5.2).

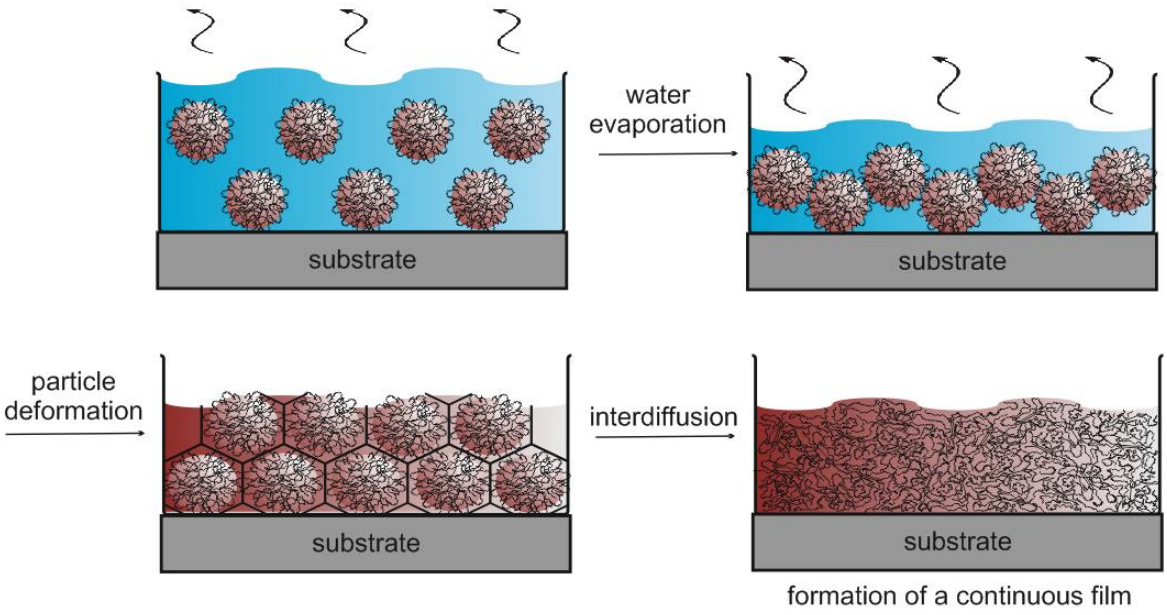

***Figure 2.5.7**: Simplified illustration of the film formation process for polymer dispersions. The process occurs in three stages: evaporation of water until the particles come in contact with one another, deformation of particles due to capillary forces, and lastly interdiffusion to create a homogeneous film.*

2.5.5.2. Physical crosslinking

Once a film is formed, the polymer (in this case PU) chain structure determines factors such as modulus, cohesion, etc.. Polyurethanes synthesized from diisocyanates and diols are segmented polymers.[41] The low molecular weight diisocyanates are transformed into short, rigid segments with urethane or urea groups on either side whereas the higher molecular weight diols constitute longer, more flexible segments which can be at the origin of different, interesting properties (see below).

In terms of film properties, the distinctive characteristic of polyurethanes lies in the strong interactions between urethane and urea groups through hydrogen bonding (see ***Figure 2.5.8***). Hydrogen bonding can occur between urethane groups, urea groups, and groups from the polyol segments. Of all possible couples, the H-bonds formed between two (symmetrical) urea groups are the strongest. Due to their high interaction, the urethane and urea groups tend to form associates. Those urethane- and urea-rich domains are called “hard segments” and can serve as physical crosslinking sites.[63] The polyol-rich domains are called “soft segments” due to their increased chain flexibility caused by weaker inter- and intramolecular interactions. In practice, those interactions can easily be adjusted through the molecular weight of the starting materials. Using predominantly

higher molecular weight diols and few diamines will lead to a lower concentration of urethane and urea groups and therefore to weaker interactions in the film. Conversely, employing lower molecular weight diols and particularly short diamines will increase film interactions. [42, 50, 64]

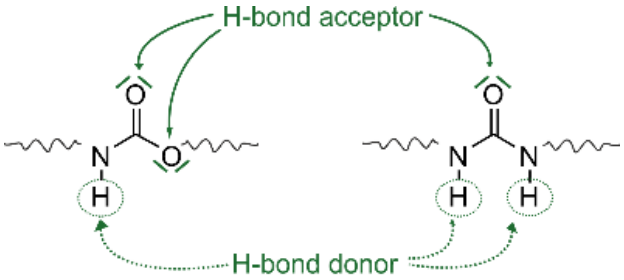

***Figure 2.5.8**: Possible H-bond donor and acceptor sites in urethane and urea groups.*

Depending on the isocyanate and diol structures, the hard segment interactions can lead to amorphous or crystalline structures. With the isocyanate IPDI which was employed in all PUD syntheses of this work, amorphous hard segment structures are usually obtained. However, with symmetrical isocyanates like HDI or MDI, and in some cases with TDI, crystalline domains can result. The corresponding melting ranges reported were commonly above 150 °C, even though hard segment melting at temperatures as low as 25 °C has also been observed.[65-67]

The soft segments generally provide flexibility and elasticity to the PU films. However, the soft segment compositions can be very diverse and hence the attainable properties can be as well.[42] For instance, polyester polyols can be employed which can provide crystalline domains in the soft segments. Such macromonomers can be produced from polyols and dicarboxylic acids or their anhydrides by polycondensation. Common polyols include ethylene glycol, 1,4-butanediol or neopentyl glycol, common dicarboxylic acids or anhydrides include adipic acid, terephthalic acid or phthalic anhydride, for example.[63] Nowadays, the synthesis of polyesters by ring opening polymerization of lactones is also largely used.[68]

The incorporation of crystalline domains can be used as yet another way to form physical crosslinks inside a PU film.[47] Those crosslinks are reversible and highly sensitive to temperature (see ***Figure 2.5.9***). Heating the film above the melting temperature of the crystalline domains will lead to an adhesive, flexible, and easily deformable film. Decreasing the temperature will, after crystallization, lead to a non-sticky, rigid film.[63] This property is highly desirable for a number of different applications and will be used as an important feature throughout this work. Furthermore, the crystallization of the soft segments also gives valuable insight into PU microstructure modifications. In fact, the crystallization behavior is very sensitive to changes in the PU chain structure caused by, for example, different chain lengths of the constitutive blocks,[69, 70] varying

proportions of hard and soft segments,[71] the type of soft segment used,[72] the type of chain extender,[64] etc.. Thus, the PU microstructure can also be expected to be affected by a functionalization of the particles and it will therefore be analyzed here to draw conclusions to this end.

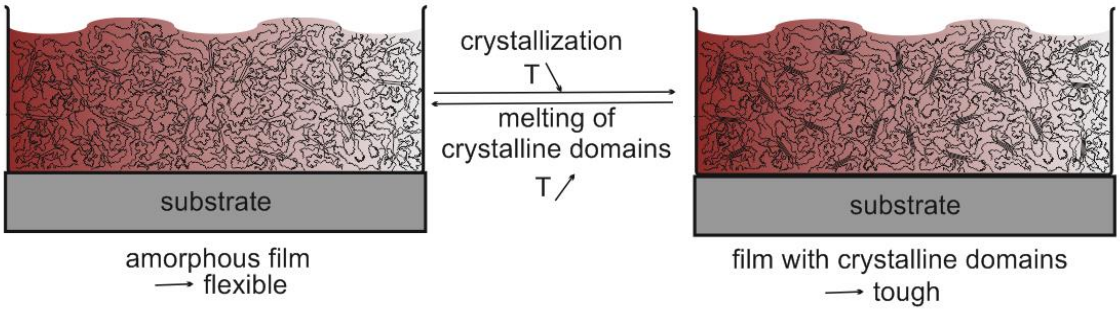

***Figure 2.5.9**: Illustration of the reversible formation and dissolution of physical crosslinks due to crystallization in PU films.*

In order to permit an analysis of the crystallization behavior of the PUDs synthesized here, a general understanding of the crystallization process is necessary. Crystallization generally describes the association of chain segments to form highly ordered structures with translational symmetry.[73] In the absence of external influences, it is a two-stage process which begins with the association of individual chain segments in Brownian motion to form small clusters.[74, 75] An interface between the clusters and the surrounding, amorphous bulk is thus created. From an energetic point of view, cluster formation can be seen as a competition between the energetically unfavorable creation of an interface and the energetically favorable interactions in the cluster volume.[76] Small clusters (clusters with a small radius) have a high surface-to-volume ratio and are thus less stable. In fact, a critical radius value exists below which clusters cannot remain stable and redissolve. Larger clusters, however, are stable and will evolve into crystals.[77] This first stage is termed (homogeneous) crystal nucleation. In the presence of impurities, the so-called heterogeneous nucleation occurs. In this case, clusters form at the surface of the impurities because the interfacial area to the bulk and hence the energetic cost of cluster formation is thereby greatly reduced.[74] It should be noted that in confined systems, such as in the case of dispersions of polymer chains capable of crystallizing, homogeneous nucleation is predominant due to the generally small number of heterogeneous nuclei distributed over a great number of particles. In order to induce a homogeneous nucleation in each particle individually, a much larger supercooling is required and the crystal morphologies obtained from homogeneous and heterogeneous nucleation processes can therefore be very different.[78] The second stage, crystal growt.h, then consists of the growt.h of the stable nuclei to form large crystals. This is a dynamic process characterized by the addition and redissolution of polymer segments.[79]

The final crystallite size and structure are highly dependent on the polymer structure and on the conditions in which crystallization occurs.[73] Hence, on the one hand, a constant heating-and-cooling protocol was employed throughout this work (see chapter 6 for details) in order to provide a constant "thermal history" for all films. On the other hand, an analysis of the crystalline structure of the films was conducted in order to analyze the effects of a given functionalization on the crystallization.

2.5.5.3. Chemical crosslinking

Polymer chain interdiffusion during film formation is crucial for the consequent cohesion in the film. If incomplete or only minor interdiffusion occurs, the remaining particle interfaces constitute weak junctions along which fractures can easily propagate. Interdiffusion depends on chain mobility in the film which, in turn, depends on chain length, crosslinking density, and temperature.[80-82] If the chains are short and linear, at a temperature above the polymer's glass transition temperature, interdiffusion can easily take place. In the extreme case of a densely crosslinked, infinite network, on the other hand, interdiffusion can be suppressed. However, following the same line of reasoning, short, linear chains also lead to poor film cohesion. In practice, for dispersion coatings and adhesives, crosslinking after film formation is usually used to solve this dilemma.

Two types of crosslinking mechanisms can be used: chemical and physical crosslinking. Whereas chemical crosslinking usually provides stronger, irreversible connections, physical crosslinking provides reversible and weaker interactions. For chemical crosslinking of PUs, hydrophilic polyisocyanates can be dispersed in the water phase. Upon film formation, the polyisocyanates are evenly distributed inside the film and can react with hydroxyl or amine groups of the polyurethane. A similar method entails the addition of a curing dispersion consisting of hydrophilic polyisocyanates and hydrophobic polyols.[8] In both cases, however, the high reactivity of polyisocyanates must be taken into account. The polyisocyanates should therefore be added to the dispersion directly before application.

Stability of the curing component is achieved in latent reactive systems in which, for example, solid, aromatic isocyanates are dispersed in an amine solution. The surface groups of the isocyanates in this case react with the amines, forming a protective shell. After film formation, further reactions take place at temperatures above 60 °C.[83] The main drawback of this method is the microscopic distribution of the isocyanates inside the film due to the micrometer-size dispersion which leads to inferior film properties.

Many other methods, including blocked isocyanates, entirely different crosslinkers like epoxides, carbodiimides, etc. can also be used and all possess respective advantages and disadvantages.[8]

As mentioned previously, physical crosslinking due to intra- and intermolecular interactions in the polyurethane film and due to the incorporation of polyester segments was a central aspect of the present investigations. However, chemical crosslinking was intentionally not included because the primary focus was the surface functionalization and subsequent interfacial interactions.

2.6. Studied model surfaces

We will now take a closer look at the types of surfaces investigated. Three different model surfaces where chosen to represent different surface categories used in various fields of application. Human hair was chosen as an example of a proteinaceous, filamentous type of substrate often encountered in personal care or biological applications. Hydroxylapatite was selected to represent crystalline, hard surfaces present in medical and health care applications as well as organic pigment surfaces encountered in coating and paint applications. Lastly, stainless steel was designated to represent metallic, conducting surfaces used in construction, consumer products, and medicine. In order to better understand the challenges associated with improving the interactions with the above-named surfaces, a general knowledge of their composition and surface chemistry is important.

2.6.1. Hair surfaces

2.6.1.1. Basic hair structure

Hair is a highly hierarchical material with a structure and chemical composition which greatly vary throughout.[84] The apparent surface composition depends on the exposed area and thus, the general structure of the entire fiber will be presented here. ***Figure 2.6.1*** shows the overlay of an electron microscopy image and a schematic depiction of a hair fiber and its constitutive parts.

A hair fiber typically has a diameter between 10 µm and 100 µm and is composed of two basic components: the cuticle and the cortex.

The cuticle is the outer layer of the fiber and consists of dead, overlapping cells which are arranged like tiles on a roof or scales on a fish. The scales point to the tip of the fiber. The cuticle consists of four layers of varying amounts of disulfide and isodipeptide bonds whose cohesion is provided by the cell membrane complex. From the exterior inwards, the first layer is the epicuticle which is only 5 nm thin and hydrophobic. Next is the a-layer, followed by the exocuticle, and the endocuticle.[85]

The cortex is composed of different, spindle-shaped cells: the ortho-, para-, and meso-cortical cells which differ in abundance and cystine (dimer of cysteine) content.[86, 87] Each cortical cell, in turn, consists of 5-8 macrofibrils, each with a maximum diameter of 300 nm. Macrofibrils are surrounded by a matrix consisting of cytoplasmic and nuclear remnants of keratinocytes. Each macrofibril is composed of 500 – 800 microfibrils (also called intermediate filaments proteins (IFP) or keratin proteins (KP)) bundled together and surrounded by intermediate filament- or keratin associated proteins (IFAP or KAP).[88-90] For more information on the amino acid composition of IFPs, see section 4.1.2. A microfibril contains 7 or 8 single or paired protofilaments. A protofilament is an association of four chains: a pair of right-handed alpha-helices with each helix consisting of two keratin chains. The two right-handed alpha-helices arrange in a left-handed coiled coil structure. The cross-section of a microfibril thus contains 32 keratin chains.

Coarse hair fibers may also contain a medulla at their center which is composed of hollow cells made up of amorphous proteins and fine filaments.[91]

Furthermore, pigment granules are also present in the hair fiber which range from black to brown eumelanin and yellow to red pheomelanin. A granule is a disc-like arrangement of a diameter of 46 Å and a height of 12 Å. It is made up spheres with a diameter of 70-500 nm which, in turn, consist of associations of 5 nm large particles. Those particles are composed of stacked oligomer sheets of protomolecule. In fact, it is this well-defined, ordered structure which is responsible for hair color: the color is thus a so-called physical color (due to a geometrical arrangement rather than to the presence of chromophores).[92]

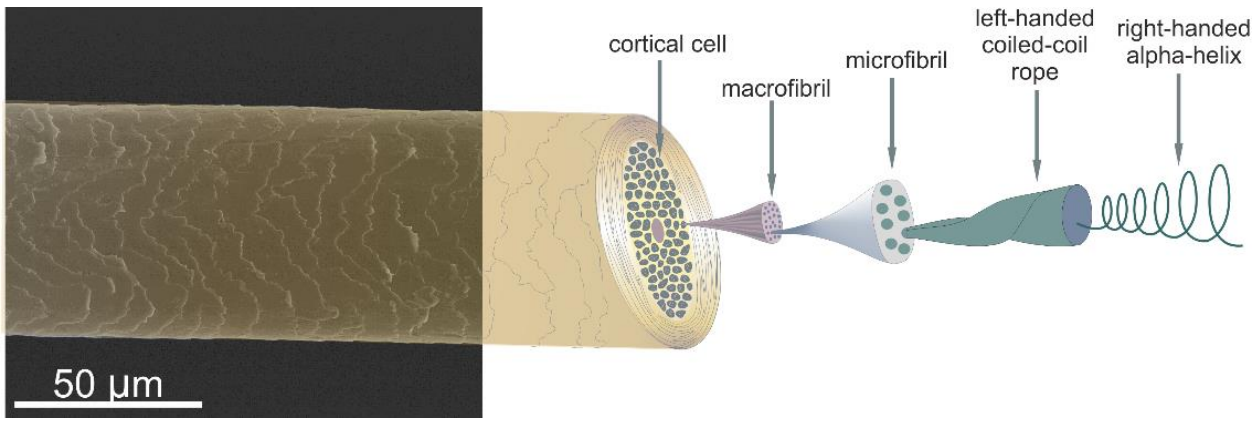

***Figure 2.6.1**: Major components of a hair fiber. Reproduced according to similar diagrams found in the literature.*[86]

2.6.1.2. Properties of hair fibers

A consequence of the complex, heterogeneous composition of a hair fiber is the "hair paradox."[93] The phenomenon describes that the exterior of undamaged hair is hydrophobic because the cuticle cells present predominantly aliphatic chains of fatty acid groups to the exterior.[94] The interior of a hair fiber, however, is hygroscopic because it contains many hydrophilic amino acid residues (see section 4.1.2). Furthermore, chemical treatments such as oxidation lead to an increase in surface tension and hence to an increase in hydrophilicity. The apparent nature (hydrophilic/hydrophobic) of the hair surface therefore very much depends on the exposed area and on its history. In practice, swelling of hair fibers is also a very important factor which can affect the mechanical behavior.

The general insolubility of hair fibers, their high wet strength and thermal stability are a curtesy of disulfide bridges.[95] S-S bonds, along with isodipeptide links, are the only covalent interactions amongst peptide chains, resulting in cross-linked structures of high resistance to external influences. This tool is also exploited in hair care and textile applications. In both cases, the S-S bonds are broken under the influence of a reducing agent (*e.g.* thioglycolic acid for human hair or sodium bisulfite for wool), the fibers are molded into the desired shape (*e.g.* rolled onto curlers or pressed), and the S-S bonds are then reformed under the influence of an oxidizing agent (like H_2O_2).[96]

2.6.1.3. Damage to the hair fiber

In healthy hair, the surface of the epicuticle cells is exposed, presenting a hydrophobic surface. However, in practice, different factors contribute to the gradual destruction of the hair fiber and can therefore be at the origin of a varying, apparent surface chemistry and morphology.

Mere mechanical grooming, *i.e.* regular combing of hair can affect the hair structure. Exerting a mechanical stress on the fiber causes it to expand and retract and a cyclic stress may therefore cause abrasion of cuticle layers, cracking, or even breaking of the fiber.[97]

Natural ultraviolet (UV) irradiation may also cause damage to the fiber because melanin granules and keratin fibers absorb UV light. A destruction of the granule structure and a general decrease in their size lead to a lightening or even to a loss of hair color. Furthermore, a loss of proteins from the hair is observed due to UV-induced separation of protein and matrix associations or even cleavage of intermolecular bonds, leading to a general weakening of the hair structure.[98]

The application of heat to the fiber, for instance through blow-drying after washing, also causes a gradual degradation of the hair. Cracks are formed during blow-drying, originating at particularly

dehydrated cell junctions and propagating several cell layers deep into the fiber. In this manner, repeated blow-drying can cause severe damage to the hair and eventually lead to it breaking.[99]

Chemical alterations to the hair structure, for instance due to bleaching, permanent weaving or straightening, also cause great damage. During chemical bleaching, a destruction of the granule structure is observed: hydrogen peroxide binds to the melanin sheets and causes a delayering of the discs, and lastly an elimination of the oligomeric sheets. In consequence, the granules shrink and the apparent hair color is shifted to lighter shades. During weaving or straightening, damage is due to the formation of cystine by-products and the consequent decrease in available cysteine for stabilizing the fiber. It has been reported that only about 91% of initially present cystine bonds were rebuilt after a single standard waving process.[100] For cosmetic and textile applications, processes have thus been developed to reduce this degradation effect (see below).[101, 102]

2.6.1.4. Adhesives for hair

In order to try and avoid or repair damage inflicted to the hair, different methods have been developed in the cosmetic industry. In general, natural polymers such as proteins or polysaccharides have been investigated and it has been demonstrated that some compounds are capable of attaching to the hair surface, providing a protective superficial layer.[103, 104] In particular, it has been shown that keratin hydrolysates can be formulated into shampoos and rinse-off conditioners which are then integrated into the hair fiber and deposited at cuticle junctions.[105] Lipid-modified keratins are also useful for reconstructing the lipid layer which is gradually eroded during a hair's lifecycle.[106]

For styling applications, it has been established that hairsprays which wet the hair surface and which consist of polymers with a low glass transition temperature adhere well to the hair surface and provide an elastic surface layer.[107] Due to the great similarities in surface structure of healthy hair and wool, many studies treat both cosmetic and textile applications.[93]

In this work, a hydrolyzed protein from wool will be used to promote the adhesion of PUDs to hair fibers. In spite of a slightly different amino acid composition due to insoluble products from the hydrolysis, favorable interactions can be supposed due to generally similar structure motifs and compositions of the hydrolyzed fragments as compared to the native hair. Furthermore, due to the cost-efficient manufacture of hydrolyzed proteins from natural resources, we thereby hope to extend their range of applications from food products and cosmetic additives to more sophisticated structures and uses.

2.6.2. Hydroxyapatite

2.6.2.1. Basic structure and occurrence[108]

Hydroxyapatite (HAP) is a naturally occurring crystal with a color ranging from colorless or white to yellowish green. It is a type of calcium apatite, which is a group of phosphate minerals also including fluoroapatite and chloroapatite. The chemical formula of hydroxyapatite is $Ca_5(PO_4)_3(OH)$, although it is customarily written as $Ca_{10}(PO_4)_6(OH)_2$ to reflect that apatites crystallize in the dipyramidal class of the hexagonal crystal system and a unit cell contains 2 entities.[109] It has a hardness of 5 on the Mohs scale and is very brittle.

Aside from its natural occurrence in rocks, hydroxyapatite is also the major constituent of mammal bone and teeth. During bone formation, hydroxyapatite crystallizes in a proteinaceous scaffold of tropocollagen in the form of small crystallites. The resultant material is hard, but rather flexible.[110] Enamel, the top layer of teeth, is made up to 96 wt% of hydroxyapatite in the form of large rod- or prism-shaped crystals (about 30 nm thick, 60 nm wide, and several micrometers long), rendering enamel the hardest tissue in the body.[111] The underlying dentine is similar in composition to compact bone.[112] Due to its natural presence in the body, hydroxyapatite is biodegradable and bioactive (*i.e.* it bonds to bony tissue) and has thus been extensively investigated for the use as hard tissue replacement. However, due to its weakness in tension and low resistance to fatigue, the general consensus is that hydroxyapatite should not be used as a bulk material, but rather as a superficial coating layer or in the form of small granules to repair minor defects. The probably most-investigated use is that of a coating for titanium implants.[112, 113] It is therefore very important to study the affinity of potential adhesives for bone or tooth replacements to the underlying substrates and hydroxyapatite will be used here as a model surface.[114]

2.6.2.2. Adhesion to hydroxyapatite

Many routes have been developed in the past in order to improve the compatibility of generally hydrophobic resins with hydroxyapatite-containing surfaces. A popular approach is to etch the substrate, *i.e.* to partially remove the top layer by dissolution prior to application of the adhesive. The goal is commonly to remove any pollutants from the interface and create cavities for the adhesive to diffuse into, favoring intimate contact.[115] Most often, acrylates or methacrylates are used and after etching, polymerization is carried out *in situ*. The wide-spread use of acrylates and methacrylates is mostly due to their low cost, fast polymerization, and high mechanical stability.[116, 117] However, inherent drawbacks include general hydrophobicity, monomer volatility, and possible

diffusion into tissues.[118] Different kinds of acids have been used for etching and the incorporation of phosphonic acid groups has been demonstrated to result in better biocompatibility and adhesion.[10] The much improved interaction with the tooth surface results from a dual interaction *via* the adhesion/decalcification concept with hydroxyapatite.[119] The acid groups partially dissolve calcium ions from and bond to HAP,[120] a process which is largely determined by the solubility of the resulting salts in their own solutions, regardless of concentration and pH.[11] The dissolved Ca^{2+} ions further act as crosslinkers at the interface[121] and the bond strength largely depends on the structure of the acid.[122, 123]

In this work, the interactions between phosphonic acid groups and HAP surfaces will be exploited. PUDs functionalized comporting phosphonic acid groups as chain termini will be synthesized and their adhesive behavior to HAP will be evaluated.

2.6.3. Stainless steel

2.6.3.1. Basic description[124]

Since ancient times, iron has been used and mended for various uses such as weapons, containers, utensils of different sorts, *etc*. due to its high abundance, durability and ductility. In order to adapt mechanical properties like tensile strength and hardness, alloying elements such as carbon, manganese, chromium, nickel, molybdenum, or tungsten were added. Although steel is the general term for alloys of iron and carbon (with typically a maximum of 2 wt% carbon), the above-named elements may also be present in small amounts, yielding a large palette of steel types with diverse properties. In particular, stainless steels contain a considerable amount of chromium (typically at least 10.5 wt%) which confers a highly desired property to the materials, namely corrosion resistance. In fact, iron corrodes readily in humid, oxygen-containing environments to form an oxide layer through which oxygen can diffuse. As a result, corrosion continues throughout the material, leading to a drastic deterioration of properties. In contrast, in the case of stainless steel, chromium forms a protective oxide layer through which oxygen cannot diffuse, thereby effectively hindering corrosion. Depending on the properties demanded by the application, various kinds of stainless steels of different composition were developed. As a model, we will investigate stainless steel type SS2343 which consists of carbon (max 0.05 wt%), silicon (max 1.0 wt%), manganese (max. 2.0 wt%), phosphorus (max. 0.045 wt%), sulfur (max 0.03 wt%), chromium (16.0-18.5 wt%), nickel (10.5-14.0 wt%), and molybdenum (2.5-3.0 wt%).

2.6.3.2. Adhesion to stainless steel

Due to the extensive use of stainless steel in construction, automotive, and other industrial applications, the adhesion of coatings, adhesives, and other materials has been widely investigated. In most cases, the goal of such investigations is to avoid damage to the materials due to corrosion or separation of an adhesive joint. Different methods have thus been developed which may rely on a pretreatment of a polymer to be attached using oxidative treatments such as corona discharge or plasma treatments, or a pretreatment of the surface using *e.g.* acid treatments,[125] or on the use of reactive species.[126] Oxidative treatments aim at increasing the polarity of the polymeric coating and hence favor wetting between a metal of high surface tension and a polymer of rather low surface tension. In the latter cases, the goal is to take advantage of specific surface-coating interactions due to acid/base interactions, coordination of the metal, interfacial reactions, *etc.*.[127-129]

For stainless steel in particular, phosphonic acid pretreatment has become a standard process in the industry. The phosphonic acid groups bind to the metal oxide surface through strong acid/base interactions in different bonding modes.[130] Aside from pretreatments, phosphonic acids can also be blended with an adhesive or covalently attached to it. The main drawback of the former method, however, is that the distribution of phosphonic acid groups in the coating will not be homogeneous and a loss of adhesion may result.[131] It is therefore preferable to covalently attach the phosphonic acid group to the coating, either *via* reaction *in-situ* or *via* a coating containing phosphonic acid groups. Many researchers have focused their attention on such investigations.[132, 133]

Another promising alternative consists in the use of adhesive peptides. Due to the monodispersity of the peptide structure, peptide-substrate interactions are specific and can therefore be modified at will.[134, 135] Whereas for synthetic polymers, unspecific interactions like hydrogen bonds or charge interactions often determine their adhesive behavior[129], peptide adhesion may be modulated through single amino acid side chains (their degree of oxidation, their orientation in space, etc.); factors which can change dramatically due to minor modifications in the environment.[136] This characteristic renders peptides particularly well-suited for playing the role of a functional component of polymers, even bestowing upon them reversible adhesion to a particular substrate.[137] Similarly to other adhesion promoters such as phosphonic acid groups, peptides can also be covalently attached to a coating using many different approaches.[5, 6, 138] We will investigate here the use of an amino acid sequence which has been shown to adhere to stainless steel (see section 4.2.3).[139]

3. Relevant Characterization Methods

The following chapter describes the main characterization techniques employed in this work. When appropriate, the theoretical background will also be explained. Practical details are given in chapter 6.

3.1. Isocyanate titration according to the Spielberger method

The titration of isocyanate groups using the Spielberger method[140] is a type of endgroup analysis and a convenient method for monitoring the polymerization of polyurethanes. Aliquots are taken from the reaction medium and reacted with an excess of a secondary amine (such as DBA) in an organic (usually aromatic) solvent. The reaction product does not possess the general, basic character of amines. Therefore, the residual, unreacted amine can be quantified by titration with hydrochloric acid. Prior to the titration, a cosolvent (usually an alcohol) is added in order to improve the miscibility of the aromatic solvent with the aqueous acid. The equivalence point can easily be determined using a pH indicator (such as bromophenol blue). If the exact concentrations of both the amine solution and the hydrochloric acid solution are known (for instance through reference titrations of the amine solution with the HCl solution), then the residual NCO content can be quantified.

An exemplary experimental procedure can be as follows (according to ISO 14896:2009-07 method A): ca. 1 g of sample are precisely weighed and 4.00 mL dibutyl amine solution (0.5 M in xylene) is added. 50 mL each of xylene and isopropanol are added and the sample is stirred while heating moderately until the polymer is completely dissolved. Several drops of a bromophenol solution (saturated solution in ethanol) are then added and titrated using a 0.5 M HCl solution. If the equivalence point for a mass C (in grams) of polymer corresponds to a certain volume B (in mL) of HCl solution and a blank reference measurement (same procedure without the addition of polymer) corresponds to a volume A (in mL) of HCl solution, then the isocyanate content (in wt%) can be calculated as follows:

$$\%NCO = \frac{2.1\frac{g}{mL} * (A - B)}{C}$$

This method was used for following the PU synthesis for all prepolymers (see sections 6.2.1, 6.3.1, and 6.4.1).

3.2. Particle size measurements

Two techniques, namely dynamic light scattering (DLS) and laser diffraction (LD) measurements were used to determine the size of the particles in dispersion.

3.2.1. Dynamic light scattering[141]

DLS is a method for determining the hydrodynamic size and the size distribution of nanoparticles in dispersions.A laser sends photons of coherent light which pass through the sample and are scattered in all directions by the particles. Interference of the scattered photons causes regions in space of high intensity (constructive interference) or low intensity (destructive interference). Due to the fact that all colloids in solution are in Brownian motion, the position of the scattering particles and hence the interference pattern change overtime. The diffusion coefficient D_z of non-deformable, spherical particles in Brownian motion can be related to their hydrodynamic radius r_h using the Stokes-Einstein equation as follows:

$$D_z = \frac{k_B T}{6\pi\eta r_h}$$

with k_B the Boltzmann constant, T the temperature, and η the dynamic viscosity of the surrounding medium.

As a result of the diffusion of the particles, a detector placed at a given point in space will recollect an intensity of light which fluctuates overtime. The fluctuations can be described by an autocorrelation function $g_1(t)$ using the Wiener-Kinchim theorem:

$$g_1(t) = e^{-D_z q^2 t}$$

With t the time and q the wave vector. Measuring the intensity of scattered light overtime thus allows to determine the diffusion coefficient of the particles in motion which in turn permits to calculate their hydrodynamic radius.

Generally, DLS can be used to determine particle sizes ranging from a few nanometers to a few micrometers. Limitations merely arise in the case of small particles due to the low scattering intensity and in the case of large particles due to their slow Brownian motion, requiring long measurement times.

The particles synthesized in the present study were generally a few hundred nanometers in size and therefore fall into the range of DLS sensitivity. However, in some parts of the work (section 4.1.4),

particle stability was assessed through the formation of agglomerates. In that case, a method for the detection of larger entities was necessary, *i.e.* laser diffraction.

3.2.2. Laser diffraction[142]

LD is another method for determining particle size. It is also based upon the analysis of a light pattern observed when light from a coherent source is scattered by a dispersion of particles. However, whereas in DLS, the variation overtime of the intensity of light at a given point in space is used to determine particle sizes, in LD measurements, characteristic variations in space of the diffraction pattern (intensities and line spacing) at a given point in time are measured. Since the observed pattern may not only be due to diffraction but also to other scattering phenomena (such as refraction, reflection, *etc.*), this must also be taken into account.

The description of the scattering phenomena largely depends on the ratio of the particle diameter D and the wavelength of incident light λ. If the particles are very large with regard to the wavelength of light ($D/\lambda > 5$), the so-called Fraunhofer scattering occurs. If $D/\lambda \approx 1$, Mie scattering occurs, and if $D/\lambda < 0.1$, Rayleigh scattering occurs. In order to accurately describe the scattering pattern observed, the Mie solution to Maxwell's equations can be used which expresses the scattered light intensity as a function of the scattering angle. The solution regroups all three cases, comporting a term of Fraunhofer scattering and a term for Rayleigh scattering. According to the theory, the scattering pattern intensities can thereby be related to the particle diameter, the scattering angle, and the optical parameter of the system. Since the latter factor only appears in the Rayleigh term of the Mie solution, it can be neglected if the particles are large with respect to the incident light. This approximation is known as the Fraunhofer analysis and strictly speaking only applies for $D/\lambda > 6$, which for most light sources translates to particles larger than 4.5 µm (for λ = 750 nm).

Thus, if the scattering angle and the intensity of light are measured (if the Fraunhofer analysis is applicable) and additionally the optical parameter is known (in cases in which it is not, the full Mie solutions must be considered), the particle diameter can be deduced.

Aside from the above-named theoretical considerations, another limitation arises from the fact that smaller particles scatter little and at large angles whereas larger particles scatter a lot of light to smaller angles. Since the experimental setup is such that primarily diffracted light is measured (meaning light scattered at small angles with regard to incident light), the sensitivity with regard to smaller particles is reduced and there is an effective detection limit for particles smaller than 400 nm (for λ = 750 nm).

The above-named limitations can be overcome by measuring with more than one wavelength of light and by placing detectors at both large and small scattering angles. For instance, the device used in this study thereby provided an extended measuring range from 10 nm to 5000 µm.

3.3. Particle charge measurements

Two methods, namely Zeta potential (ZP) measurements and particle charge detection (PCD) measurements, were carried out in order to determine the charge of the PUDs synthesized.

3.3.1. Zeta potential analysis[143]

ZP measurements can be used to give information about the superficial charge of a particle. When a charged particle is placed in an aqueous environment, a double layer of oppositely charged ions will form around it (as explained previously in section 2.2.2.). The first layer is composed of strongly adsorbed, immobile ions whereas the second is composed of more loosely attracted ones (due to the repulsion originating from the first layer). Further from the surface of the particle, ions in the solution will be less and less affected by the presence of the charged particle and therefore move more freely. The ZP describes the potential at the slipping plane separating the double layer from the surrounding medium.

In practical measurements, an electric field is applied across the dispersion which causes the particles to move along the field lines due to osmosis. The particle motion can be tracked using a laser and related to the particles' zeta potential using the Smoluchowski equation.

The ZP is an important factor for determining particle stability. In fact, for particles such as PUDs which are stabilized (an)ionically, as a rule of thumb, a zeta potential (ζ) inferior to -30 mV or superior to +30 mV is necessary for long-term stability. In the case of -40 mV < ζ < -10 mV or +40 mV > ζ > +10 mV, particles may be stable for short periods of time. For zeta potentials close to zero, however, coagulation usually occurs rapidly. Thus, in this study, zeta potential measurements were used to assess the mode of stabilization through functionalization in some cases, and to assess the effect of functionalization on the stability in other cases.

3.3.2. Particle charge detection

A particle charge detector is a device used for measuring the surface charge of colloids and macromolecules through titration with an electrolyte. It consists of a measuring cell containing the dispersion or solution to be analyzed, two electrodes at the cell wall, and a piston moving up and down in the cell. This movement (which commonly has an amplitude of 5 mm and a frequency of 4 Hz) creates a stream of solvent in the cell which carries the charged particles with their fixed

counterion layers along (see ***Figure 3.7.1***). A displacement of the particles and their fixed counterion layers relative to the mobile counterion layers is thus created. This effect is at the origin of the creation of a streaming potential which is detected at the cell wall.

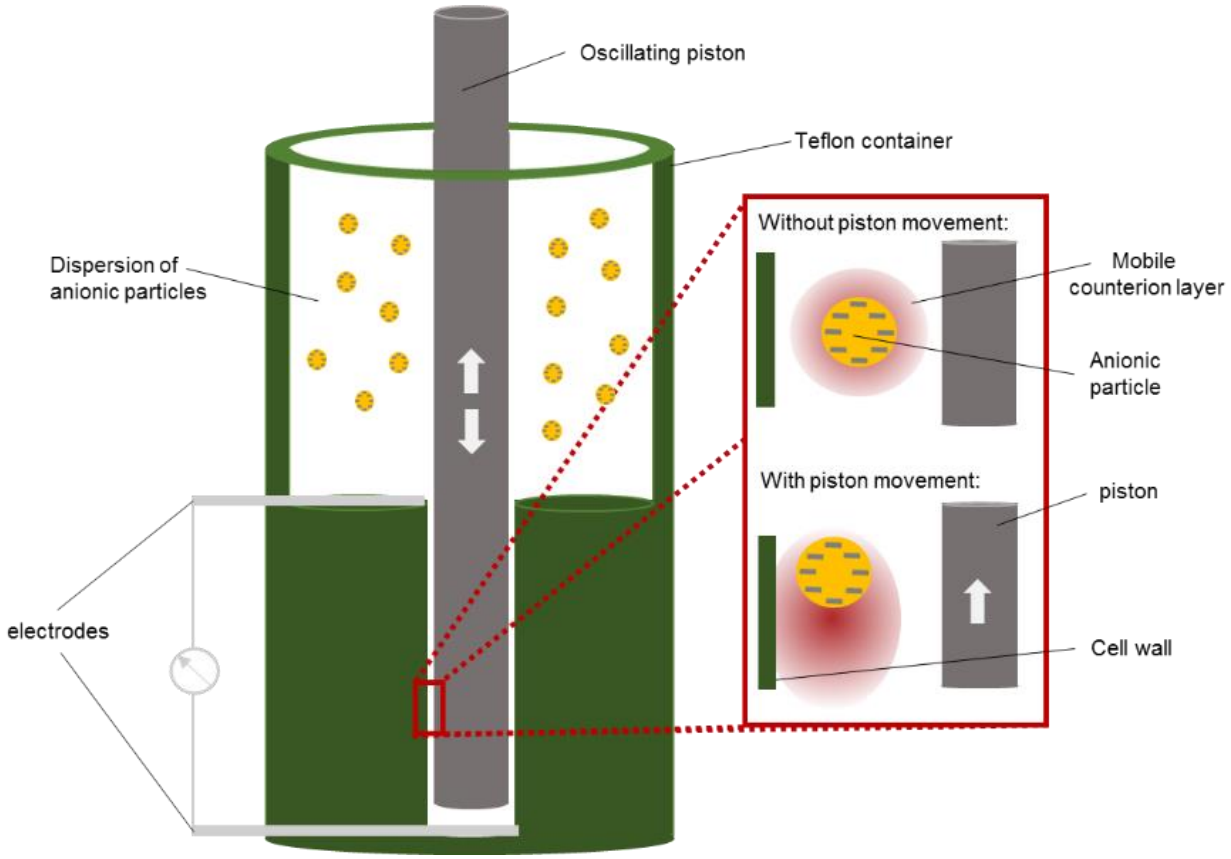

***Figure 3.7.1**: Illustration of a particle charge detector. Reproduced according to similar illustrations found in the literature.*[144]

Measurements are carried out repeatedly during titration with a polyelectrolyte (usually Polydiallyldimethylammoniumchlorid (PDADMAC) for anionic analytes and sodium polyethylene sulphate (PES-Na) for cationic ones, see ***Figure 3.7.2***). The latter have a stretched conformation due to repulsion of the charged monomer units and are insensitive to changes in pH and to addition of ions over a large range.[144]

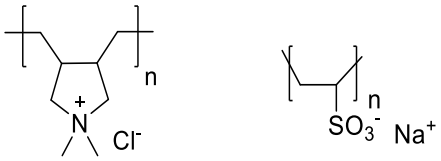

PDADMAC PES-Na

***Figure 3.7.2**: Chemical structures of PDADMAC and PES-Na, polyelectrolytes often used in PCD titrations.*

The volume of added electrolyte at which a reversal of the streaming potential occurs gives the equivalence point in the titration. Using the concentration of the electrolyte, the solid content of the dispersion, and other characteristics of the dispersion (hydrodynamic diameter of the particles, density of the polymer), and assuming certain conditions are met (all charges are accessible to simplex formation, 1:1 stoichiometry of simplex, no coagulation during the measurement), the charges per particle $q_{particle}$ can be calculated using the following equation:[145, 146]

$$q_{particle} = \frac{8q\pi d{r_h}^3\rho}{6}$$

With r_h the hydrodynamic radius of the particles, ρ the density of the polymer, and q the charges per gram of polymer which are calculated as follows:

$$q = \frac{VcN_A}{s}$$

Where V is the volume of electrolyte consumed, c the concentration of the electrolyte, N_A the Avogadro constant, and s the solid content of the dispersion.

Here, titrations with PDADMAC of the phosphonic acid-functionalized PUDs were conducted in order to calculate the number of phosphonic acid groups per particle (section 4.3.3.2 and 4.3.4.2).

3.4. Measurements of particle functionalization

For the three types of particle functionalization, three different techniques were used in order to assess the extent of particle functionalization. For the first project of functionalization using a hydrolyzed protein, the Bicinchoninic acid assay (BCA assay) was used (see section 4.1.5). For the second project of functionalization using an adhesive peptide of defined sequence, the Ellman's test for free thiols was used (see section 4.2.4.). And for the third project of phosphonic acid-functionalization, inductively-coupled plasma optical emission spectroscopy (ICP-OES) was used (see sections 4.3.3.2 and 4.3.4.2).

3.4.1. Bicinchoninic acid assay

The BCA assay is a method to quantify peptide concentrations in solution. It relies on the biuret reaction between peptides with alkaline Cu^{2+} to give a purple complex. The divalent copper is coordinated by at least two peptide links as shown in ***Figure 3.9.1***, causing the color shift. It has been shown that the intensity of the complex increases linearly with the amount of peptide present.[147] A colorimetric measurement thereby easily permits a quantification. However, the complexation interactions are rather unspecific; particular residues (such as Tyrosine) have also been shown to be capable of coordinating copper and generating the purple color.[148] In this study, the BCA assay was used to quantify a hydrolyzed protein, *i.e.* a mixture of different peptide components. The hydrolyzed protein itself was used to establish a calibration curve to try and avoid uncertainties arising from specific residues.

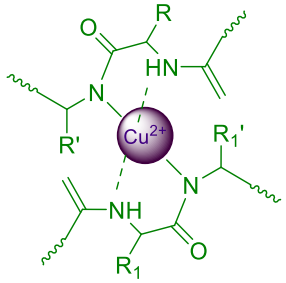

***Figure 3.9.1**: Schematic representation of the biuret reaction between two peptides with Cu^{2+} to generate a purple complex.*

3.4.2. Ellman's test for free thiols

Alternatively, specifically for cases in which the peptide's amino acid composition is known, individual residues can be used for quantification. In the case of the Ellman's test, cysteine residues react with the colorless 5,5'-Dithiobis(2-nitrobenzoic acid) (DTNB) to produce equimolar quantities of 5-Mercapto-2-nitrobenzoate (MNB) (see ***Figure 3.10.1***).[149, 150] The characteristic absorption of MNB at 412 nm increases linearly with concentration and can therefore be used for quantification of the peptide.[151]

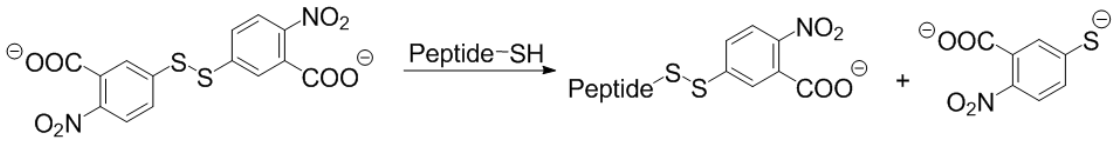

***Figure 3.10.1**: Reaction between DTNB and a cysteine-containing peptide. The reaction product MNB displays a characteristic absorption at 412 nm which allows for the quantification of the peptide sample.*

3.4.3. Inductively-coupled plasma optical emission spectroscopy[152]

Inductively-coupled plasma optical emission spectroscopy (ICP-OES) is a common technique for determining trace elements in soils and rocks, drinking and waste water, in biological and medical tissues and liquids, *etc.*. Liquid or gaseous samples are measured; solid samples may be measured after extraction or acidic decomposition to generate solutions. Solutions or liquids are in turn nebulized and channeled towards the first part of the device, *i.e.* the inductively coupled plasma. Due to the high temperature of the ICP (ca. 10 000 K), the sample is vaporized and the elements present are freed and excited through further collisions in the ICP, often generating excited ions. Those excited atoms and ions may then return to the ground state through the emission of photons. A measurement of the wavelength and of the quantity of photons emitted can then be used to characterize and quantify the elements present, respectively. This is achieved in the second part of the instrument, the spectrometer. The emitted photons are collected and focused using a lens or a concave mirror, then specific wavelengths are selected using a monochromator. The signal detected is amplified and converted to an electronic signal which is lastly used for the analysis.

It was used here to measure the amount of phosphorus present in dispersions for the phosphonate-functionalization of PUDs for adhesion to hydroxyapatite (see section 4.3). Freeze-dried samples before and after dialysis were measured in order to calculate the conversion of the endcap reaction.

3.5. Quartz crystal microbalance with dissipation[153]

The quartz crystal microbalance with dissipation (QCMD) is a measuring device to monitor adsorption phenomena in gaseous or liquid environments and to simultaneously investigate the characteristics of the adsorbed layer. It consists of a quartz sensor across which an electric field is created through the deposition of electrodes. As the piezoelectric effect (or more precisely, the reverse piezoelectric effect) describes, the application of an electric field across a piezoelectric material (such as a quartz) causes a mechanical strain. Similarly, the application of an alternating current causes an oscillation of the sensor with the frequency of oscillation being proportional to its mass. Thus, if the sensor is immersed in a medium containing absorbing species, a shift in the frequency of oscillation can be related to a change in mass caused by adsorption or desorption. Sauerbrey was the first to propose a model for this phenomenon.[154] He defined the area density of the quartz by $m_q = t_q r_q$ with r_q the density of the quartz plate and t_q its thickness. Assuming that for small changes in mass, the

adsorbed layer can be treated as an extension of the thickness of the quartz itself, he derived that the change in frequency *Δf* is given by

$$\Delta f = \frac{f}{m_q}\Delta m = -\frac{f}{t_q r_q}\Delta m = -\frac{n}{C}\Delta m$$

with *Δm* the change in mass, *C* the so-called mass-sensitivity of the QCMD, and *n* the order of the frequency (for the fundamental frequency *n* = 1, for the first overtone *n*=2, and so on). In this manner, a change in mass can be calculated from a change in frequency of the sensor. In fact, an increase in mass (through adsorption) manifests itself through a decrease in frequency (see ***Figure 3.12.1***).

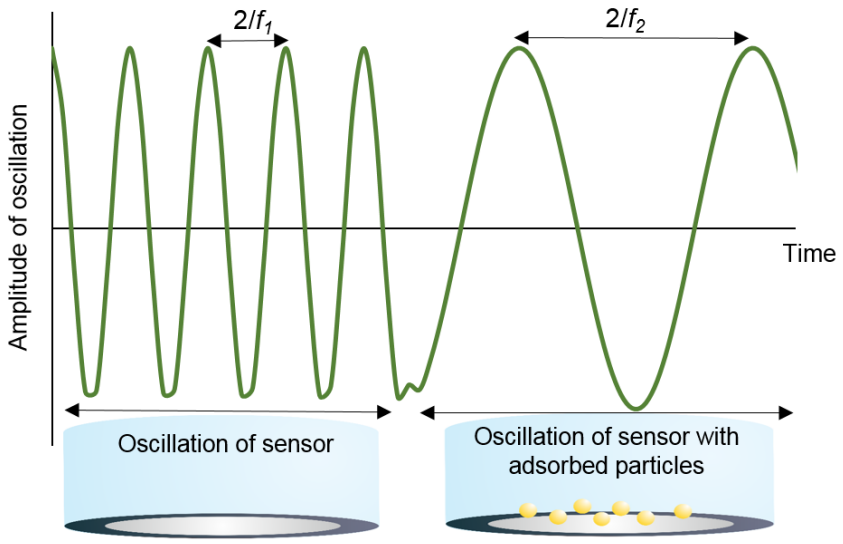

Figure 3.12.1: *Illustration of the change in frequency of oscillation of a sensor due to the adsorption of particles.*

Sauerbrey further showed that the crystal vibration only occurs in the area of overlap of the electrodes (which is termed the active area of the crystal) and that it decreases along a Gaussian curve radially from the center (see ***Figure 3.12.2***).[155]

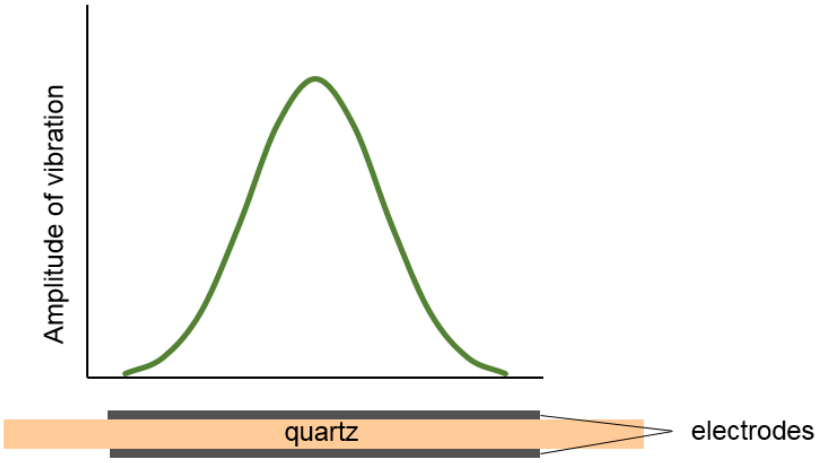

Figure 3.12.2: *Schematic representation of the decrease of the amplitude of vibration radially outwards from the center of the quartz.*

Another important aspect of QCMD measurements is the determination of the dissipation factor *D* which is defined by

$$D = \frac{E_{dissipated}}{2\pi E_{stored}}$$

With $E_{dissipated}$ and E_{stored} the energy dissipated and stored during one period of oscillation of the quartz, respectively. D regroups all causes for dissipation of energy in the system, particularly losses from a viscous behavior of the adsorbed layer. It can be determined from the decay rate of the oscillation after the excitation current has been switched off. In practice, this means that a current is applied to excite the sensor into oscillation, and when the current is switched off, the response of the system (meaning the decay of the oscillation) is measured. The resulting oscillation curve can be seen in ***Figure 3.12.3***. The higher the dissipation, the faster the signal decay.

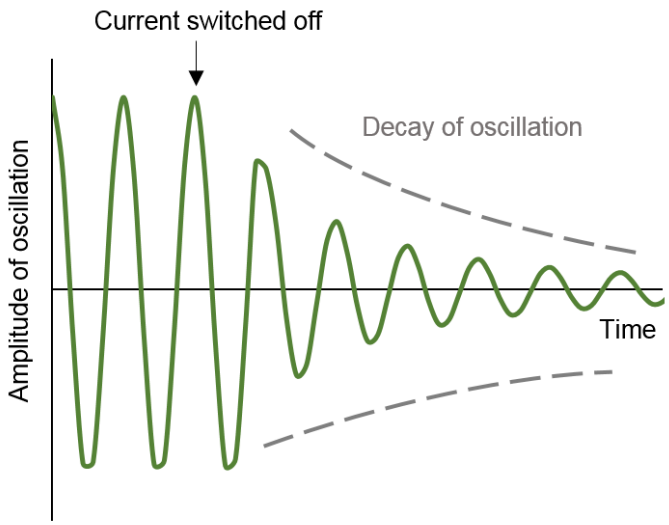

Figure 3.12.3: *Illustration of the evolution of the amplitude of oscillation upon switching off of the current. This method is used to determine the dissipation of the system: the faster the decay of the system, the higher the dissipation.*

In this work, QCMD was used to compare the affinities of the functionalized dispersions for the surfaces in question, *i.e.* stainless steel and hydroxyapatite. The respective QCMD sensors are commercially available and of highly reproducible surface composition and morphology. Unfortunately, to our knowledge, there are no QCMD sensors currently available which mimic the hair surface.

3.6. Differential scanning calorimetry[156, 157]

Differential scanning calorimetry (DSC) is a technique for measuring the thermal properties of a sample and changes thereof as a function of time and temperature. Two general types of DSC exist, namely heat-flux DSC and power-compensated DSC. Only the former will be explained because it is the method used in this work. The analyte is placed in a pan and subjected to a temperature protocol (heating/cooling) in parallel to an empty reference pan under adiabatic conditions. Both pans are placed on the same thermoelectric disk equipped with a furnace in order to ensure a uniform heating or cooling. The pans are thus heated indirectly through the disk and thereby experience a linear heating rate. Due to differences in heat capacity of the sample and of the empty reference pan, a change in temperature would result which can be detected by area thermocouples. From this, differences in heat flow can be deduced by using a relation reminiscent of Ohm's law

$$Q = \Delta T/R$$

with Q the heat flow of the sample, ΔT the temperature discrepancy between the sample and the reference, and R the resistance of the thermoelectric disk.

Differences in heat flow may occur due to various phenomena, for instance due to chemical reactions, and in particular due to phase transitions such as melting or crystallization. Recording changes in heat flow as a function of time when the sample is heated linearly can therefore be translated directly to changes in heat flow as a function of temperature. For polymers specifically, depending on the heating rate used (commonly 2 K/min – 10 K/min), precise measurements of melting temperature ranges, glass transition temperatures, *etc.* can be conducted using DSC. Melting is a so-called first order transition, *i.e.* it is characterized by an abrupt change in fundamental thermodynamic properties. In practice, melting is represented by an endothermic peak in the DSC diagram giving the heat flow as a function of temperature. A glass transition, on the other hand, is a second order transition because it is characterized by an abrupt change in heat capacity of the sample. In a DSC diagram, glass transitions are therefore detected as baseline shifts. In this work, DSC was used in order to detect melting of the partially crystalline PUs and to observe changes therein due to the different functionalizations conducted.

4. Results and Discussion

This chapter regroups the results from the three functionalization projects. Section 4.1 illustrates the synthesis of peptide-decorated PUDs for adhesion to hair and fibers, section 4.2 explains the specific coupling of peptides for adhesion to stainless steel, and section 4.3 is about the phosphonic acid-functionalization of PUDs for adhesion to ceramic and metallic surfaces.

4.1. Unspecific coupling of a hydrolyzed protein to PUDs for adhesion to hair*

4.1.1. Introduction and aim of the project

The first project of the thesis concerns the synthesis of peptide-decorated PUDs in a simple and cost-efficient manner in order to generate a system which may later serve for textile or hair care applications. As explained in the theoretical background chapter (section 2.6.1), natural polymers such as proteins or polysaccharides have been investigated for avoiding or repairing damage inflicted to the hair. In this context, it has been demonstrated that some compounds are capable of attaching to the hair surface, providing a protective superficial layer.[103, 104] In particular, it has been shown that keratin hydrolysates can be formulated into shampoos and rinse-off conditioners which are then integrated into the hair fiber and deposited at cuticle junctions.[105] The aim of this project is thus to try and combine those types of hydrolyzed proteins with PUDs and in order to fully exploit the vastness of possibilities in both PUD and peptide properties, a rather complex system was chosen.

On the one hand, a PU structure was designed which combines chemically dissimilar soft segment blocks to enrich the material microstructure and to obtain an adaptive material with temperature-response properties. We utilized poly(dimethylsiloxane) (PDMS) soft segments which possess a low interaction parameter and hence total incompatibility with the polyurethane hard segments and other soft segments.[159] The very low T_g of the PDMS segments further leads to a polymeric backbone structure with low activation energy for morphological changes. Furthermore, we incorporated polyester diols based on poly(tetramethylene adipate) (PTMA) with a strong tendency to crystallize.[160] The corresponding polymeric materials are able to undergo a soft segment crystallization, which is a well-known mechanism of physical crosslinking for reinforcement of polyurethane films (see section 2.5).[45, 70]

*This section is based on the publication "Polyurethane Dispersions with Peptide Corona: Facile Synthesis of Stimuli-Responsive Dispersions and Films" by Laura Breucker, Susanne Schöttler, Katharina Landfester, and Andreas Taden, published in 2015 in *ACS Biomacromolecules*, volume 16 on pages 2418 to 2426.[158] Reprinted with permission. Copyright 2015 American Chemical Society.

On the other hand, a hydrolyzed protein from wool was used as natural counterpart. Traditional routes of peptide synthesis yield monodisperse macromolecules, but involve relatively tedious and costly synthetic steps, requiring large amounts of different solvents, and consuming a lot of energy. The method of obtaining mixtures of peptides through enzymatic cleavage or hydrolysis of naturally occurring proteins from wool, corn, soya, and so on is much more cost-efficient and thus particularly attractive industrially.[161, 162] Although they are not sequence-defined and show considerable molecular weight distributions, hydrolyzed proteins can still display desired properties such as amphiphilicity, stimuli-responsiveness, and pronounced interactions with certain molecules and interfaces.[105, 163] For the purpose of this study, a peptide mixture was used to serve as dispersion stabilizer and in order to introduce stimuli-responsiveness in dispersion through pH-triggered coagulation.

Presented below are thus PU-peptide hybrid particles which can be synthesized easily. During emulsification of the PU prepolymer in a hydrolyzed protein solution, attachment and adsorption of the peptides to the forming particles can be achieved simultaneously. Although covalent attachment could not be proven directly, a comparison of properties between hybrid particles consisting of a reactive prepolymer and those consisting of a nonreactive prepolymer show markedly divergent properties. In particular, a major focus of this work was stabilization of particles through the peptide component and sustained colloidal stability could only be achieved using reactive dispersions. The peptide corona surrounding the particles is hereby used to introduce particle repulsion and enable more specific interactions at the same time. The attached peptide chains can also be viewed as a multifunctional hard segment. Upon film formation, the biological hard segment influences the PU microstructure, affecting in particular the crystallization behavior of the films. We present a general approach to hybrid nanoparticles with hydrolyzed proteins, proceeding *via* a preliminary characterization of the hydrolyzed protein using isoelectric focusing. Consequently, laser diffraction is used to monitor long-term colloidal stability and the particle-water interface is characterized through a quantification of the unattached peptide. A pH-triggered coagulation of the particles in the same pH-range as can be observed for the hydrolyzed protein solution is demonstrated using titration experiments. The effect of the peptide segments on the film properties is shown using differential scanning calorimetry.

4.1.2. Characterization of the starting materials

As a first step, both the synthetic and the natural starting materials were characterized using different techniques such as sodium dodecyl sulfate polyacrylamide gel electrophoresis (SDS-PAGE)

and isoelectric focusing (IEF) for the hydrolyzed protein, and gel permeation chromatography (GPC) and endgroup titration for the macrodiols used in the PU synthesis. A detailed explanation of the experimental procedures and apparatuses can be found in section 6.2.

4.1.2.1. Characterization of the peptide mixture

The peptide mixture is derived from the keratin type I microfibrillar 48 kDa protein from wool, component (C-1), also known as low-sulfur keratin[164] (see section 2.6.1 for information on the general structure of hair fibers). For the present study, the presence of potentially reactive amino acid side chains in the peptide mixture is important and the latter was shown to comport hydroxyl, amino, guanidinyl, α- and ß-carboxyl groups, imidazolyl groups, thioether, indoyl, and phenolic hydroxyl groups.[165, 166]

SDS-PAGE of the mixture was conducted (see ***Figure 4.1.1***) to show a broad distribution of molecular weight fragments, as expected with this type of protein fragmentation.

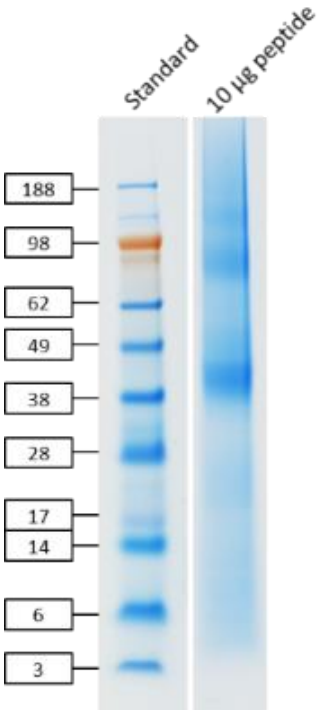

***Figure 4.1.1**: Results of SDS-PAGE analysis of the hydrolyzed protein, showing a broad distribution of molecular weight fractions. Noticeably, slightly smaller fractions than the native protein (of 48 kDa) were detected. The presence of a wide variety of molecular weight species is expected due to the hydrolysis; distinct bands can commonly only be observed in the case of enzymatic degradation.*
This figure is reproduced from the publication "Polyurethane Dispersions with Peptide Corona: Facile Synthesis of Stimuli-

Responsive Dispersions and Films" by Laura Breucker, Susanne Schöttler, Katharina Landfester, and Andreas Taden, published in 2015 in ACS Biomacromolecules*, volume 16 on pages 2418 to 2426.*[158] *Reprinted with permission. Copyright 2015 American Chemical Society.*

In order to maximize the reactivity of the different amino acid moieties present in the peptide mixture towards the NCO endgroups in the PU, the peptide was also analyzed using IEF. IEF is a type of electrophoretic method useful for separating peptides and proteins based on their isoelectric point (IP). Generally, the peptide solution is distributed over an immobilized pH gradient gel. Due to the fact that peptides are charged at any pH different from their IP, the application of an electric current causes the peptides to move to the spot on the gel at which they are not charged, *i.e.* to their IP. Fragments with IPs of 3.9, 6.0, and fragments with IPs between 4.2 and 4.8 were identified. In order to ensure that a large quantity of residues was available to react with the NCO endgroups in the polymer and to favor this reaction over hydrolysis, a pH well above the highest IP in the peptide mixture was chosen for the dispersion solution, *i.e.* a pH of 6.5 to 6.8. These pH values were reached when the hydrolyzed protein was dissolved in water such that no additional acid or base was added.

4.1.2.2. Characterization of the macrodiols

GPC and endgroup analyses were used in order to allow for an accurate determination of molecular weights of the macrodiols used in the PU synthesis and results thereof are displayed in ***Figure 4.1.2***. The molecular weights from endgroup analysis were used for subsequent calculations (see section 6.2.1 for details).

a)

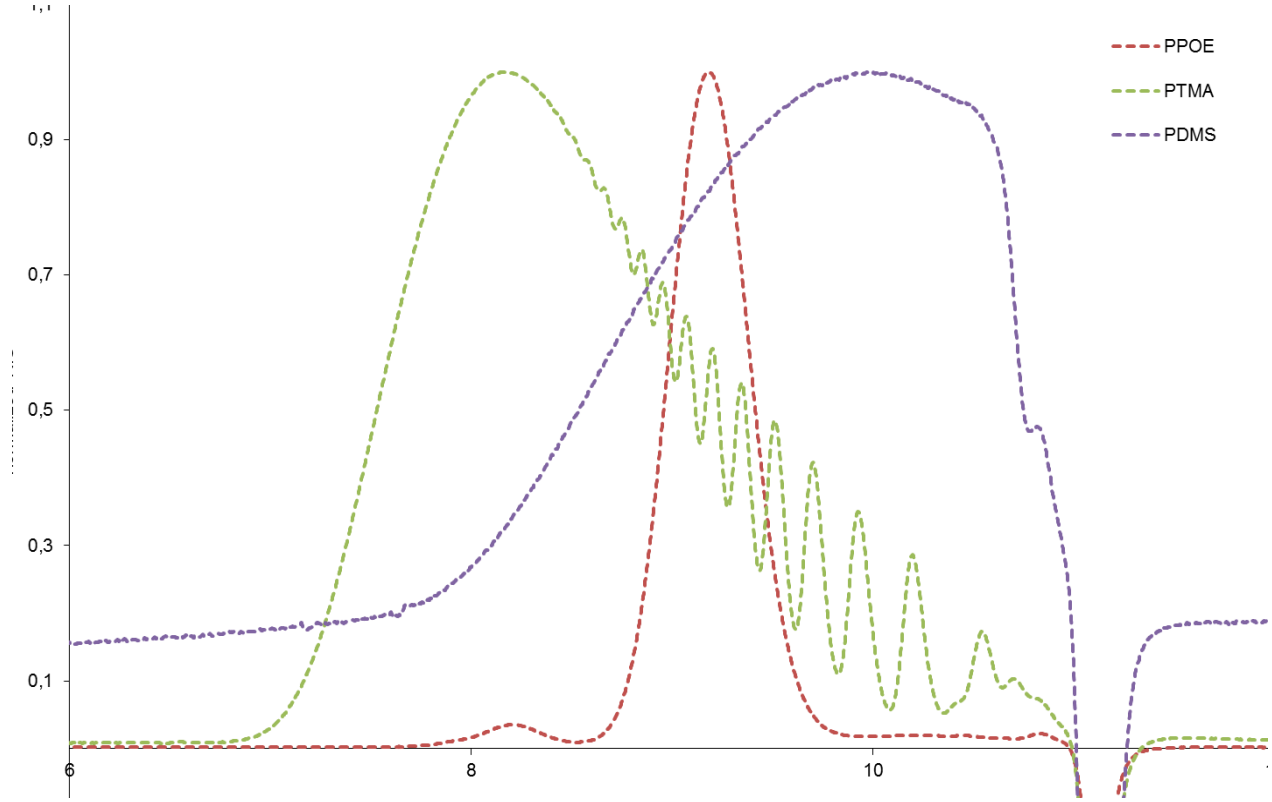

b)

Polymer	GPC		endgroup analysis[1]
	M_n (g/mol)	PDI	M_n (g/mol)
PPOE	2600	1.2	2200
PTMA	2700	2.1	2100
PDMS	1300	1.8	2200

1) Hydroxyl titration according to DIN 53240

***Figure 4.1.2**: Characterization of macrodiols using GPC and hydroxyl titration according to DIN 53240. a) GPC elution diagram overlay of the three macrodiols used in the synthesis, i.e. poly(oxypropylene, oxyethylene) (PPOE) (red dotted line), PTMA (green dotted line), and PDMS (purple dotted line). GPC was carried out in tetrahydrofuran (THF) against a polystyrene standard. b) Table showing the number-average molecular weights (M_n) and PDI as determined by GPC and endgroup analyses. Due to the fact that GPC-derived molecular weights are relative values which depend on many factors (solubility in the solvent used, similarity in structure to the standard, etc.), results from endgroup analysis were deemed more appropriate to be taken as basis for theoretical calculations. This figure is reproduced from the publication "Polyurethane Dispersions with Peptide Corona: Facile Synthesis of Stimuli-Responsive Dispersions and Films" by Laura Breucker, Susanne Schöttler, Katharina Landfester, and*

Andreas Taden, published in 2015 in ACS Biomacromolecules, *volume 16 on pages 2418 to 2426.*[158] *Reprinted with permission. Copyright 2015 American Chemical Society.*

4.1.3. Method

The general synthesis route employed is shown below (***Figure 4.1.4***). A linear PU prepolymer with a calculated M_n of 8 000 g/mol was synthesized and the polymerization was monitored by isocyanate endgroup titration (according to ISO 14896:2009-07 Method A, see section 3.1 for details). The obtained, so-called reactive prepolymer was also characterized by nuclear magnetic resonance (NMR) spectroscopy in order to demonstrate the presence of urethane links and to show the absence of urea links. The NMR spectrum is shown in ***Figure 4.1.3***. Signals at δ = 121-122 ppm can be attributed to the presence of residual NCO.[167] The signal at δ = 174 ppm stems from the carbonyl of the polyester. The two double peaks detected at δ = 155.8-157.2 ppm can be attributed to urethane links with the double peak at lower chemical shift originating from the secondary urethanes and the one at higher chemical shift stemming from the primary urethane. The chemical shift values are in good agreement with results found in the literature.[167-169] The splitting is most likely due to the detection of *cis*/*trans* conformations thanks to the high measurement frequency (600 MHz). Urea links were not detected and would appear at slightly higher chemical shift than urethane links (δ = 157.9-158.8 ppm).[168]

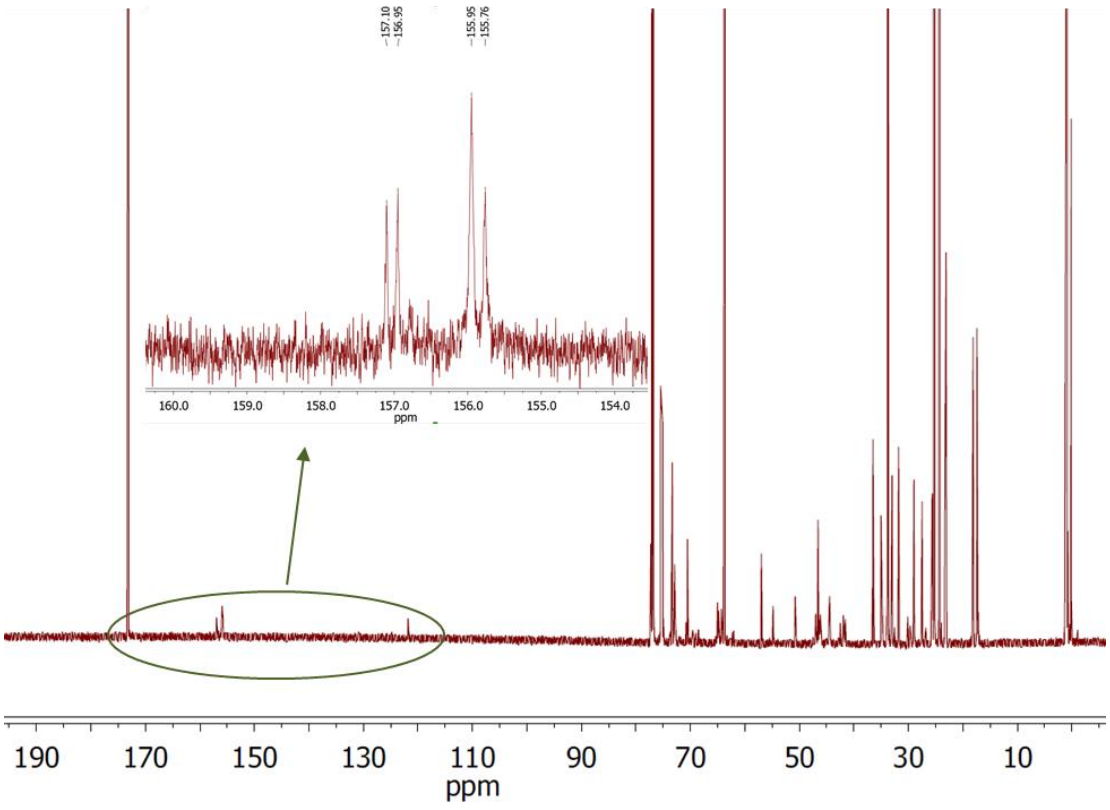

Figure 4.1.3: *^{13}C NMR spectrum of the reactive PU prepolymer to investigate the presence of urea links in the polymer.* *This figure is reproduced from the publication "Polyurethane Dispersions with Peptide Corona: Facile Synthesis of Stimuli-Responsive Dispersions and Films" by Laura Breucker, Susanne Schöttler, Katharina Landfester, and Andreas Taden, published in 2015 in* ACS Biomacromolecules, *volume 16 on pages 2418 to 2426.*[158] *Reprinted with permission. Copyright 2015 American Chemical Society.*

The prepolymer was then dissolved in ethyl acetate and dispersed in different concentrations of the peptide (0 wt%, 4 wt%, 6 wt%, and 8 wt%) with regard to the prepolymer. The amount of continuous phase was chosen such that after dispersion, the initial concentration of NCO functional groups in the system was 0.175 wt%. A nonreactive PU prepolymer was synthesized alongside the reactive one (by simply reacting the residual NCO groups with DBA prior to emulsification), in order to investigate the importance of potential, covalent peptide attachment.

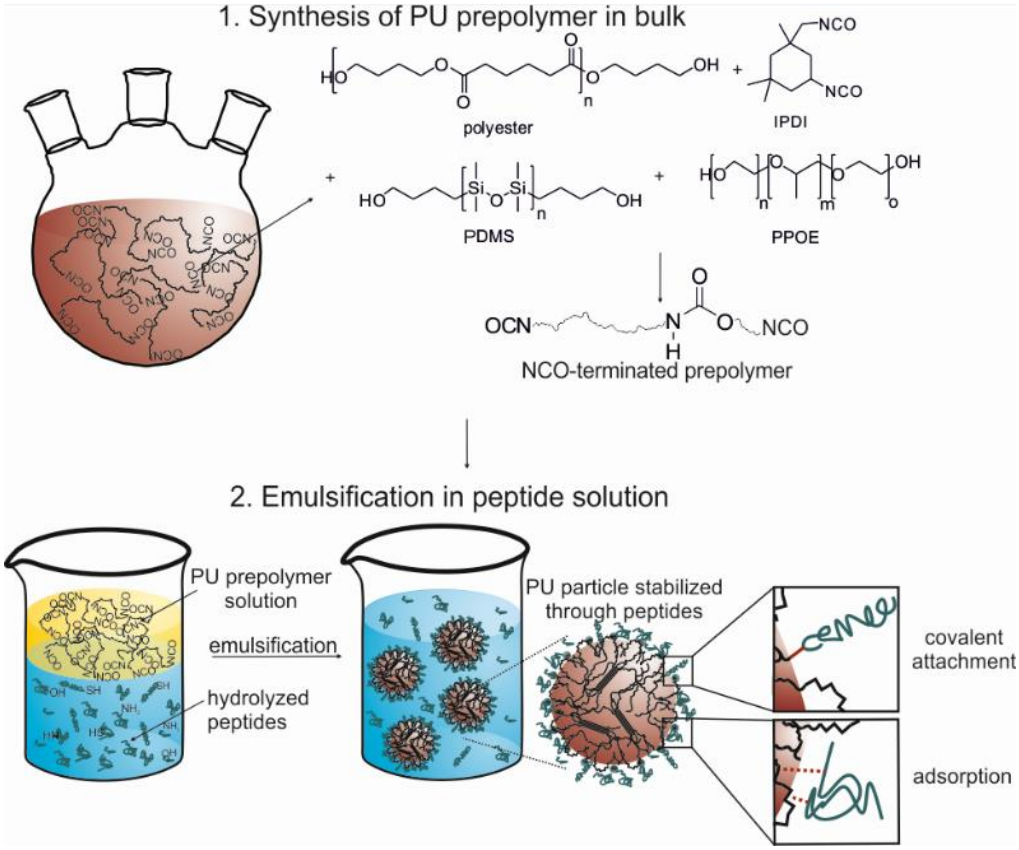

Figure 4.1.4: *General synthesis scheme showing as a first step the synthesis of the PU prepolymer in bulk, followed by the emulsification of the latter in a peptide solution to obtain peptide-decorated PUDs.* *This figure is reproduced from the publication "Polyurethane Dispersions with Peptide Corona: Facile Synthesis of Stimuli-Responsive Dispersions and Films" by Laura Breucker, Susanne Schöttler, Katharina Landfester, and Andreas Taden, published in 2015 in* ACS Biomacromolecules, *volume 16 on pages 2418 to 2426.*[158] *Reprinted with permission. Copyright 2015 American Chemical Society.*

The FTIR spectrum of the endcap reaction is shown below (***Figure 4.1.5***). The disappearance of the NCO band at 2300 cm^{-1} indicates the complete reaction of the terminal NCO groups.

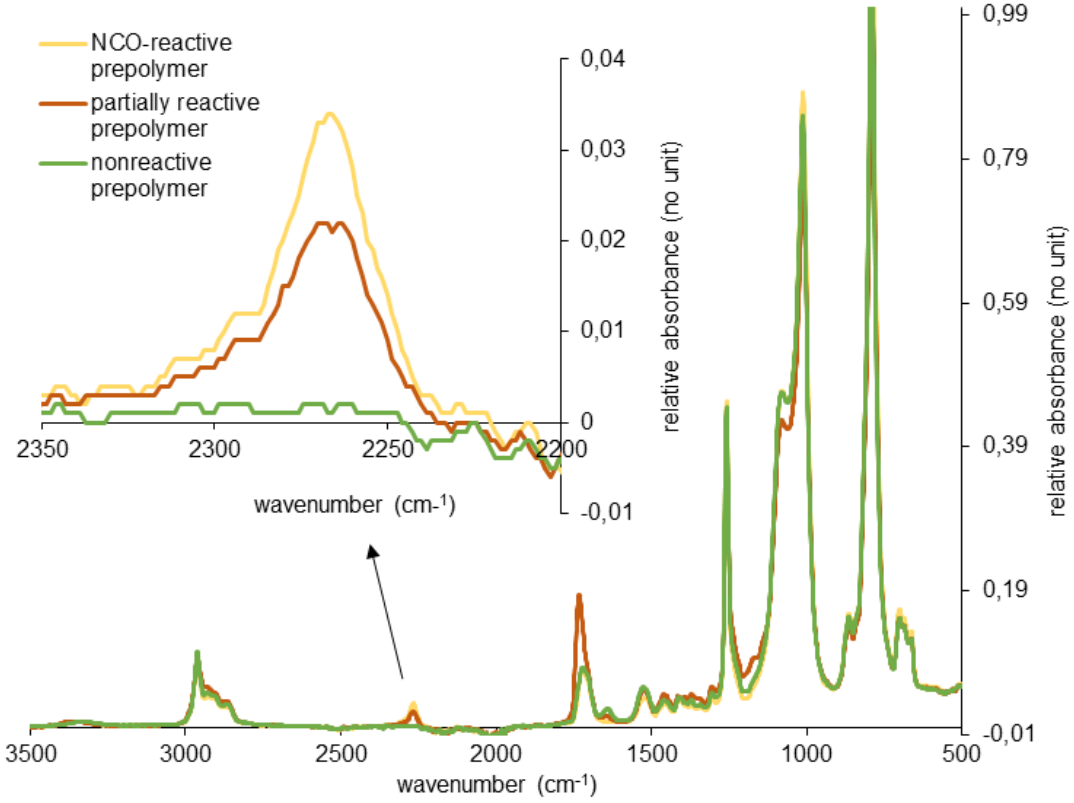

***Figure 4.1.5**: FTIR spectroscopy graphs of the prepolymer during the endcap reaction with DBA. The green line shows the absence of NCO groups in fully endcapped prepolymer (termed "nonreactive prepolymer"). This figure is reproduced from the publication "Polyurethane Dispersions with Peptide Corona: Facile Synthesis of Stimuli-Responsive Dispersions and Films" by Laura Breucker, Susanne Schöttler, Katharina Landfester, and Andreas Taden, published in 2015 in* ACS Biomacromolecules*, volume 16 on pages 2418 to 2426.[158] Reprinted with permission. Copyright 2015 American Chemical Society.*

4.1.4. Peptide-stabilization of particles

Commonly, PUDs are designed as self-stabilizing ionomers.[170] Self-stabilization in water is most often achieved *via* the incorporation of ionic polyols like dimethylolpropionic acid (DMPA) or sulfated/sulfonated segments which induce repulsive electrostatic interactions. PUDs obtained from quarternization with methyl iodide are also known.[171] In our approach, we have purposefully neither incorporated ionic polyols, nor utilized any external synthetic surfactant in order to attempt stabilizing PUDs in another way. It is known in the literature that proteins and peptides can be used

as stabilizers for emulsions, and hence are of high interest for food science and pharmaceutics.[172, 173] However, they typically do not serve as multifunctional building blocks. For investigating the stabilization through peptide attachment, particle stability overtime was studied using LD. For comparison, the NCO-reactive prepolymer and the non-reactive prepolymer were both used for monitoring. Measurements were carried out every week over the course of 1 month and results are displayed in ***Figure 4.1.6***.

We can first note that the 8 wt% sample of the reactive dispersion possesses an average particle size of 290 nm and a narrow size distribution. No changes in particle size distribution could be measured over the course of one month, indicating sustained long-time stability. Particles synthesized with less peptide, on the other hand, showed broader size distributions as well as significant coagulation occurring after one week. Strikingly, the nonreactive dispersions all show poorer particle stability than the reactive ones. In particular, even for the 8 wt% sample of the nonreactive dispersions, larger particle sizes were measured as early on as one week after synthesis. This observation is most likely due to the dynamic nature of the interface: peptides adsorb and desorb reversibly, leaving the particle surface “unguarded” for short periods of time and thereby allowing for coagulation to occur. The fact that particle stability is consistently enhanced for the reactive dispersions suggests that in this case, peptide desorption is inhibited through covalent attachment.

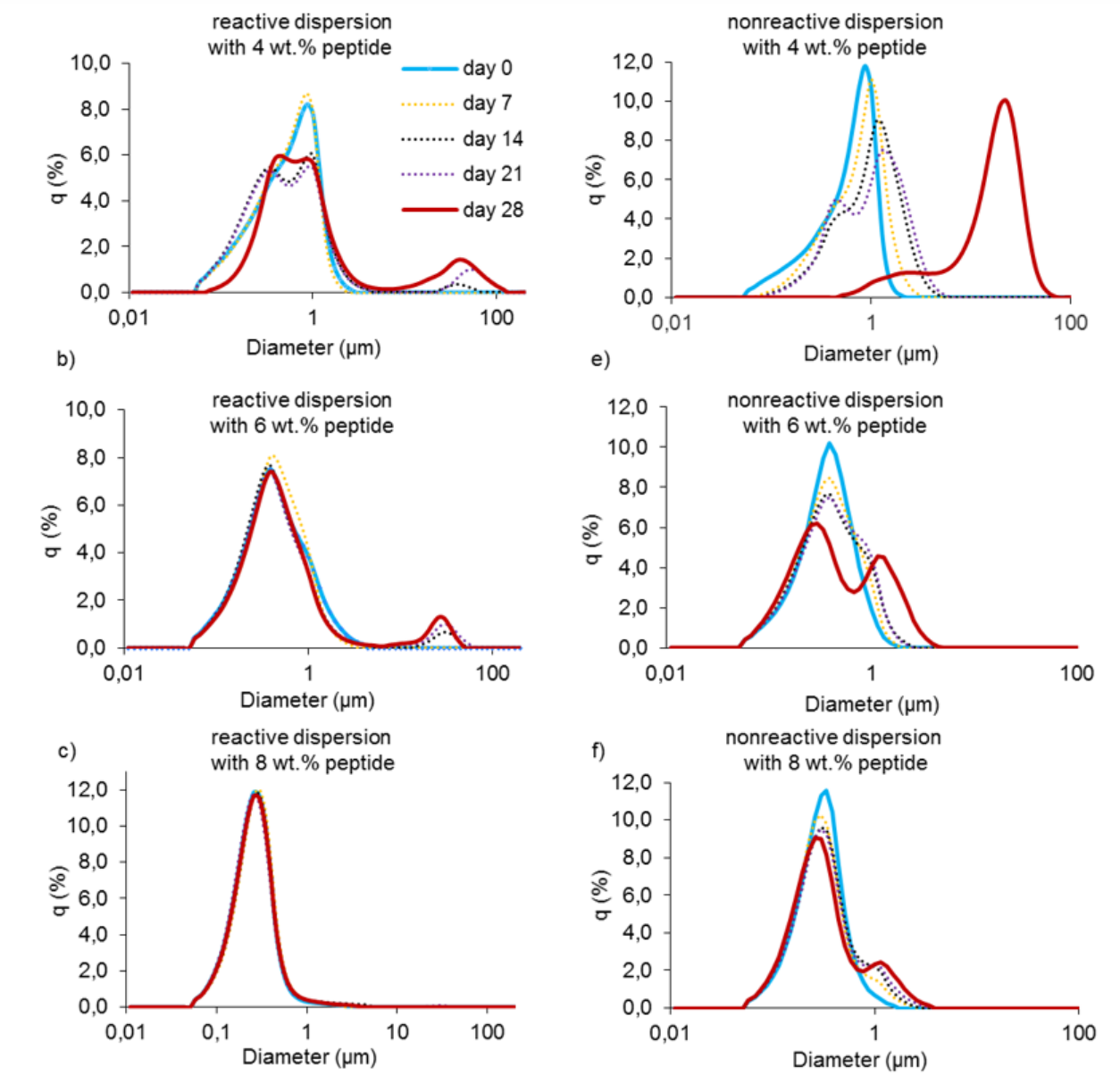

***Figure 4.1.6**: LD measurements of PUDs synthesized with 4 wt%, 6 wt% or 8 wt% peptide using a reactive prepolymer (a-c) or a nonreactive one (d-f). The legend in a) applies to all graphs. Measurements were carried out every week for 1 month and show the average of 3 individual measurements. Particles of small size (about 290 nm) could be synthesized which remained perfectly stable for over 1 month using a reactive prepolymer emulsified in 8 wt% aqueous peptide solution.* *This figure is reproduced from the publication "Polyurethane Dispersions with Peptide Corona: Facile Synthesis of Stimuli-Responsive Dispersions and Films" by Laura Breucker, Susanne Schöttler, Katharina Landfester, and Andreas Taden, published in 2015 in* ACS Biomacromolecules, *volume 16 on pages 2418 to 2426.*[158] *Reprinted with permission. Copyright 2015 American Chemical Society.*

It can also be noted that a removal of peptide, for instance through dialysis (see section 6.2.6), leads to slight sedimentation. This can be attributed to the critical stabilization of the particles, which is a well-known aspect of nanoparticles synthesized by the miniemulsion process.[174] While particle formation takes place, the high sheer forces applied lead to the arrangement of the stabilizing molecules (the hydrolyzed protein in this case) to stabilize a maximum surface area. If less peptide is used in the synthesis, as discussed above, particle stability is decreased. A posterior removal of peptide has a similar effect.

We thus found that stable PUDs could be synthesized from a reactive PU prepolymer with 8 wt% peptide.

4.1.5. Quantification of the attached peptide

For both the reactive and the nonreactive dispersions, we also investigated how much of the added peptide interacted with the particles. Extensive dialysis was performed against deionized water and the dialysis water batches were analyzed using the BCA. This assay relies on the biuret reaction between a peptide with alkaline Cu^{2+} to give a purple complex. It has been shown that the intensity of the complex increases linearly with the amount of peptide present[147] (see section 3.1.4.1). A solution of the peptide was subjected to the same treatment to show that over the course of the dialysis time, all of it passed the membrane and could be detected using the BCA.

Figure 4.1.7 shows the results of the BCA for both the reactive and the nonreactive dispersions, *i.e.* how much peptide was flushed out during dialysis at different points in time. Values represent averages of three independent dialysis experiments and error bars represent the standard deviation. It can be seen that the sample with the highest peptide content of 8 wt% also consistently shows the highest fluorescence intensity in the dialysis water. Furthermore, for all six samples, a plateau is reached at the end of the dialysis time span which shows that the system has reached a stable state at that point, *i.e.* all peptides that were either free in solution or merely weakly adsorbed have been dialyzed out. In sum, the total amount of attached peptide relative to the total amount added for the reactive dispersions ranges from 92% ± 4% to 75% ± 2% to 73% ± 1% as the amount of peptide added increases, indicating that in all three cases, a large quantity of the added peptide was attached.

The same general trend and conclusion can be drawn for the results of the BCA for the nonreactive dispersion. The amount of peptide dialyzed out increases with the initial peptide content of the dispersions. However, it can clearly be seen that the amount of unattached peptide is constantly higher in case of the nonreactive dispersions as compared to the reactive ones. Furthermore, the

total amount of peptide which is attached to the dispersions is significantly lower for the nonreactive dispersions, ranging from 70% ± 3% to 69% ± 2% to 67% ± 1% as the quantity of peptide added increases (average values and standard deviation from three independent dialysis experiments). The differences between the reactive and the nonreactive dispersions may appear small in view of the number of possible nucleophilic groups in the peptide. A plausible explanation can be given by the conformation-related, reduced reactivity of endogenous amino acids. In addition to the protonation state, steric effects strongly affect the chemical modification of peptides *via* their nucleophilic sites and typically require the presence of third parties such as transition metals or enzymes, *etc.*.[175, 176] In this case in which a mixture of peptide components of unknown sequence is used, a more thorough analysis of possible conjugation mechanisms would be necessary to draw exact conclusions with regard to the covalent attachment. However, taking into consideration the results of the dialysis experiments, we can observe that the trends shown are again indicative of the covalent attachment of the peptide to the reactive dispersions.

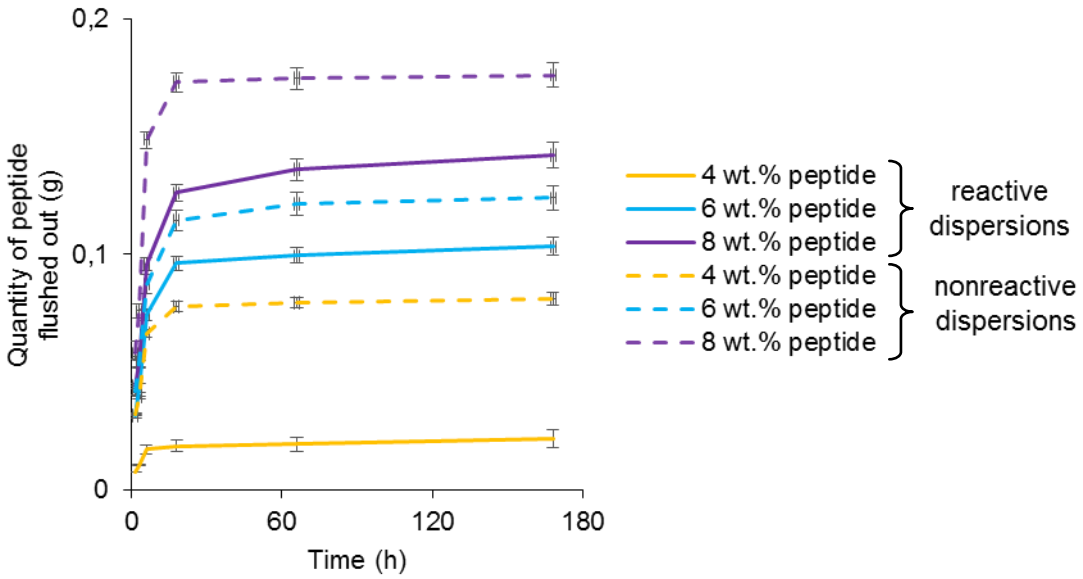

***Figure 4.1.7**: Results of the BCA for the reactive and the nonreactive dispersions. Variation of the quantity of peptide flushed out with dialysis time. Values represent averages of three independent dialysis experiments and error bars represent the standard deviation.* *This figure is reproduced from the publication "Polyurethane Dispersions with Peptide Corona: Facile Synthesis of Stimuli-Responsive Dispersions and Films" by Laura Breucker, Susanne Schöttler, Katharina Landfester, and Andreas Taden, published in 2015 in* ACS Biomacromolecules, *volume 16 on pages 2418 to 2426.*[158] *Reprinted with permission. Copyright 2015 American Chemical Society.*

It may be supposed that changing the conditions of dialysis (most importantly the pH) may alter the results of the BCA. However, we performed a control experiment in which a reactive dispersion emulsified at pH 7 in 8 wt% peptide was dialyzed in parallel at pH 7 and at pH 10 (see ***Figure 4.1.8***) and it was found that only a small increase in the amount of peptide flushed out was detected.

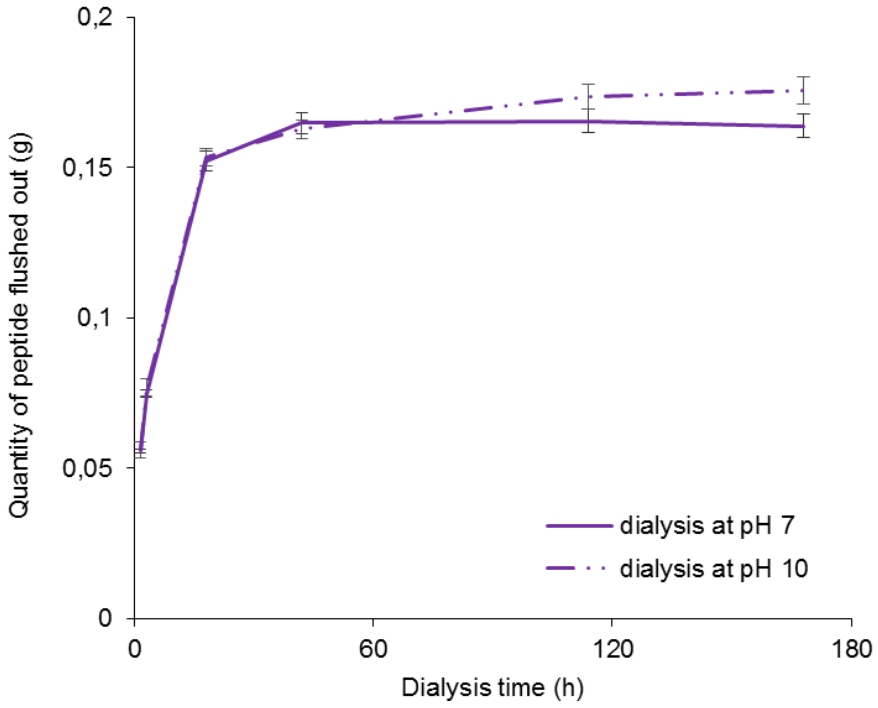

***Figure 4.1.8**: Results of the BCA for a reactive dispersions emulsified in an 8 wt% peptide solution and dialyzed at different pH for one week. Variation of the quantity of peptide flushed out with dialysis time. Values represent averages of three independent dialysis experiments and error bars represent the standard deviation. Results suggest that the effect of the elevated pH on the peptide solubility and hence on the dialysis is very small. This figure is reproduced from the publication "Polyurethane Dispersions with Peptide Corona: Facile Synthesis of Stimuli-Responsive Dispersions and Films" by Laura Breucker, Susanne Schöttler, Katharina Landfester, and Andreas Taden, published in 2015 in* ACS Biomacromolecules*, volume 16 on pages 2418 to 2426.[158] Reprinted with permission. Copyright 2015 American Chemical Society.*

In addition, the amino acid compositions of the initial hydrolyzed protein and of the unattached peptides were determined. See ***Figure 4.1.9*** for details. However, a detailed analysis is not presented here due to inherent limitations to the technique, in particular regarding the detection of cysteine.

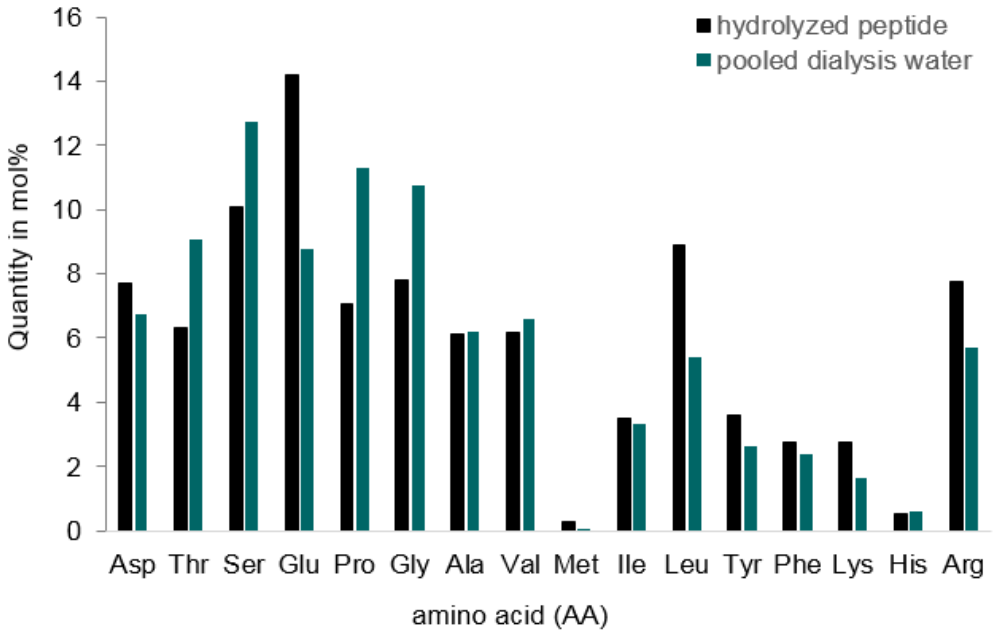

***Figure 4.1.9**: Amino acid profiles of the hydrolyzed peptide and of the pooled dialysis water from the 8 wt% peptide sample. Results are displayed in mol% relative to the total amount of amino acids found.* *This figure is reproduced from the publication "Polyurethane Dispersions with Peptide Corona: Facile Synthesis of Stimuli-Responsive Dispersions and Films" by Laura Breucker, Susanne Schöttler, Katharina Landfester, and Andreas Taden, published in 2015 in* ACS Biomacromolecules, *volume 16 on pages 2418 to 2426.*[158] *Reprinted with permission. Copyright 2015 American Chemical Society.*

4.1.6. Stimuli-responsive dispersions and films

Surface functionalization with and stabilization through the peptide component might also confer an additional property to the dispersions: by using stimuli-responsive peptides which undergo conformational changes through a slight change in pH, temperature, ionic strength, *etc.*, one might be able to transfer this responsiveness to the particles. Here, our intention was to show that the anionic stabilization can be bestowed by the peptides when using a mixture of peptides with low IPs. Thus, the zeta potential of the particles from reactive and nonreactive dispersions after dialysis were measured. Indeed, the measured ZPs of all peptide-containing samples ranged from -28 mV to -38 mV, with no significant differences between reactive and nonreactive dispersions. The colloidally completely unstable particles without peptides are virtually uncharged with a zeta potential of 1 mV (measurement directly after emulsification, accompanied by partial coagulation and precipitation; afterwards, complete phase separation). In addition to characterizing the dispersions in the way of their stabilization, stability, and morphology, titration experiments of the dispersions

after dialysis were performed and results thereof for the 8 wt% sample are displayed in ***Figure 4.1.10***. The pH value and the turbidity of the dispersions were measured while titrating with an acid or a base. It was observed that in basic conditions, the dispersion remained turbid and thus stable throughout the measurement. When titrating with an acid, however, coagulation occurred abruptly as the pH dropped below 5.5. It was therefore concluded that even a slight change in pH suffices in order to trigger a destabilization of the particles. The pH-induced destabilization is probably the simplest experiment to demonstrate that stimuli-response properties originating from the biological component were successfully transferred to the otherwise long-term stable peptide-PUDs and this in fact is a very interesting feature for many applications.

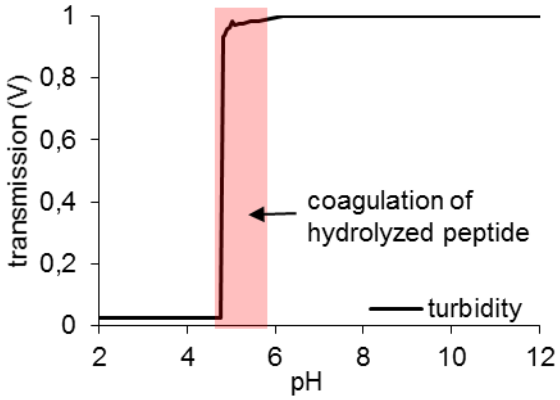

Figure 4.1.10**: Results of titration experiments of the 8 wt% peptide reactive dispersion after dialysis. Turbidity of the dispersion is displayed as a function of the pH. It can be seen that a pH change below 5.5 leads to an abrupt destabilization of the dispersions. This figure is reproduced from the publication "Polyurethane Dispersions with Peptide Corona: Facile Synthesis of Stimuli-Responsive Dispersions and Films" by Laura Breucker, Susanne Schöttler, Katharina Landfester, and Andreas Taden, published in 2015 in* ACS Biomacromolecules*, volume 16 on pages 2418 to 2426.[158] Reprinted with permission. Copyright 2015 American Chemical Society.*In order to elucidate the thermal properties of the peptide-decorated dispersions, DSC measurements of their respective films were carried out with a heating rate of 10 K/min. The heating rate was chosen in order to visualize possible polymorphism and microstructure variances and is too fast to progressively drive formation of the thermodynamically preferred α-form crystals of PTMA segments during the measurement.[45, 46] Prior to this, the films were subjected to a heating and cooling protocol (see section 6.2.14) in order to ensure a uniform thermal history. ***Figure 4.1.11 shows the heat flow as a function of temperature. It can first be noted that the peptide (green curve) does not show any type of crystallinity. The prepolymer possesses the most pronounced and the narrowest melting peak (with a T_m of 50 °C), which can be explained by the fact that the short PU prepolymer chains have the highest mobility in the film. Correspondingly, a relatively high degree

of crystallization can be achieved and the crystallites formed are more uniform, have fewer defects and a high melting point regime.

For the three nonreactive, peptide-containing dispersions (dashed yellow, blue and purple lines), the displayed melting behavior is very similar. A single melting peak is observed which occurs in the same temperature range as for the nonreactive prepolymer. The melting enthalpy is reduced (ranging from 11.5 J/g to 10 J/g), indicating a lower degree of crystallinity caused by the presence of the peptides. Those two facts indicate that a high degree of phase separation seems to occur between the peptides and the PTMA segments of the polymer. As a result, the crystallization still proceeds in the same way, but leads to the formation of fewer crystallites.

In contrast, for the three reactive samples dispersed in peptide solution (solid yellow, blue or purple lines), similar heating curves are observed. In all cases, melting occurs over a very broad temperature range (between 35 °C and 45 °C) with a significantly reduced melting enthalpy which points to the formation of fewer and smaller crystallites. This is also indicated by the reduced melting enthalpies (ranging from 8.5 J/g to 7.5 J/g) with increasing quantity of peptide present during dispersion, which is again indicative of a covalent attachment of the peptides. A plausible explanation is that the peptides act as multifunctional chain extenders and lead to a branched or even locally crosslinked macromolecular structure that prevents the pronounced formation of crystalline structures of high order. However, it should be noted that in all cases, homogeneous films were obtained.

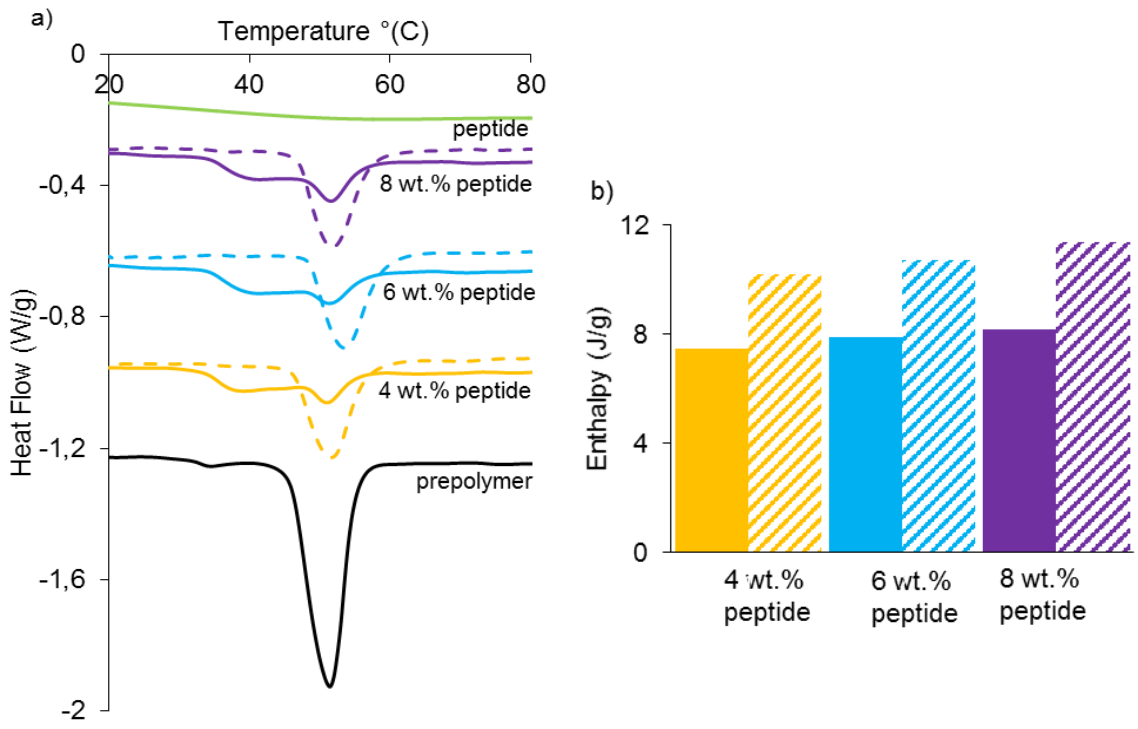

***Figure 4.1.11**: a) DSC results of the different samples showing the melting peak(s) of the crystalline domains within the PU. b) Comparison of melting enthalpies. The solid green line represents the pure peptide, the solid black line represents the nonreactive prepolymer. Solid yellow, blue and purple lines represent the reactive dispersions with 4 wt%, 6 wt%, and 8 wt% peptide, respectively, and the dashed lines and bars represent their nonreactive analogues. This figure is reproduced from the publication "Polyurethane Dispersions with Peptide Corona: Facile Synthesis of Stimuli-Responsive Dispersions and Films" by Laura Breucker, Susanne Schöttler, Katharina Landfester, and Andreas Taden, published in 2015 in* ACS Biomacromolecules*, volume 16 on pages 2418 to 2426.[158] Reprinted with permission. Copyright 2015 American Chemical Society.*

Furthermore, TEM was also conducted from highly diluted dispersions after drying and astonishingly revealed some highly crystalline areas (see ***Figure 4.1.12***). Both TEM images show selected areas where nucleation has taken place and other areas which appear amorphous. This phenomenon can be explained by an altered crystallization behavior in confined areas on the nanoscale particles, which especially in polymer systems requires strong undercooling.[78] Depending on the system, homogeneous and surface-catalyzed nucleation can occur in parallel, leading to the observed structures.

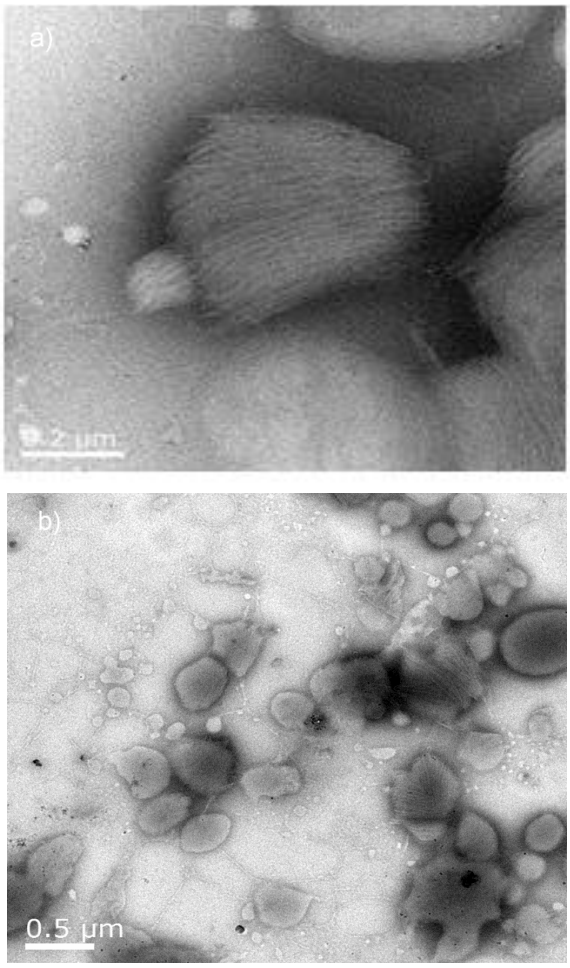

***Figure 4.1.12**: TEM images prepared from the PUD with 8 wt% peptide showing a) highly crystalline domains and b) general morphology of the particles. Images were kindly recorded by Ingo Lieberwirth.* *This figure is reproduced from the publication "Polyurethane Dispersions with Peptide Corona: Facile Synthesis of Stimuli-Responsive Dispersions and Films" by Laura Breucker, Susanne Schöttler, Katharina Landfester, and Andreas Taden, published in 2015 in* ACS Biomacromolecules, *volume 16 on pages 2418 to 2426.*[158] *Reprinted with permission. Copyright 2015 American Chemical Society.*

The reversible, temperature-induced transition from a semi-crystalline to an amorphous film and *vice versa* is of high importance for many applications, for example as physical setting mechanism for adhesives or other applications. In particular, the model system represented throughout this investigation could be used for hair care products, intended to form a film on the hair which is later curled or straightened through the application of heat.

4.1.7. Adhesion to hair

As mentioned above, the peptide-decorated PUDs described in this part of the work are intended to serve for hair care and textile applications. The hydrolyzed peptide used is derived from wool, so the peptide's primary structure resembles that of human hair and a favorable interaction with the hair surface is expected. In fact, the manufacturer claims that the smaller molecular weight fragments in the mixture penetrate into the hair fiber while the larger molecular weight fragments serve for film formation, thereby protecting the hair from external influences.[177] The PU, on the other hand, may protect the hair from heat damage and permit for shaping of the hair through partial crystallinity in the film. ***Figure 4.1.13*** shows how the dispersion may be applied to form a continuous, tough film with crystalline domains. Through the application of heat, the film becomes amorphous and hence flexible and can be used to give the hair a desired shape. Cooling then leads to recrystallization of the film and hence a retention of the hair shape.

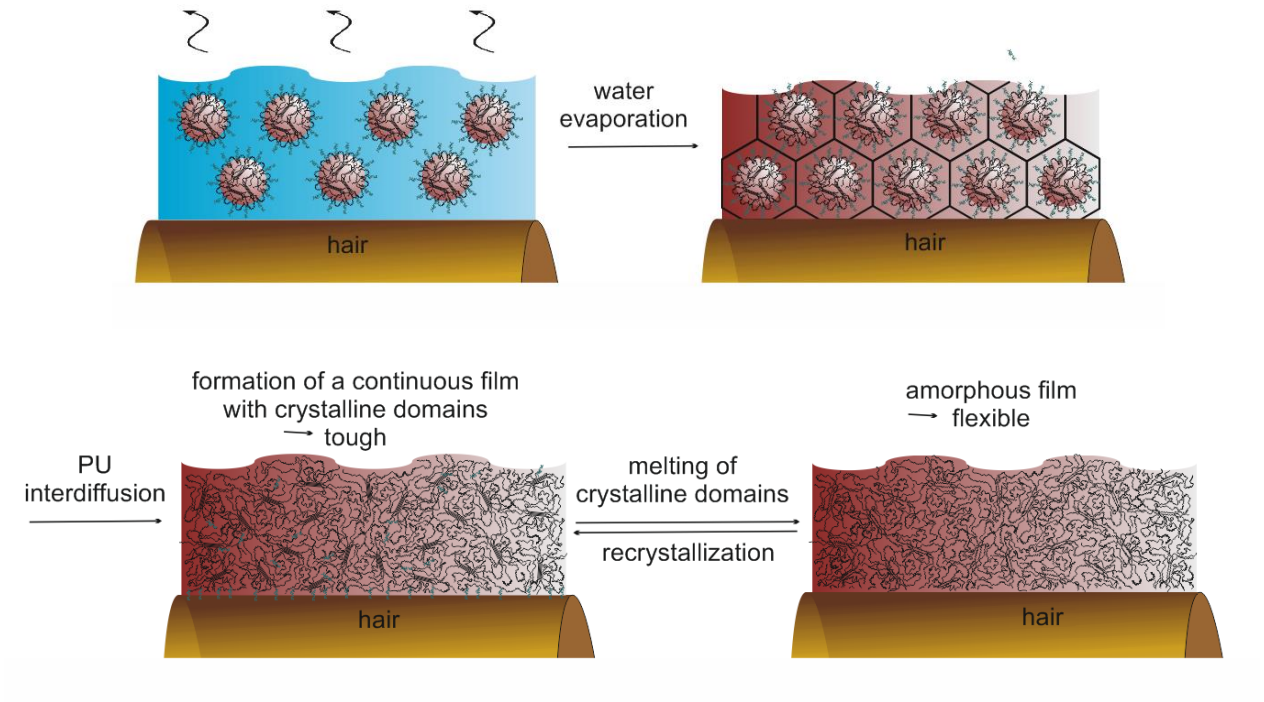

Figure 4.1.13: *Illustration of the use of peptide-decorated PUDs for hair applications. The peptide component provides a good affinity for the hair fiber and the partially crystalline PU can be used for shaping and smoothing of the hair and for heat protection.*

In order to obtain a qualitative assessment of the affinity of the dispersions for hair surfaces and to estimate the effect on the topology, we treated damaged (bleached) hair strands with the 8 wt%

reactive dispersion. ***Figure 4.1.14*** shows scanning electron microscopy (SEM) images in two magnifications of the untreated, bleached hair (left-hand column) and of the bleached hair treated with the dispersion (right-hand column). The observed surface structure of the bleached hair is rough with cuticle cells angled away from the core and partly chipping off due to the bleaching treatment. For the hair treated with the 8 wt% peptide reactive dispersion, the dispersion appears to have partly covered the hair surface, forming a smooth film on top of the cuticle cells. This first indication of the effect of the dispersion is a promising result for further hair care applications.

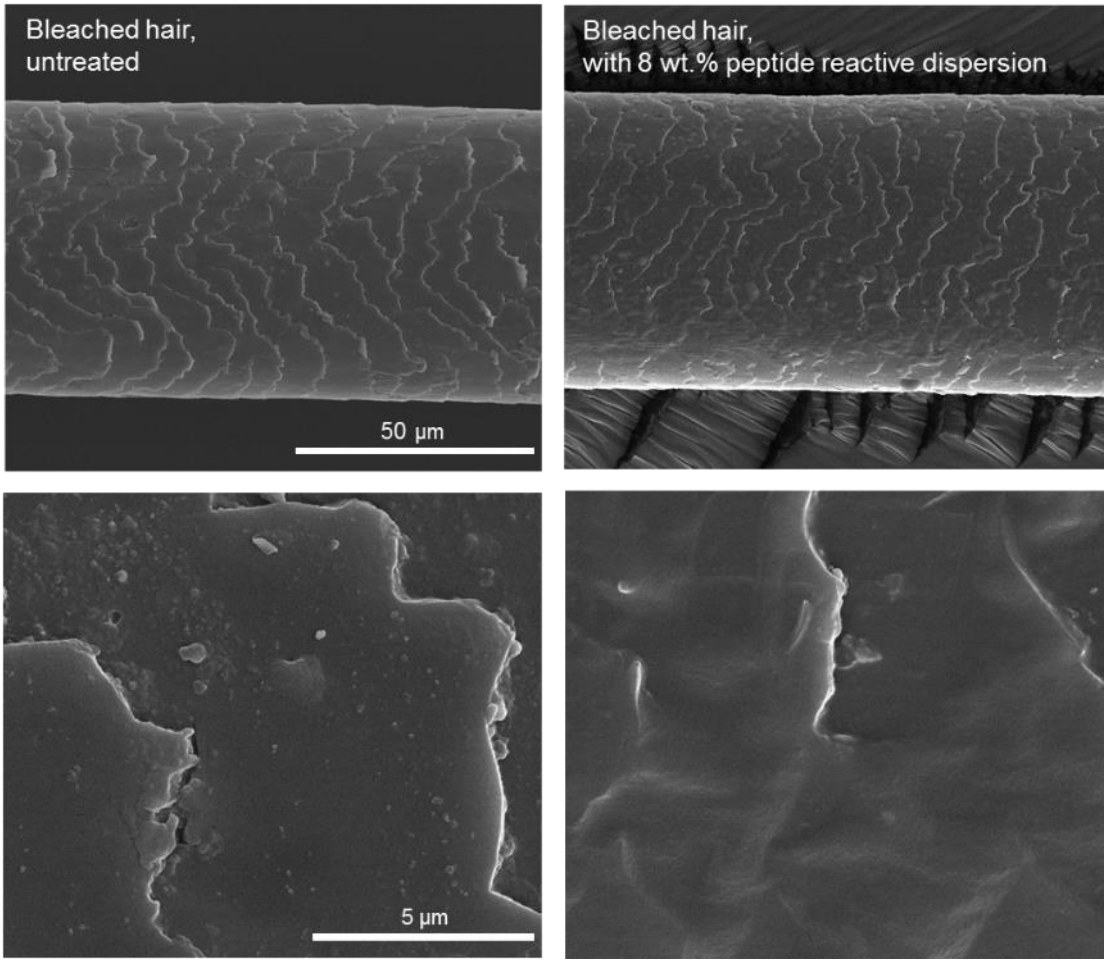

Figure 4.1.14*: SEM images of untreated, bleached hair (left-hand column) and of the same batch of bleached hair treated with the 8 wt% peptide reactive dispersion. Scale bars apply to each row. The dispersion forms a film on top of the damaged hair, smoothening its surface.*

4.1.8. Conclusions

In this section, we present a study on the synthesis of polyurethane dispersions with a peptide corona using a mixture of peptides from the hydrolysis of the intermediate filament protein from wool as model substance. Hybrid particles were obtained in a facile process by coupling of the peptides to previously synthesized NCO-functional polyurethane prepolymer chains during the emulsification step. The water-soluble peptide segments confer an electrostatic repulsion to the particles, rendering the use of charged chain segments for colloidal stabilization unnecessary. Unattached peptides can be separated from the dispersion by dialysis and were quantified using the bicinchoninic acid assay to show a high coupling efficiency. Properties of NCO-reactive dispersions are compared to nonreactive ones to suggest the effects of a covalent attachment of the peptides. The synthetic concept is highly malleable and allows for the use of various hard and soft segments to fully exploit the rich possibilities of PU chemistry. As an example, we combined two dissimilar soft segments in our model system, namely PDMS (low T_g, fully amorphous, highly flexible and strongly incompatible with other soft and hard segments), and PTMA polyester. The polyester leads to a crystallization tendency, which can be utilized as a reversible, physical crosslinking mechanism and can be triggered by temperature. In addition to colloidal stabilization and peptide-guided stimuli-response, the creation of a biopolymer corona also influenced the PU microstructure after film formation, causing a strongly modified crystallization behavior. We therefore propose to consider the peptides as multifunctional, biological hard segments, to emphasize the segmented structure and modular concept of these novel PU-bioconjugate structures. In general, our approach should furthermore also be suited for other water-soluble (bio)polymers carrying nucleophilic functionalities, *e.g.* certain polysaccharides. Due to the fact that hydrolyzed proteins are readily available and that polyurethane dispersions are already produced in large scale in the industry, we believe that the present study gives a valuable alternative to classically laborious and expensive routes for the synthesis of segmented bioconjugates and hybrid particle systems.

4.2. Specific coupling of peptides to PUDs for adhesion to steel

4.2.1. Introduction and aim of the project

In addition to the synthesis of peptide-polymer hybrid particles from hydrolyzed proteins presented in the previous section, a second project is presented here which consists in the synthesis of peptide-polymer conjugates from a single peptide of defined sequence. This project was again inspired by the great attention which peptide-polymer conjugates have received in past years. The prospect of combining the specific interactions characteristic of proteins with the high resistance to external influences (pH, temperature, *etc.*) common for synthetic polymers has sparked the interest of researchers in many fields, including biomedicine, personal care, adhesives, and so on.[6, 178]

A wide variety of peptides, ranging from large proteins like bovine serum albumin[179] or fragments thereof,[158] to smaller peptides with distinct properties[180] to single amino acids[181] have been used for coupling, demonstrating the far reach of this field. Among the sought-out, unique properties of peptides, their adhesion to particular substrates is a particularly interesting topic. Due to the monodispersity of the peptide structure, peptide-substrate interactions are specific and may be modified at will.[134, 135, 182] Whereas for synthetic polymers, unspecific interactions like hydrogen bonds or charge interactions often determine their adhesive behavior,[129] peptide adhesion is often modulated through single amino acid functionalities (their degree of oxidation, their orientation in space, *etc.*); factors which can change dramatically due to minor modifications in the environment.[136] This characteristic renders peptides particularly well-suited for playing the role of a functional component of polymers, bestowing upon them stimuli-responsive, or even reversible adhesion to a particular substrate.[137]

Concerning the synthetic polymer counterpart, initial efforts concentrated largely on water-soluble polymers like poly(ethylene glycol) (PEG).[178]However, the consequent investigations of peptide-functionalized nanoparticles and nanocapsules extend the scope to water-insoluble polymers and inorganic matter and their respective properties.[2, 7, 183] For instance, metal-incorporating particles can be used as contrast agents for magnetic resonance imaging[184] and drug-loaded particles may be used for targeted drug delivery.[185] The before-mentioned examples illustrate the traditional areas of application of peptide-polymer conjugates. Nevertheless, polymer-peptide hybrids are also gaining importance in other fields of application like coatings and adhesives,[180, 186] where polymer backbones other than PEG may be desirable. One versatile class of polymers which is often used in those fields are polyurethanes. PUs are variable in structure, they may incorporate crystalline

domains, charged moieties or water-swellable segments, conferring properties to them like heat-activation, charge interactions and dispersibility in water (see section 2.5).

In order to obtain peptide-polymer hybrids, two routes have been investigated which proceed either *via* coupling of pre-synthesized natural and synthetic polymers (the "grafting-onto" approach) or *via* an *in-situ* polymerization, starting from the peptide moiety (the "grafting-from" approach).[178] Although the latter method has been used successfully,[179, 187] the possible polymer structures are somewhat limited and the PU structure envisioned here, for instance, cannot be synthesized in this way. However, the main drawback of the grafting-onto method consists in unspecific coupling which can greatly affect peptide activity. Formerly, coupling was often achieved *via* lysine residues, several of which are usually present in a peptide chain and a precise control of the attachment site was therefore difficult.[188] A valuable alternative consists in using cysteine residues for coupling[189] because free cysteines (which are not engaged in disulfide bridges) are rare in peptides. Cysteines are reactive towards molecules like vinyl sulfones, acrylates, or maleimides, and often undergo a Michael addition of the SH function to a C=C double bond to form a chemically stable thioether bond.[190] Furthermore, in case of maleimide-functionalized polymers, a precisely controlled pH allows for a selective addition.[138]

Thus, in contrast to the previous approach (section 4.1), this project aims to take advantage of the monodisperse peptide structure and the associated properties in order to obtain a well-defined peptide-polymer system with tunable adhesive properties. In more detail, we show how maleimide-reactive PU particles can be functionalized with cysteine-containing peptides to transfer the adhesive behavior of the peptide to stainless steel surfaces onto the dispersions. The PU particles are complex in structure, containing segments which crystallize upon film formation and moieties rendering the particles self-stabilizing in water. The peptide sequence was chosen due to its unique and tunable adhesion to stainless steel surfaces investigated previously.[139] We show a high degree of control over the extent of particle functionalization and provide a detailed investigation of the functionalization as well as of the resultant dispersion and film properties.

4.2.2. Synthesis of maleimide-functionalized PUDs

The first step in the synthesis of peptide-functionalized, adhesive PU particles consisted in the synthesis of the PU prepolymer in bulk. In employing a slight excess of diisocyanate with regard to diol monomers, a PU with terminal NCO endgroups is obtained. Subsequently, hydroxyethyl maleimide (HEMI) is added to functionalize the linear polymer chains with terminal maleimide groups, as previously reported in the literature.[191] The chemical structure of HEMI as well as the functionalization reaction occurring are shown in ***Figure 4.2.1***.

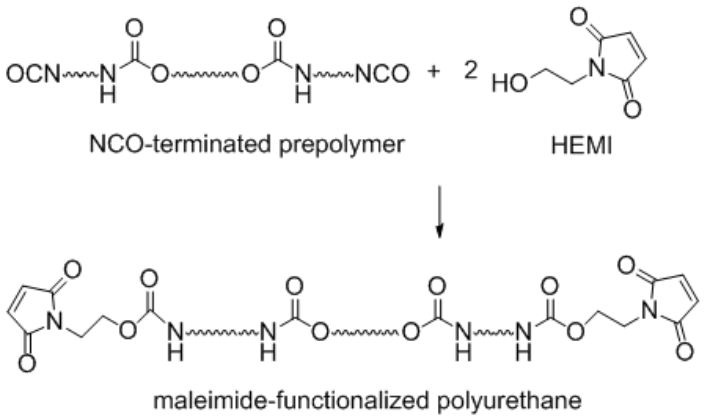

***Figure 4.2.1**: Reaction between an NCO-reactive PU prepolymer and HEMI to yield terminally maleimide-functionalized PU chains.*

An excess of HEMI is used in order to ensure that every chain end is functionalized. The reaction can be monitored by FTIR and the results thereof are displayed in ***Figure 4.2.2***. The decrease in the NCO band at 2300 cm^{-1} confirms that the reaction has taken place.

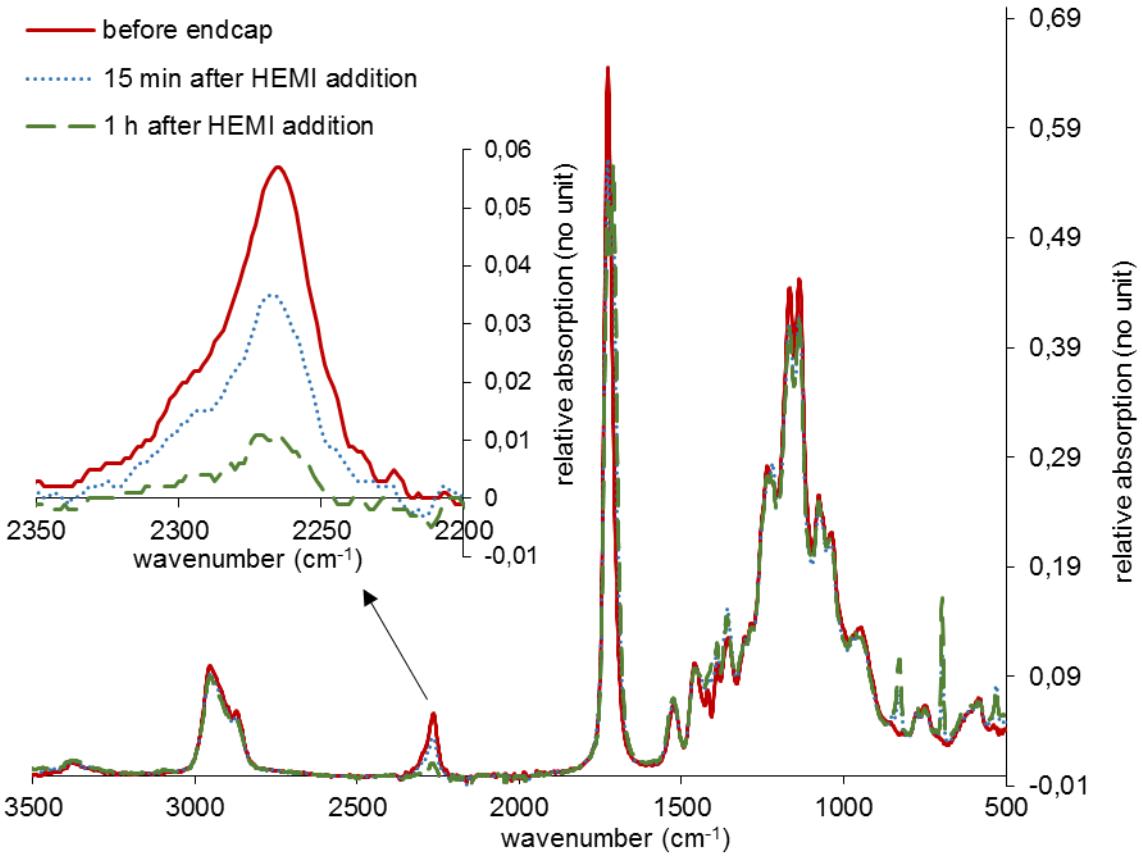

***Figure 4.2.2**: FTIR spectra of PU before (red line), during (blue dotted line), and after (green dashed line) successful endcap with HEMI. The inlay shows the NCO band at 2300 cm^{-1} which permits to conclude that 1 h after HEMI addition, the endcap reaction is virtually complete.*

Then, an auxiliary solvent (acetone) was added to facilitate the subsequent dispersion in water. Maleimide-functionalized particles (MI-PUDs) were obtained with a z-average particle diameter of 223 nm and a PDI of 0.115. After dialysis to remove the excess HEMI, it was found that the solid content of the dispersion was 9.85% (measured by freeze-drying), and the average particle size of the MI-PUDs was 204 nm with a PDI of 0.125.

4.2.3. Use of a peptide designed for adhesion to stainless steel

The peptide sequence to be used for coupling originates from a previous project for the screening, identification, and sequencing of peptides which adhere to stainless steel surfaces, described in a recent patent.[139] After a large-scale prescreening of randomly generated peptide sequences consisting of twelve amino acids, ten peptides were selected for cell expression investigations. *Escherichia coli* cells were transfected to express those peptides at the cell surface using the autodisplay method.[192] The latter consists in the transfection of cells to not only synthesize the desired sequence, but also a barrel domain which allows the sequence to pass the cell membrane and hence be presented at its surface. It is therefore a useful technique to investigate the properties of the expressed peptides, circumventing the laborious step of peptide isolation.[193]

The transfected cells were incubated on stainless steel platelets and subjected to a repeated washing protocol with phosphate-buffered saline solution. The adhering cells were harvested and sequenced in order to identify the most strongly binding peptides. The peptide sequence HMISTMNAASRR (see ***Figure 4.2.3a***) was found to adhere rather strongly to stainless steel as well as to porcelain surfaces and was therefore selected for this study. In order to couple this peptide motif to the MI-PUDs, a slight alteration was made to the sequence: at the C-terminus, the four amino acid long linker GSGC was added (see ***Figure 4.2.3b***). The sequence HMISTMNAASRRGSGC was thus used for the subsequent peptide-functionalization of the MI-PUDs through a cysteine-maleimide reaction.

a)

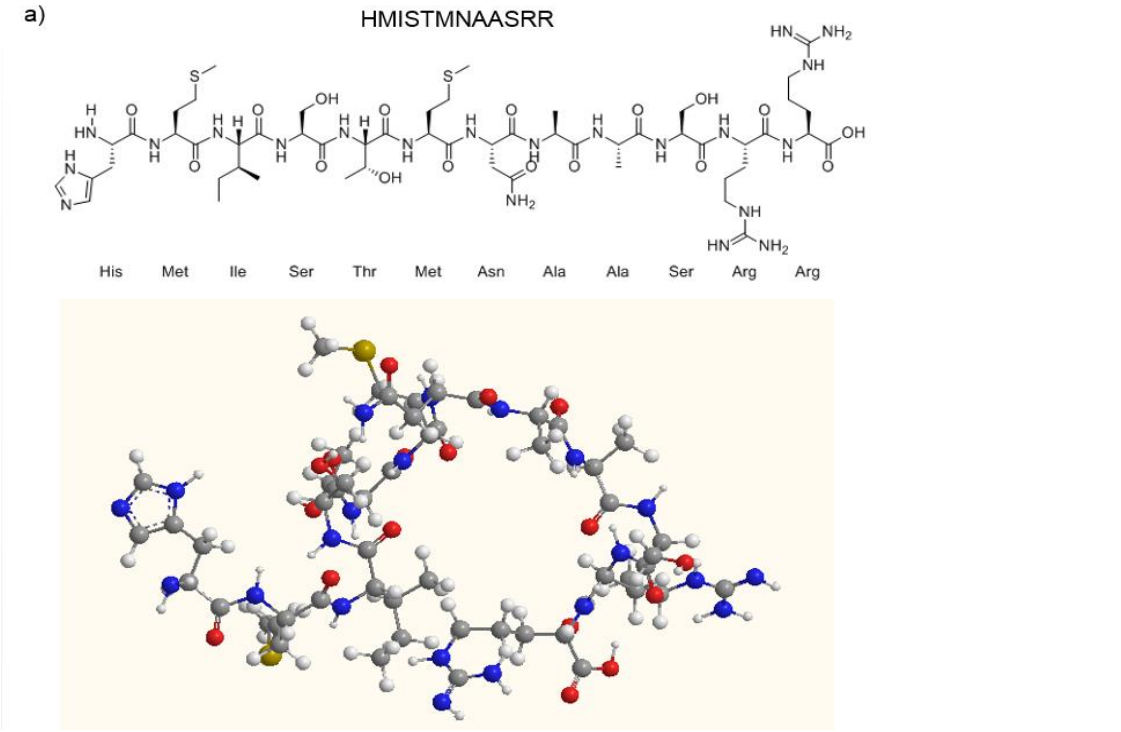
HMISTMNAASRR
His Met Ile Ser Thr Met Asn Ala Ala Ser Arg Arg

b)

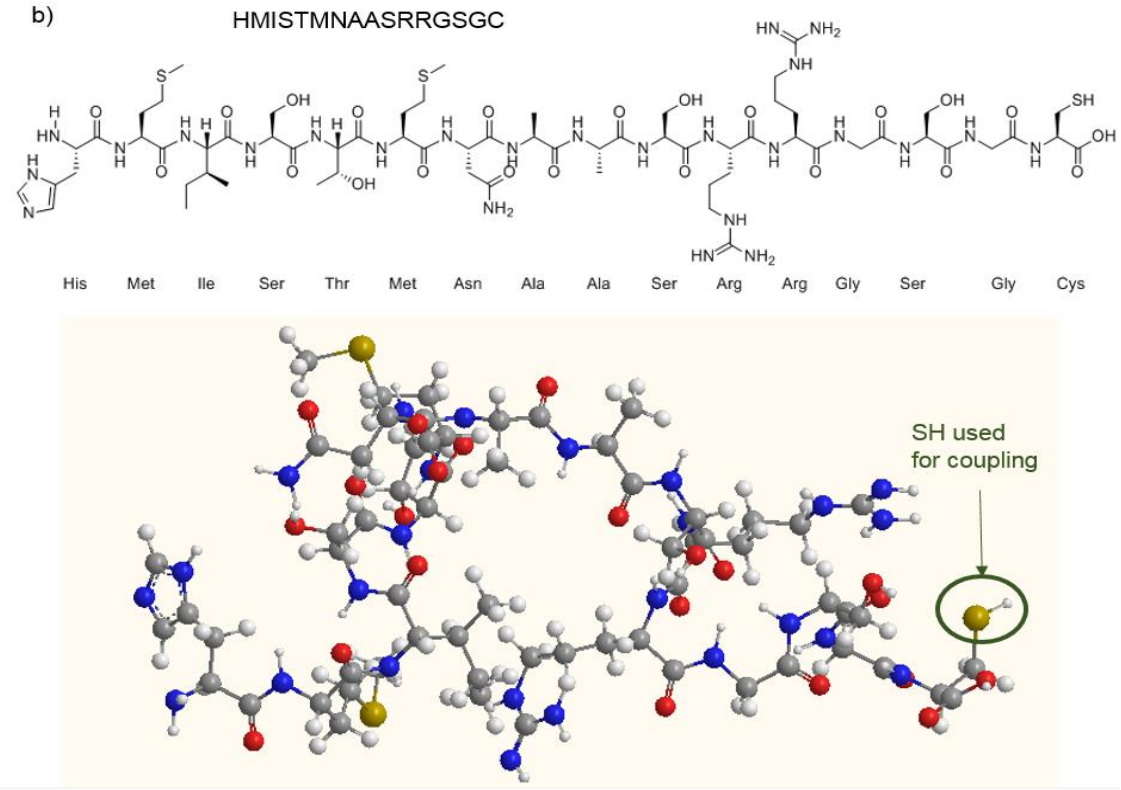
HMISTMNAASRRGSGC
His Met Ile Ser Thr Met Asn Ala Ala Ser Arg Arg Gly Ser Gly Cys
SH used
for coupling

***Figure 4.2.3**: Sequence, chemical structures, and three dimensional illustrations of a) the peptide sequence identified in the binding assay on stainless steel,[139] and b) the slightly altered sequence used for coupling.*

4.2.4. Coupling of the peptide to the PUDs

Cysteine residues in peptides have been used previously for a selective coupling to synthetic polymers *via* the cysteine residue.[189] A possible reaction pathway is a Michael addition of the SH function to a C=C double bond (present in acrylates, maleimides, and other compounds) to form a chemically stable thioether bond (see ***Figure 4.2.4***).[190] Furthermore, in case of maleimide-functionalized polymers, a precisely controlled pH set between 6.5 and 7.5 allows for a selective addition of cysteines with respect to other nucleophilic side chains.[138] In specific, at pH 7.0, the Michael addition of cysteines occurs 1 000 times faster than that of amines, whereas at higher pH, the reaction with lysine residues becomes more important. It can therefore be concluded that a carful control of the reaction conditions (*i.e.* the pH value) permits to selectively couple cysteine-containing peptide structures to maleimide-functionalized polymers.[190] The peptide sequence described above (HMISTMNAASRRGSGC) allows for this type of coupling reaction.

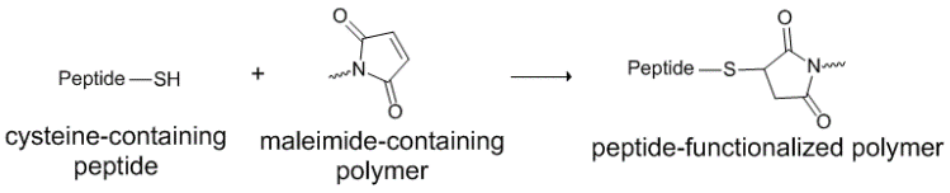

***Figure 4.2.4**: Michael addition between a cysteine-containing peptide and a maleimide-containing polymer to form a stable peptide-polymer conjugate.*

The Ellman's test is a type of colorimetric method for detecting free thiols in solution and has previously been proven useful to quantify the concentration of a cysteine-containing peptide.[149, 150] The test relies on the reaction between the colorless DTNB and the thiol group of the peptide, producing equimolar quantities of 5-mercapto-2-nitrobenzoate (MNB) (see also section 3.10). The characteristic absorption of MNB at 412 nm increases linearly with concentration and can therefore be used for quantification of the peptide.[151]

In this work, as a first step, the MI-PUD was analyzed with regard to the amount of MI available for reaction. Thus, the MI-PUD was incubated with a large excess of N-acetyl-L-cysteine (ACC) (n(MI):n(SH) =1:3) at room temperature and the Ellman's test was performed immediately after

addition and after 24 h. The chemical structure of ACC as well as the reaction between the maleimide-containing polymer and ACC are shown in ***Figure 4.2.5***.

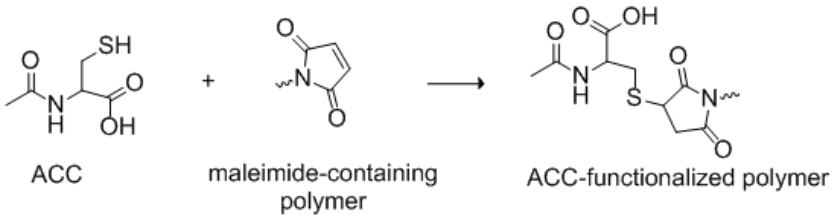

Figure 4.2.5*: Michael addition between ACC and a maleimide-containing polymer to yield an ACC-functionalized (and hence nonreactive) polymer.*

It was assumed that the reaction was completed after 24 h. Furthermore, since SH groups are susceptible to oxidation in solution, forming unreactive disulfide links, a non-reactive control dispersion was treated in the same way to quantify this side-reaction. The amount of available MI was calculated according to the equation:

$$\%\ \text{available MI} = \frac{(\Delta n_{ACC\ detected\ for\ MI-PUD} - \Delta n_{ACC\ detected\ for\ control\ PUD})}{n_{theoretical\ MI\ groups\ in\ dispersion}}$$

With $\Delta n = n_{ACC\ detected\ after\ 0\ h} - n_{ACC\ detected\ after\ 24\ h}$.

And with the theoretical number of MI groups in the dispersion being calculated from the amount of dispersion used, the solid content (9.85% by freeze-drying), and the theoretical number average molecular weight of dually functionalized polymer chains (M_n = 8282 g/mol). We calculated that 99% of theoretical MI groups have reacted after 24 h which indicates a successful functionalization, a good stability of the MI groups in the dispersion, and a good superficial availability of MI groups for reaction. Using this information, dispersions were prepared with 50% and 25% functionalization through incubation with the corresponding amounts of ACC, termed MI-PUD(50), and MI-PUD(25), respectively.

Subsequently, the Ellman's test was used to follow the reaction between the MI-PUDs and the cysteine-containing peptide. A control PUD was again measured in parallel to account for dimerization of the peptide. As can be seen in ***Figure 4.2.6***, the oxidation of cysteine accounts for a loss of 20% of the initially added amount of peptide over the course of 24 h. The oxidation is rather fast, seen as 15% have already reacted within the first hour. In comparison to this, when the MI-PUD is present in the peptide solution, about 60% of the cysteine groups present react within 24 h. The amount reacting within the first hour is also much greater (about 55%), indicating that coupling

strongly predominates over oxidation. It may further be noted that coupling is virtually complete after 6 h with the cysteine content reaching a plateau. The same trends are observed for the two dispersions with intermediate MI-functionalization.

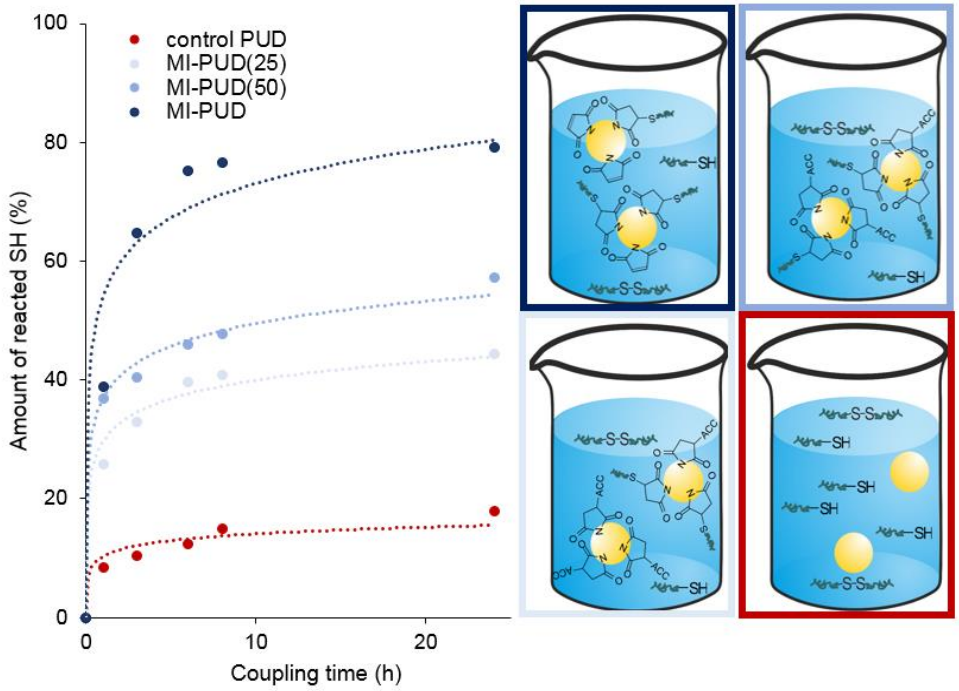

***Figure 4.2.3**: Results of the Ellman's test performed during incubation of three maleimide-functionalized dispersion and one unreactive control dispersion with a slight excess (molar ratio 1:1.5) of a cysteine-containing peptide. The test shows that the coupling is very fast and predominates over the oxidation of the peptide in solution. In case of the MI-PUD, 40% of the cysteine present in the reaction medium are thus covalently attached to the particles.*

4.2.5. Effect of the coupling on dispersion properties

It should be noted that during both coupling and dialysis, despite low solid contents (*ca.* 0.35%), minor coagulation of particles was observed. Coagulation was interestingly lowest for the functionalized MI-PUD and higher in case of the MI-PUD(50) and the MI-PUD(25). For electrostatically-stabilized particles, coagulation is most commonly due to high salt concentrations weakening the effectiveness of the electrostatic stabilization (see section 2.2.2 on electrostatic forces). However, we observed that coagulation could not be remedied by decreasing the buffer concentration, but rather seemed to stem from the peptide attachment because all MI-PUDs were stable in the 0.01 M P-buffer in absence of the peptide. Charge calculations of the peptide (see section 6.3.10 for details)

indicated that it is positively charged with a net charge of 2.1 at pH 7 (see ***Figure 4.2.4a***). We therefore concluded that during peptide coupling, the electrostatic repulsion between particles is compromised, leading to coagulation. Since coupling is fastest for the MI-PUD (see ***Figure 4.2.3***), coagulation is least pronounced. We further conducted zeta potential measurements during addition of increasing amounts of peptide to the MI-PUDs and observed that the ZP of the particles remained negative as long as n(SH)/n(MI) < 0.08. For larger values, the ZP of the particles was reversed (see ***Figure 4.2.4b***).

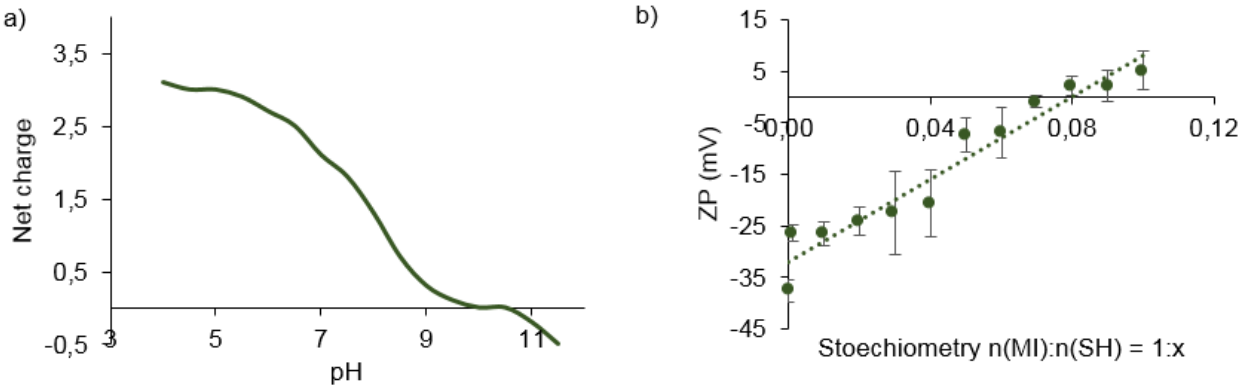

Figure 4.2.4*: a) Net charge of the peptide as a function of pH, calculated using a charge calculator.*[194] *The peptide is cationically charged below pH 10. b) Zeta potential measurements of the dispersion during addition of small amounts of peptide. The ZP of the anionically stabilized particles is approximately zero for a stoichiometry of n(MI):n(SH) = 1:0.08 and becomes positive with increasing amounts of peptide added.*

The phenomenon of ZP reversal is well-known for the layer-by-layer technique for particle synthesis or modification where oppositely charged polyelectrolytes are consecutively and alternatingly adsorbed to particle surfaces. Due to the fast adsorption kinetics, stability can be maintained.[195, 196] We therefore attempted to increase the reaction kinetics by increasing the concentration of both reaction partners by a factor of up to 10 and by increasing the stoichiometry of n(SH):n(MI) by a factor of 3. Although improvements were observed, neither approach completely avoided coagulation. We therefore also attempted the more economical alternative of partial functionalization, *i.e.* using very small stoichiometries of n(MI):n(SH) of 1:0.01 to 1:0.03. Although those functionalized dispersions remained perfectly stable, they did not show the desired, improved adhesion to stainless steel and the approach was therefore not pursued further. All subsequent results therefore relate to the mostly stable, previously mentioned MI-PUD functionalized with the peptide.

4.2.6. Effect of the coupling on film properties

DSC measurements were conducted in order to assess the effect of the peptide functionalization on the film properties. The dispersions were dialyzed to remove any remaining, unattached peptide and films were cast and tempered to ensure a uniform thermal history (see section 6.2.15 for the temperature treatment protocol). Results of the DSC measurements are shown in ***Figure*** 4.***2.5***. The melting enthalpy for the maleimide-functionalized dispersion and for the peptide-functionalized dispersion after dialysis are 99 J/g and 64 J/g, respectively. Those values indicate that crystallization is greatly affected by the presence of the peptide. Furthermore, the graph indicates the presence of two peaks, one at 49 °C and one around 52 °C corresponding to two types of crystallites formed. The maleimide-functionalized dispersion shows both peaks with a greater proportion of crystallites melting at 52 °C. The peptide-PUD shows the same behavior although in comparison, the proportion of crystallites which melt at lower temperatures is higher. This observation indicates that the presence of the peptide impedes the formation of larger crystallites from the small ones during tempering, as is observed for the unfunctionalized sample.

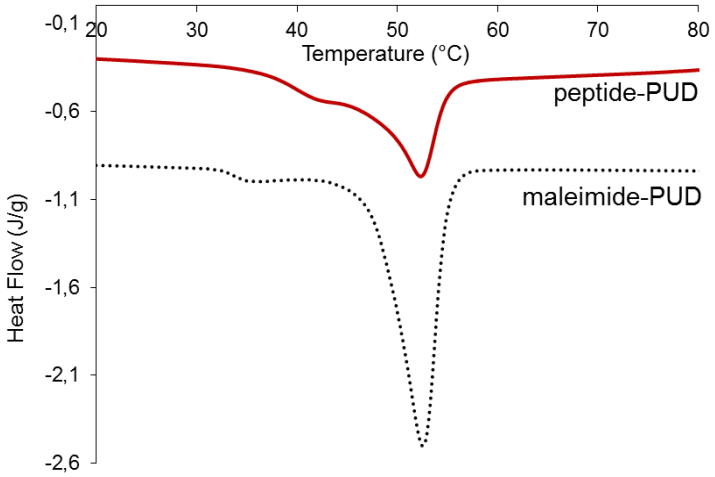

Figure 4.2.5*: DSC measurements of the MI-PUD and of the peptide-functionalized dispersion. Results show that peptide coupling greatly affects the degree of crystallization.*

4.2.7. Adhesion to stainless steel surfaces

In order to investigate if the peptide's adhesive properties have been transferred to the particles, QCMD measurements on stainless steel (type SS2343) sensors were performed using the dialyzed peptide-functionalized dispersion, the nonfunctionalized MI-PUD, and a solution of the peptide at the calculated concentration at which it was present in the peptide-functionalized dispersion (0.45

µmol/ml). Results thereof are displayed in ***Figure 4.2.6***. It can firstly be noted that the peptide itself does not seem to show a measurable adhesion to the surface at the concentration used. This may appear puzzling in light of the strong affinity for stainless steel measured in the assays used for selecting the peptide sequence. However, it is very likely that the concentration used here is too low for a pronounced frequency shift to be detected. This is due to the fact that a frequency shift is on the one hand due to the number of adsorption events taking place, but on the other hand, it is also due to the mass of the adsorbing species. In consequence, it is much more difficult to detect small molecules than large ones. We are observing here a combination of two factors: firstly, the concentration of the peptide is very low and hence the adsorption events are few, and secondly, the peptide itself is small and as a consequence, the frequency shift is very small as well. Also, it can be seen that the maleimide-functionalized particles adsorb to a small extent to the stainless steel surface, resulting in a frequency change of about -12 Hz. Furthermore, the fact that the dissipation does not increase significantly and that the frequency overtones hardly spread indicates that the particles form a rather rigid film on the sensor surface. This observation can be explained by the deposition of single, isolated particles which do not coalesce. The extent of adsorption is too little to allow for a continuous polymer film to form which would show a viscoelastic behavior. In contrast, to those two control samples, the peptide-functionalized particles adsorb very well to the stainless steel surface, leading to a frequency change of about -75 Hz. In addition, after the initial decrease, the frequency change is lessened with ΔF increasing by about 5 Hz. This behavior is characteristic of the adsorption of peptides. When in solution, the latter are surrounded by water molecules which adsorb to the sensor surface alongside the peptides in a first step. Consequently, when the peptide layer condenses, the water molecules are expulsed, leading to a decrease of adsorbed mass and causing the increase in the frequency change observed here. Upon close examination, we can see the same effect mirrored in the dissipation curves. We can therefore conclude that the adhesion of the peptide-functionalized particles is indeed due to the attached biomolecules.

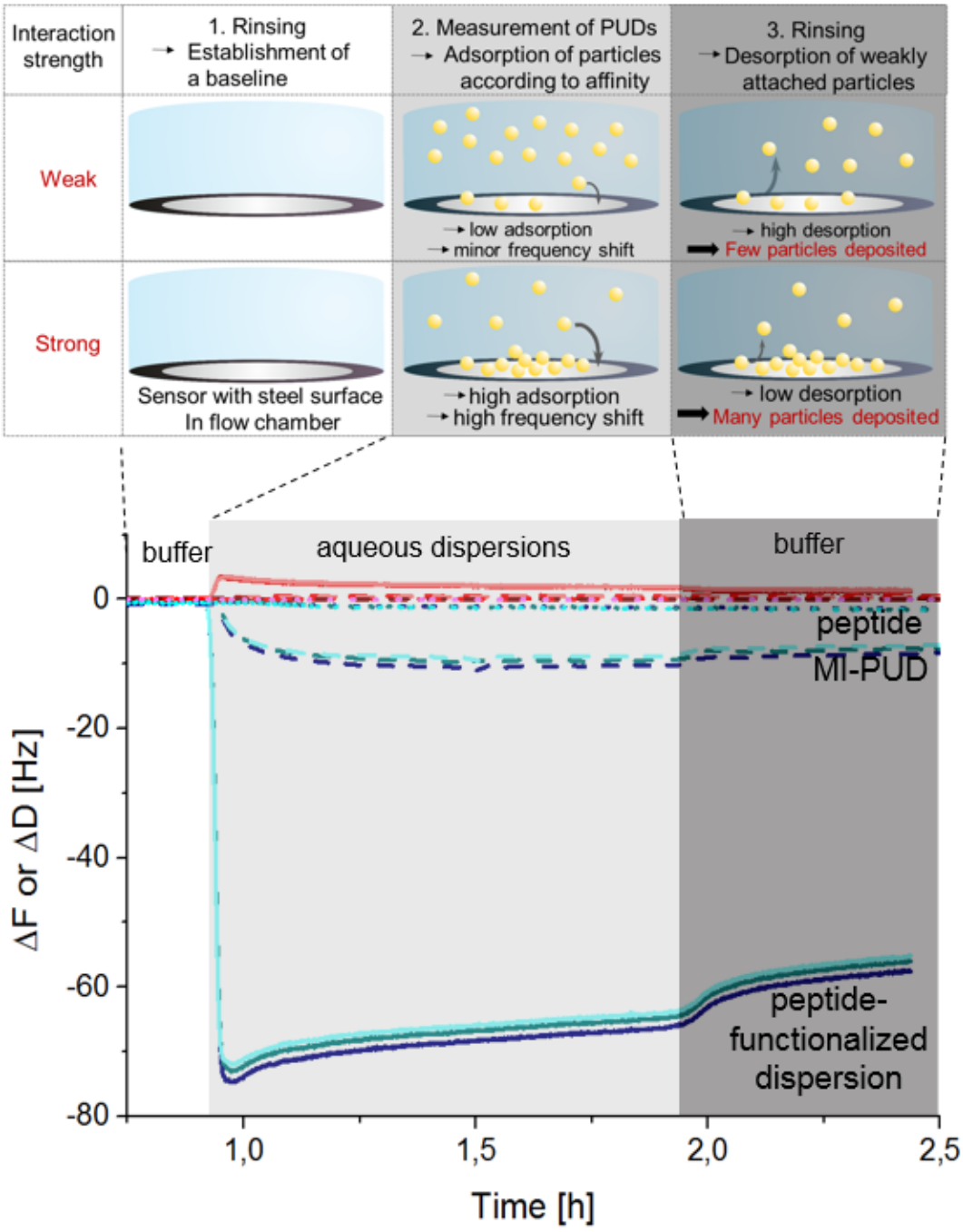

***Figure 4.2.6**: Results of QCMD investigations performed on stainless steel sensors using a solution of the peptide (dotted lines), a maleimide-functionalized dispersion (dashed lines), and a peptide-functionalized dispersion (solid lines). Measurements include three phases: 1 h of rinsing with deionized water, then 1 hour of letting the dispersion run over the sensor and lastly another hour of rinsing with deionized water. The graphs show that adsorption is much more pronounced for the peptide-functionalized dispersion than for the reference samples.*

4.2.8. Conclusion

Presented in this section are results on to the synthesis of peptide-polyurethane conjugates using a peptide of defined sequence and designed for adhesion to stainless steel surfaces.[139] We use a cysteine-maleimide coupling and provide a detailed analysis of the reaction kinetics. The peptide's cationic charge at the working pH (pH 7) is shown to cause a reversal of the zeta potential of the particles and is therefore at the origin of a slight destabilization of the particles, particularly for partial peptide functionalizations. The peptide coupling also affects the film properties of the polyurethane backbone, leading to a pronounced decrease in the film's degree of crystallinity. We finally show that the peptide's adhesive properties can be transferred to the particles, as demonstrated with quartz crystal microbalance with dissipation measurements. Although the peptide itself does not show a pronounced adhesion at the concentration at which it is present in the functionalized dispersions, we observe a distinct, peptide-mediated adhesion of the latter. The results presented are taken as first indications of the viability of this method to transfer the peptide's specific properties to the PUDs. Further investigations are planned which will include the coupling of the same peptide to cationically charged PUDs in order to circumvent stability issues as well as investigations of the adhesive properties of the system at different pH values. The system and method presented here will be taken as basis for such additional studies. This project as well as the planned work is intended to be of great interest for paints and adhesives for stainless steel and shows, in relation to the previous section on peptide-polymer hybrids, how sequence-defined peptides may also be used in order to confer interesting adhesion properties to polyurethane dispersions.

4.3. Phosphonate-functionalization of PUDs for adhesion to hydroxyapatite[#]

4.3.1. Introduction and aim of the project

The third project of the thesis consisted in the functionalization of PUDs with phosphorous-functional groups for adhesion to metallic and organic surfaces. Polymers containing phosphorus-groups can possess fascinating properties like complexation and ion conductivity,[198-200] biodegradability, biocompatibility,[201, 202] and flame retardancy,[203, 204] and govern vital interactions in biological and technical systems.[205-207]

Depending on the desired function, low degrees of phosphorous functionalization can already cause strong effects, *i.e.* drastically increased adhesion and pigment-binding. Phosphoric and phosphorous acid units for example are well-known adhesion promoting sites and especially enhance the interaction towards metals and inorganic substrates. For durable applications, phosphonates are typically preferred over the corresponding phosphate derivatives due to the higher hydrolytic stability of the former.[208] In any case, phosphorous functionalization in general has become an important tool for many applications like anti-corrosion coatings, structural adhesives, biomedicals, and dental fillings.[10, 116]

Similarly to solvent-born polymer systems, phosphorous units have also been introduced in their aqueous analogs, *i.e.* water-based polymer dispersions. For instance, polymer dispersions based on free-radical polymerization have received much attention. The obtained materials and their respective applications are diverse and are described mostly in recent patents, concerning for example paints and coatings with improved pigment binding and increased gloss,[209] liquid applied sound dampening systems for automotive,[210] anti-corrosion,[211] and adhesive applications.[212] Accordingly, examples of enhanced binding interactions of vinyl-based dispersions were also reported in the peer-review literature, again based on different phosphorous monomers, special designed surfmers (combining surfactant and monomer properties in one molecule) or preparation techniques, and describing a variety of applications, like biomineralization, biomedical implants, cellular uptake, or corrosion protection.[9, 146, 213-215]

[#]This section is based on the publication "Phosphonic Acid-functionalized Polyurethane Dispersions with Improved Adhesion Properties" by Laura Breucker, Katharina Landfester, and Andreas Taden, to be published in 2015 in *ACS Applied Matierals & Interfaces*, DOI: 10.1021/acsami.5b06903.[158] Reprinted with permission. Copyright 2015 American Chemical Society.

In light of the great importance of phosphate- and/or phosphonate-functionalization *via* free-radical emulsion polymerization, it seems surprising that PUDs have rarely been investigated in this regard. As explained in more detail in the theoretical background (section 2.5), PUs already serve a wide variety of applications, including foams and construction materials, flexible and shock-absorbing layers, adhesives and coatings. They further display an extraordinarily rich chemistry due to the reversibility of isocyanate-based bonds[40, 46] (urethane, urea, biuret, allophanate, etc., see section 2.5 for details) and allow for facile modification reactions, *e.g.* to integrate thermal- or UV-curing capabilities.[216, 217] In the recent past, due to a rising environmental concern and increasingly stringent governmental regulations restricting the production of volatile organic compounds, researchers have begun to shift their focus from traditional, solvent-based PUs to aqueous PUD systems.[42, 46] In particular, complex structures may be obtained which range from, for instance, self-stabilization and specific surface functionalization of the dispersions to semi-crystallinity in the film.[158, 218] Surprisingly, only a few reports on PUDs comporting phosphorous groups can be found in the literature. For flame retardancy purposes, a polyphosphate polyol[219, 220] and a phosphorous spiro compound were utilized.[221] Mequanint et al. synthesized soft segments based on 1,2,4-phosphonobutane tricarboxylic acid[57] and investigated the basic wetting and adhesive properties of the respective P-PUDs.[222] Finally, phosphorous-containing aziridinyl curing agents were combined with classical PUDs to improve flame retardancy, but remain questionable in terms of health and safety considerations and were not designed to improve adhesive properties.[218]

The previously reported phosphorus-containing PUDs are limited to a certain composition, *i.e.* the use of phosphorous diols as specialty soft segments, and are prone to hydrolysis (polyphosphate backbone) or gelation (triacid-based polyol with functionality > 2). In consequence, the attainable thermomechanical properties of the polymer films are rather limited and desirable features such as partial crystallinity in the film may not be obtained. So far, only few systems were investigated in terms of substrate interaction and adhesion. However, none of these previous reports describe dynamic adsorption behaviors of the dispersions, interactions with substrates other than metals, utilization of bisphosphonic adhesion moieties. Furthermore, they do not provide the synthetic freedom and thermos-responsive properties explained above.

In this part of the work, a facile route to obtain PUDs comporting phosphonate groups (P-PUDs) with improved adhesion properties is presented. HAP, stainless steel, and gold serve as model substrate in QCMD measurements to observe and quantify enhanced substrate interactions, which can also be expected for other inorganic materials and metal interfaces. The conversion of the functionalization reaction is evaluated and localization of the phosphonate groups (P-groups) is achieved using inductively-coupled plasma optical emission spectroscopy (ICP-OES) and particle charge detection

(PCD) measurements, respectively. We further show that a crystalline structure in the film can be maintained, which provides heat-activated physical crosslinks for an initial setting mechanism and is of great importance for adhesive applications.

4.3.2. Different synthetic routes to phosphonate-functionalized PUDs

As previously mentioned in the theoretical background (section 2.5), PUDs are commonly synthesized from a mixture of polyols and a polyisocyanate. Through addition of a slight excess of isocyanate with regard to alcohol functionalities, a prepolymer of moderate molecular weight with NCO endgroups is obtained. These endgroups can be used for a chain extension under aqueous conditions (after dispersion) to increase the molecular weight of the PU chains and/or for an endcap in order to introduce a desired functionality into the polymer structure.[44, 47, 158] For this procedure, highly nucleophilic chain extenders and/or functionalization agents are required in order to kinetically subdue the unwanted side reaction with water. For the same reason, most systems solely rely on aliphatic polyisocyanates because they are less sensitive towards water. To carry out the same reaction in bulk or in solution is highly unfavorable because of the associative nature of the PU macromolecules, leading to a pronounced viscosity increase with higher chain length and severe handling issues.

Functionalization of pre-synthesized PUDs *via* the aqueous phase was thus conducted here. This method allows for the use of the amine-containing Phosphonate-functionalized reagents (P-reagents) generally insoluble in organic media. Two general synthesis approaches for P-PUDs were used (see below). In either case, an NCO-reactive PU prepolymer was synthesized in bulk. For Method A (shown in ***Figure 4.3.1***), the prepolymer was dispersed in water, the endcap reagent was then added to the reactive dispersion and the pH was adjusted to allow for the reaction to occur. For Method B (shown in ***Figure 4.3.2***), the prepolymer was dispersed in the endcap reagent solution at elevated pH such that dispersion formation and endcapping occurred simultaneously. In the latter case, the endcap reaction may take place during emulsification and a higher endcap efficiency might be expected due to the high sheer forces employed and the increased mixing.

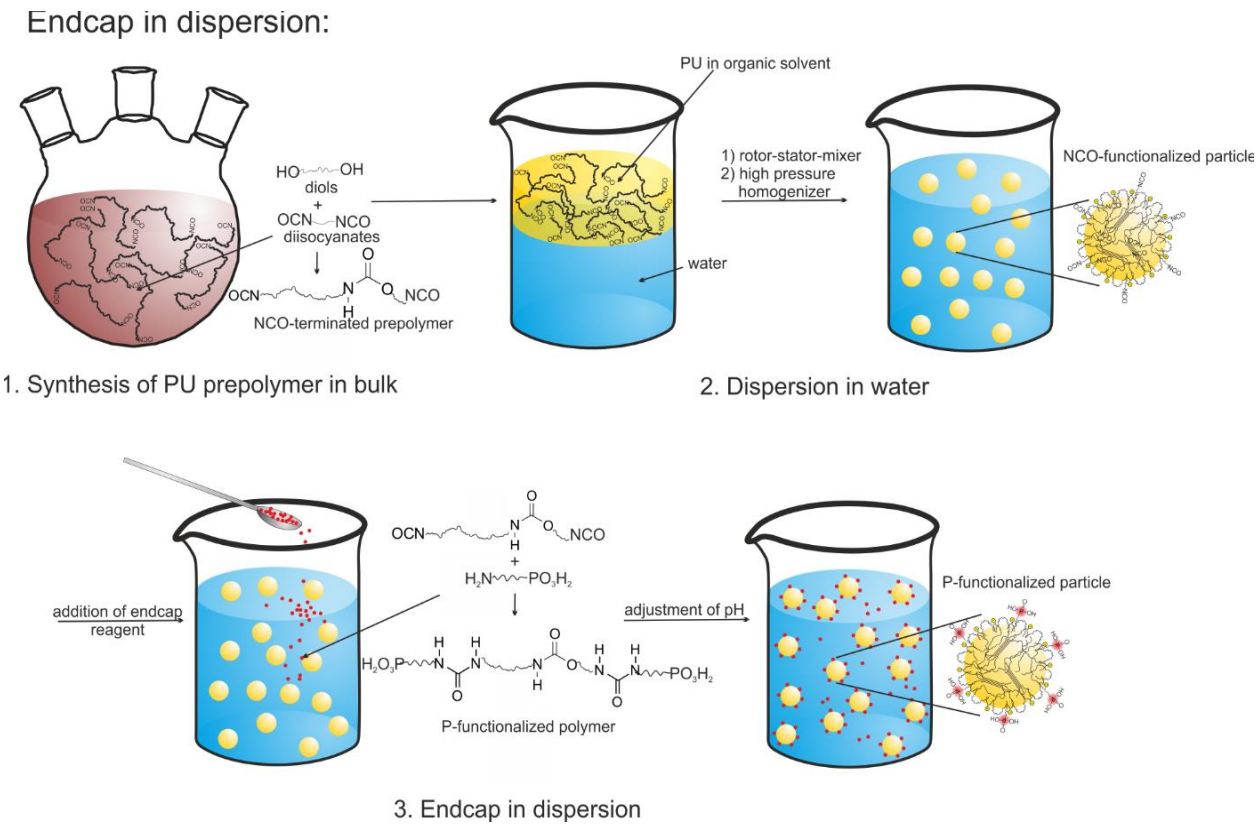

***Figure 4.3.1**: Method A for the synthesis of P-PUDs, consisting of 1. The synthesis of an NCO-terminated prepolymer in bulk, 2. Its dispersion in water, and 3. The endcap in dispersion through addition of the amine-reactive, P-containing endcap reagent and an increase of the pH to pH 12 to yield P-functionalized particles.* *This figure is reproduced from the publication "Phosphonic Acid-functionalized Polyurethane Dispersions with Improved Adhesion Properties" by Laura Breucker, Katharina Landfester, and Andreas Taden, to be published in 2015 in* ACS Applied Matierals & Interfaces, *DOI: 10.1021/acsami.5b06903.*[158] *Reprinted with permission. Copyright 2015 American Chemical Society.*

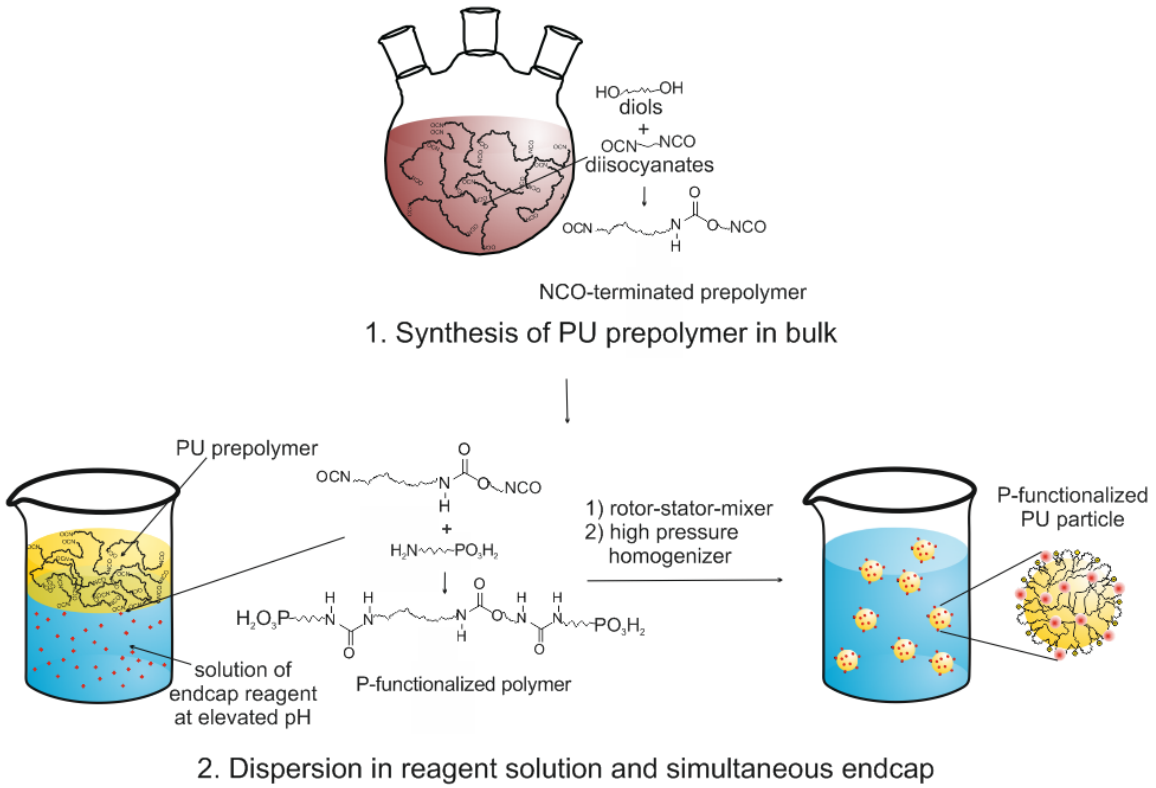

***Figure 4.3.2**: Method B for the synthesis of P-PUDs, consisting of 1. The synthesis of an NCO-terminated prepolymer in bulk, 2. Its dispersion in a solution of the amine-reactive, P-containing endcap reagent at pH 12 to yield P-functionalized particles. This figure is reproduced from the publication "Phosphonic Acid-functionalized Polyurethane Dispersions with Improved Adhesion Properties" by Laura Breucker, Katharina Landfester, and Andreas Taden, to be published in 2015 in* ACS Applied Matierals & Interfaces*, DOI: 10.1021/acsami.5b06903.[158] Reprinted with permission. Copyright 2015 American Chemical Society.*

For clarity, the two methods will be treated separately: section 4.3.3 will show results obtained with Method A and section 4.3.4 will display results from Method B.

We investigated the use of two different endcap reagents, namely neridronic acid (NA) and aminomethylphosphonic acid (AMPA). NA was chosen because previous investigations related to UV-cured, (meth)acrylate-based coatings containing bisphosphonic monomers have shown excellent results in terms of adhesion to metal and anticorrosion properties.[223] Furthermore, certain bisphosphonates, including NA, are commercially available and widely used in the biomedical field to treat bone diseases such as osteoporosis, indicating a favorable interaction with HAP.[224] AMPA only contains a single phosphonic acid group per molecule, and whereas NA was used for both Method A and Method B, AMPA was only investigated using Method B.

It should be noted that amino-alkyl-phosphonic acids form zwitterions in water. In the case of NA, the pK_a of the amino group is 11.94[225] and in case of AMPA, the pK_a is 10.2.[226] Consequently, the standard experiments were carried out at an adjusted, respective pH of 12 or 11 for amine deprotonation and to ensure a highly nucleophilic state for the endcapping reagent. Obviously, the pH and the reaction time for the endcapping reaction in aqueous dispersion are important parameters, and can also favor unwanted side reactions with water. For this reason, additional experiments at lower pH and different reaction times were conducted and are summarized in section 4.3.3.

4.3.3. Method A to obtain P-PUDs

The results presented in this section derive from the above-termed Method A where the NCO-reactive prepolymer is dispersed in deionized water, the endcapping reagent NA is added promptly and the pH of the dispersion is increased thereafter to allow for the reaction to take place. Lastly, dialysis is conducted for desalting.

Different stoichiometry ratios of isocyanate to endcap reagent (n(NCO)/ n(NA)) ranging from 1:1 to 4:1 were used in order to gain a better understanding of the system. The results were assessed based upon the conversion (*i.e.* how much of the endcap reagent that was added could be covalently attached to the PU as indicated by ICP-OES), the surface coverage (*i.e.* how many of the attached P-groups are localized at the interface), and most importantly the adhesion to HAP (*i.e.* how much strongly adsorbed to HAP surfaces as indicated by the frequency shift in QCMD measurements). As control sample, a non-functionalized dispersion was synthesized through an endcap in bulk. In this case, dibutylamine was added to the prepolymer until the NCO band at 2300 cm^{-1} in the FTIR spectrum had disappeared (see ***Figure 4.3.3***). The prepolymer was then emulsified to yield a non-functionalized PUD.

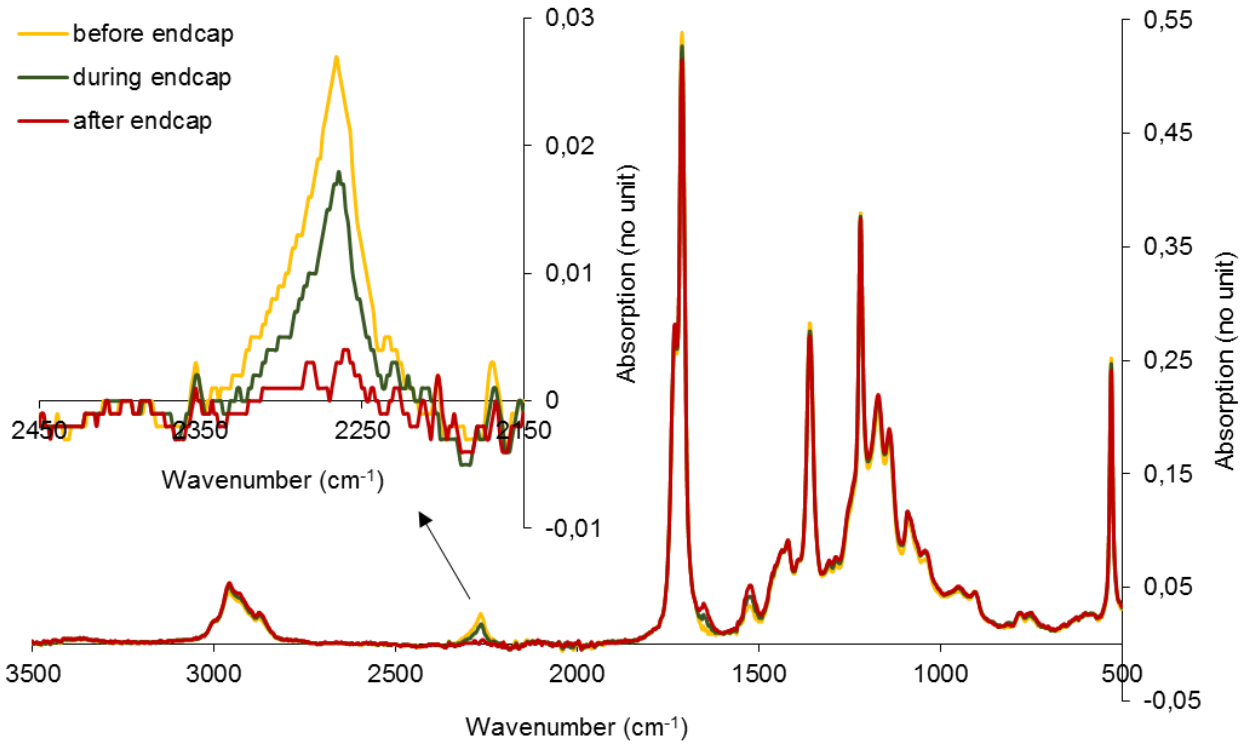

***Figure 4.3.3**: FTIR spectra showing the DBA endcap of the NCO-terminated prepolymer. The three spectra were recorded before (yellow), during (green), and after reagent addition (red). The inset shows the absorbance region associated with the isocyanate group (around 2300 cm^{-1}) and the disappearance of the peak is proof of the successful endcap. The resultant nonreactive polymer was dispersed in water to yield the control dispersion. This figure is reproduced from the publication "Phosphonic Acid-functionalized Polyurethane Dispersions with Improved Adhesion Properties" by Laura Breucker, Katharina Landfester, and Andreas Taden, to be published in 2015 in* ACS Applied Matierals & Interfaces, *DOI: 10.1021/acsami.5b06903.[158] Reprinted with permission. Copyright 2015 American Chemical Society.*

As mentioned above, the coupling pH and the coupling time are important factors in determining the endcap efficiency and the consequent dispersion properties. Thus, as preliminary experiments, the coupling time (*i.e.* the time for which the dispersion was maintained at elevated pH) as well as the coupling pH were varied and the conversion was measured. This was done using Method A and NA as endcap reagent with a stoichiometry of 1:0.25 (*n*(NCO):*n*(NA)). The results thereof are displayed in ***Figure 4.3.4***. ***Figure 4.3.4a*** shows that the conversion remains constant with about 20% for the first 2 h and is increases to 30% after 24 h. In light of the high salt concentrations necessary to increase the pH to pH 12 and the adverse effects on the stability of electrostatically stabilized dispersions, we chose 30 min as an adequate time window for the endcap reaction. ***Figure 4.3.4b*** indicates that at a pH below 7, the conversion is close to 0% and then gradually increases

between pH 8 and pH 12 to 20%. The conversion mirrors the titration of the amino group and hence, a pH of 12 (which is above the pK_a of 11.94 of the amino group) was chosen for the endcap reaction.

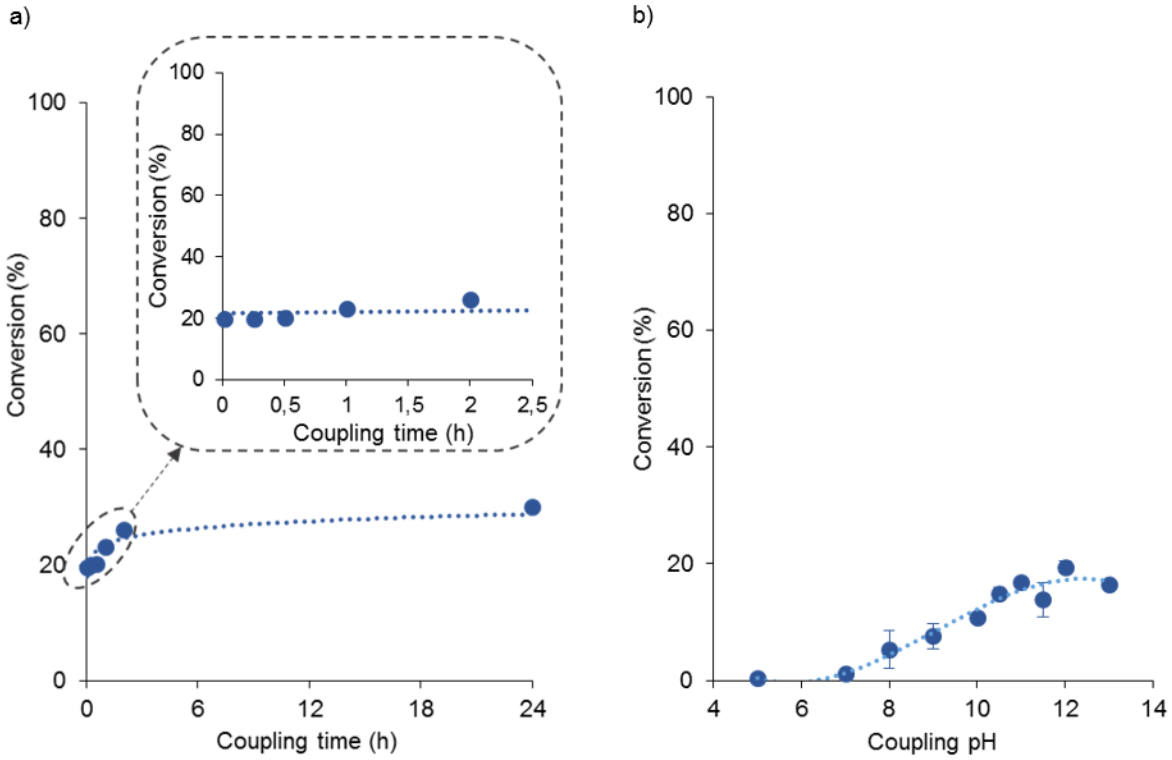

***Figure 4.3.4**: Variation of the conversion of the endcap reaction as a function of the coupling time (a) and as a function of the coupling pH (b). The conversion was calculated from the quotient of the P-content before and after dialysis in the freeze-dried dispersions (which was measured with ICP-OES). The coupling time refers to the time for which the dispersions were stirred at pH 12 in presence of the endcap reagent. The coupling pH refers to the pH at which the dispersion was stirred for 30 min, again in presence of the endcap reagent. For both investigations, a stoichiometry of 4:1 (*n*(NCO)/*n*(NA)) was chosen to minimize charge interactions at the interface. Results are averages of three independent measurements and error bars indicate the standard deviation. Coupling efficiency and localization of phosphonate groups. This figure is reproduced from the publication "Phosphonic Acid-functionalized Polyurethane Dispersions with Improved Adhesion Properties" by Laura Breucker, Katharina Landfester, and Andreas Taden, to be published in 2015 in* ACS Applied Matierals & Interfaces, *DOI: 10.1021/acsami.5b06903.*[158] *Reprinted with permission. Copyright 2015 American Chemical Society.*

4.3.3.1. Colloidal stability of the dispersions

Prior to the NA endcap, the measured z-average particle size of the dispersions was 162 nm with a PDI of 0.108. After dialysis, the NA-functionalized PUD based on a 1:1 stoichiometry (sample "NA100") had an average diameter of 233 nm with a PDI of 0.230 (see ***Table 4.3.5***). The increase in particle size and in particle size distribution can most likely be attributed to the high salt concentration during endcap and dialysis. This conclusion is supported by the fact that when less NA was used, the effect on the particle size and the PDI was much less pronounced. In any case, colloidally stable P-PUDs were obtained after desalting, which maintained their particle size distribution even at solid contents of up to 20% for at least 6 months.

***Table 4.3.5**: Chemical structure of the endcap reagent, stoichiometry for reaction, and DLS measurements before and after dialysis for the different PUDs synthesized.* *This table is reproduced from the publication "Phosphonic Acid-functionalized Polyurethane Dispersions with Improved Adhesion Properties" by Laura Breucker, Katharina Landfester, and Andreas Taden, to be published in 2015 in* ACS Applied Matierals & Interfaces, *DOI: 10.1021/acsami.5b06903.*[158] *Reprinted with permission. Copyright 2015 American Chemical Society.*

Sample name	Endcap reagent	Chemical structure	endcap in...	Stoichiometry *n*(NCO)/ *n*(endcap)	before dialysis		after dialysis	
					Particle size [nm]	PDI	Particle size [nm]	PDI
control	DBA	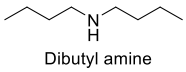 Dibutyl amine (DBA)	bulk	1:1	170	0.087	-	-
NA100	NA	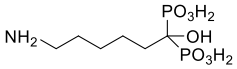 Neridronic Acid (NA)	dispersion	1:1	162	0.108	233	0.230
NA75				4:3	162	0.108	178	0.202
NA50				2:1	162	0.108	170	0.168
NA25				4:1	162	0.108	167	0.161

4.3.3.2. Quantification of the overall P-content of the dispersions

In order to assess the conversion of the functionalization reaction, samples before and after dialysis were freeze-dried and the P-content was measured using ICP-OES. The results thereof are displayed in ***Figure 4.3.6a***. The coupling efficiency is derived from the quotient of measured P contents before and after dialysis.

The results show that, for all NA samples, conversion was moderate with approximately 20%. It is interesting to notice that the conversions of the different NA samples were very similar and showed only a minor trend toward higher conversions with increasing isocyanate to endcap reagent stoichiometry. This observation is rather puzzling as one would expect that the higher the excess of NCO, the higher the conversion. The present results led us to conclude that the endcap reaction does not seem to be limited by the availability of NCO at the interface in the first place, but rather appears to be dominated by the adsorption of the negatively charged endcap reagent to the anionic particles. This is further supported by the rather similar conversions obtained for samples using the alternative method of reagent addition and pH increase in the aqueous phase prior to dispersing (see section 4.3.4). It can further be noted that surprisingly slow reaction kinetics of NCO-functional PUDs with nucleophiles have been observed before from our group, although a quite different system was investigated, namely the preparation of PUDs stabilized with a protein corona.[158] However, the results indicate that with more complex, partially charged endcapping reagents of pronounced hydrophilicity, interfacial adsorption can dominate the reaction. Additionally, macromolecular chain mobility and reorganization phenomena at the interface or inside the colloidal particle should be kept in mind, at least in PUD systems with complex interaction capabilities and a highly segmented block copolymer structure.

4.3.3.3. Quantification of P-groups at the interface

Since the crucial factor for the particles' adhesive behavior is not the bulk composition but rather the composition of the particle-water interface, titration experiments were used to quantify the effective number of interfacial P-groups. Calculations were conducted as described in the literature.[146, 217] As can be seen in ***Figure 4.3.6b***, for the NA100 sample, surface coverage is highest with 2.4 P-groups/nm^2 and decreases to a value of 0.9 P-groups/nm^2 for the NA25 sample. It is highly interesting to notice that for the former sample, only 28 mol% of P-groups were localized at the interface whereas for the latter sample, all of the P-groups are detected there. The result seems surprising, but clearly indicates a considerable spatial requirement of the P-groups and limited compressibility or stacking at the interface. The interfacial interaction between the individual P-groups is supposedly dominated by ionic repulsion, and depending on hydrophobicity, either favors dissolution into water or drives the functional groups inside the droplet. In our systems with only terminal functionalization, the hydrophobicity obviously favors the latter case. Another possible explanation is based on the partial solubility of the endcap reagent in water and in the particles, leading to the molecule's adsorption, and even its migration inside the particles, such that the endcap reaction might also take place there. This phenomenon has previously been observed for the chain extension of PUDs.[50]

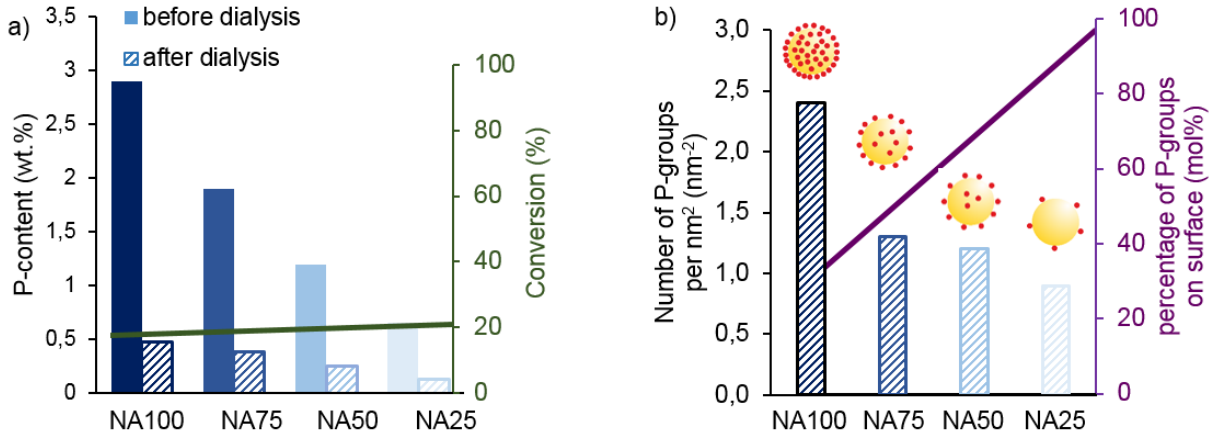

***Figure 4.3.6**: Results of ICP-OES and titration experiments. a) ICP-OES measurements were used to determine the P-content of freeze-dried samples. The conversion was determined from the quotient of the P-content before and after dialysis. All NA samples surprisingly yielded similar conversions. b) The surface coverage per unit area and the percentage of P-groups on the surface were calculated from titration experiments. The percentage of P-groups on the surface was calculated from the surface coverage and the number of P-groups after dialysis. This figure is reproduced from the publication "Phosphonic Acid-functionalized Polyurethane Dispersions with Improved Adhesion Properties" by Laura Breucker, Katharina Landfester, and Andreas Taden, to be published in 2015 in* ACS Applied Matierals & Interfaces, *DOI: 10.1021/acsami.5b06903.[158] Reprinted with permission. Copyright 2015 American Chemical Society.*

4.3.3.4. Effect of the functionalization on film properties

The polymeric backbone of the polyurethane particles was designed to be rather complex. Polyester segments capable of crystallizing were included in order to provide a temperature-induced change in modulus. Indeed, the incorporation of crystalline moieties is a well-known method to provide a reversible setting mechanism in the film.[45, 70] Furthermore, as was described in section 2.5, since crystallization in the film is strongly dependent upon polymer composition and separation between hard and soft segments in PUs, an analysis of the heat flow diagrams often gives valuable information about the film composition.[158]

As can be seen in ***Figure 4.3.7***, melting transitions can be observed in all four phosphonic-acid functionalized samples with melting enthalpies ranging from 20 J/g to 28 J/g. Strikingly, melting enthalpies are reduced by a factor of 2 approximately in phosphonic acid-functionalized samples as compared to the control sample. Furthermore, as can be seen in the heat flow diagram, the melting range is shifted from 55 °C to much lower temperatures ranging from ca. 40 °C to 50 °C and the

overall melting peak is much broader. We therefore concluded that the phosphonic acid groups greatly hinder crystallization, leading to the formation of smaller crystalline structures.

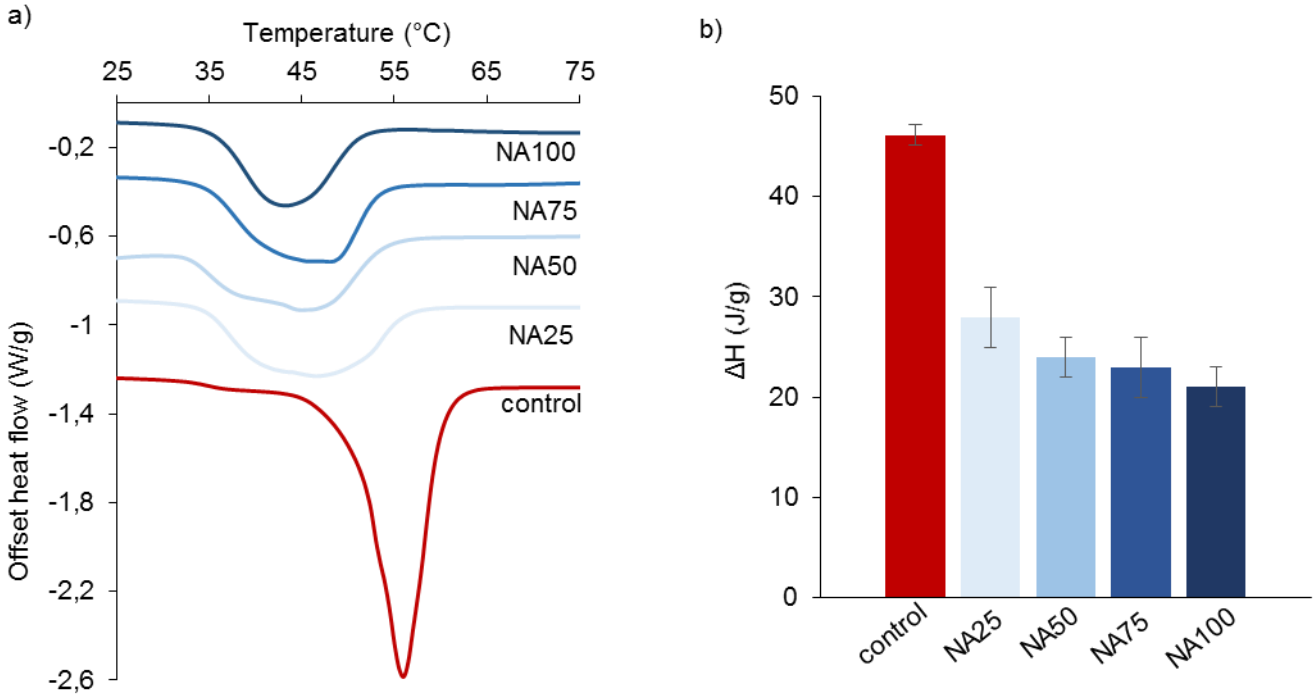

***Figure 4.3.7**: DSC results consisting of a) heat flow curves as a function of temperature and b) melting enthalpies of crystalline domains. Values are averages from three separate measurements and error bars represent the standard deviation. Results indicate a strongly modified crystallization behavior due to phosphonic acid-functionalization with an overall decrease in crystallinity and a broader melting range shifted to lower temperatures. This figure is reproduced from the publication "Phosphonic Acid-functionalized Polyurethane Dispersions with Improved Adhesion Properties" by Laura Breucker, Katharina Landfester, and Andreas Taden, to be published in 2015 in* ACS Applied Matierals & Interfaces, *DOI: 10.1021/acsami.5b06903.[158] Reprinted with permission. Copyright 2015 American Chemical Society.*

4.3.3.5. Substrate interactions

In order to assess the adhesive behavior of the P-PUDs, QCMD measurements on HAP and SS2343, as model substrates were conducted and results thereof are displayed in ***Figure 4.3.8-9***. The figures also show the general principle behind a QCMD measurement. The sensors are first rinsed with the liquid matrix (DI water in this case) until a steady state is reached. This step ensures that no adsorption or desorption events of pollutants from the tubes or from the sensors occur during a measurement. Secondly, the dispersions to be analyzed are measured. In the case of a strong

interaction with the surface, many particles adsorb to the surface, leading to a pronounced frequency shift. In the last step, the sensors are again rinsed with the liquid matrix (DI water) in order to assess whether the adsorption observed previously is reversible in the conditions used. In the case of a strong particle-surface interaction, few particles desorb and when a steady state is reached, many particles remain deposited on the surface.

In ***Figure 4.3.8***, it can be seen that the control sample without P-functionalization shows a very weak adhesion to HAP, reflecting in a frequency shift of only about -4 Hz and a strong desorption after rinsing such that almost no frequency change is detected. For all P-PUDs, on the other hand, an 8 to 10-fold higher frequency shift is observed. The highest adsorption could be measured with the NA100 sample with a frequency shift of -40 Hz. In general, the more NA was used for functionalization, the higher was the affinity for HAP. With respect to the discussion above on the quantification of P-groups at the interface of the particles, this result indicates that, upon adsorption from aqueous dispersion, significant PU chain rearrangements take place, because a large fraction of the phosphorous functionalities are expected to be buried inside the P-PUD particle. It can also be noted that a pronounced increase in dissipation (ΔD) was measured which indicates that the adsorbed layer was rather viscoelastic. Furthermore, a decrease of the dissipation values during rinsing also points towards a strong interaction between the adsorbed layer and the surrounding bulk phase. Overall, the QCMD results correlate well with the surface coverage of the particles and it can be concluded that the improved adhesive behavior is indeed due to the P-functionalization.

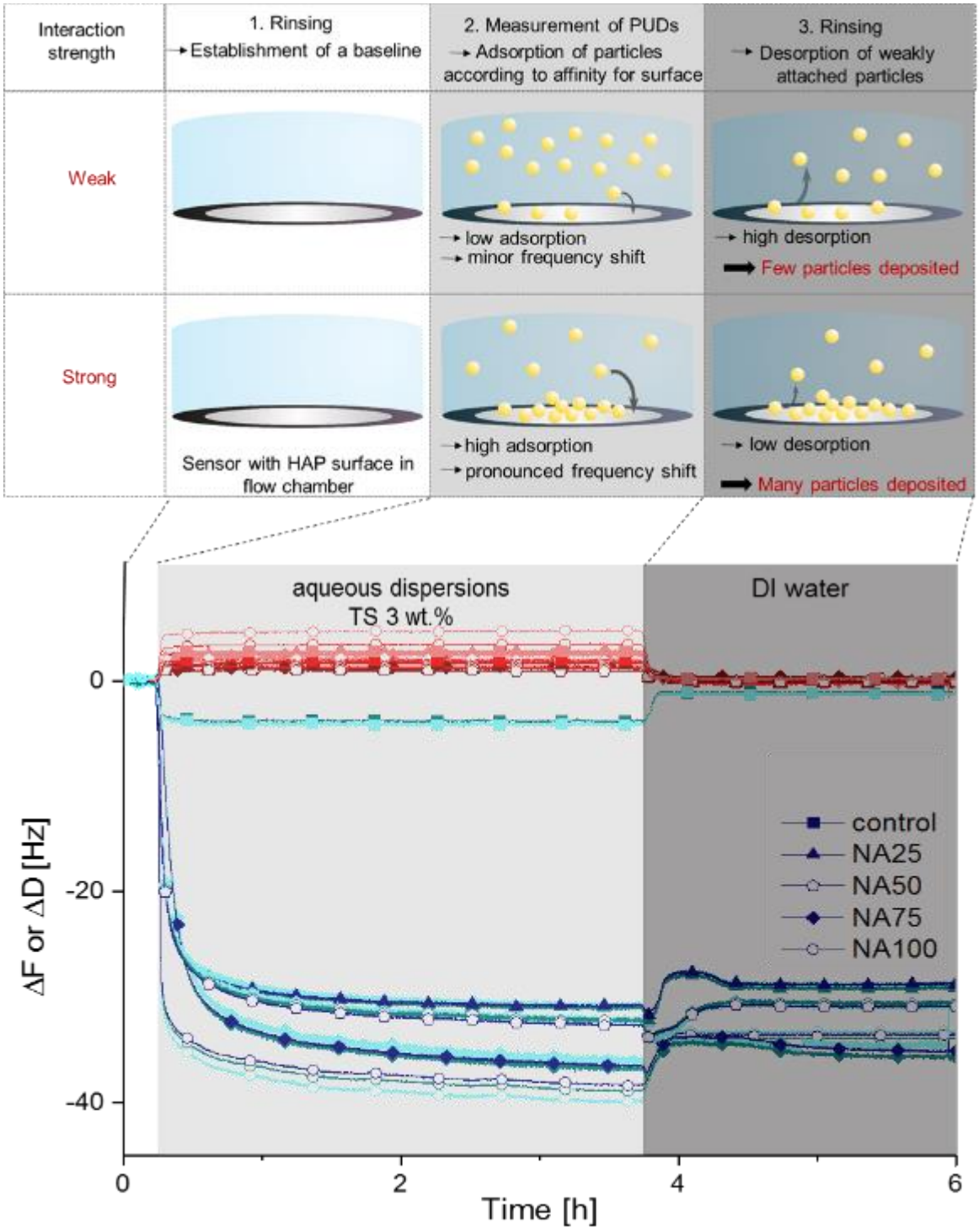

***Figure 4.3.8**: QCMD results of dispersions on HAP-coated sensors. The samples with NA endcap show strongly improved adhesion compared to the control sample. Overall, P-functionalization greatly improved the affinity for HAP.* *This figure is reproduced from the publication "Phosphonic Acid-functionalized Polyurethane Dispersions with Improved Adhesion Properties" by Laura Breucker, Katharina Landfester, and Andreas*

Taden, to be published in 2015 in ACS Applied Matierals & Interfaces, *DOI: 10.1021/acsami.5b06903.*[158] *Reprinted with permission. Copyright 2015 American Chemical Society.*

Similarly, ***Figure 4.3.9*** shows the QCMD results of the various NA-PUDs on stainless steel surfaces. It can be seen that a frequency shift of only about -10 Hz is observed for the control sample, which is indicative of a rather weak affinity for SS2343. In comparison, the adhesion of the P-PUDs is much stronger with frequency shifts ranging from -40 to -50 Hz. As in the case of HAP surfaces, the general trend of an increased affinity with an increase in NA used in the synthesis also holds true on stainless steel. However, during the adhesion step, the differences between the different NA samples are rather small, merely the NA25 sample shows a significantly lower adhesion than the other P-PUDs. Interestingly, upon rinsing, the resultant frequency shifts indicate a clearer separation of the samples, again shown through the adhesion increasing with the amount of NA used for the functionalization. It can again be noted that in all samples, a pronounced increase in dissipation was observed which is characteristic of a viscoelastic layer and that a return to very small dissipation values can be noted during the rinsing step which points towards a good interaction between the adsorbed layer and the dispersion flowing over the sensor. We can therefore see in ***Figure 4.3.9*** that the P-PUDs synthesized in this section can very well be used for improved adhesion to stainless steel, the traditional area of application of phosphonic acid-functionalization.

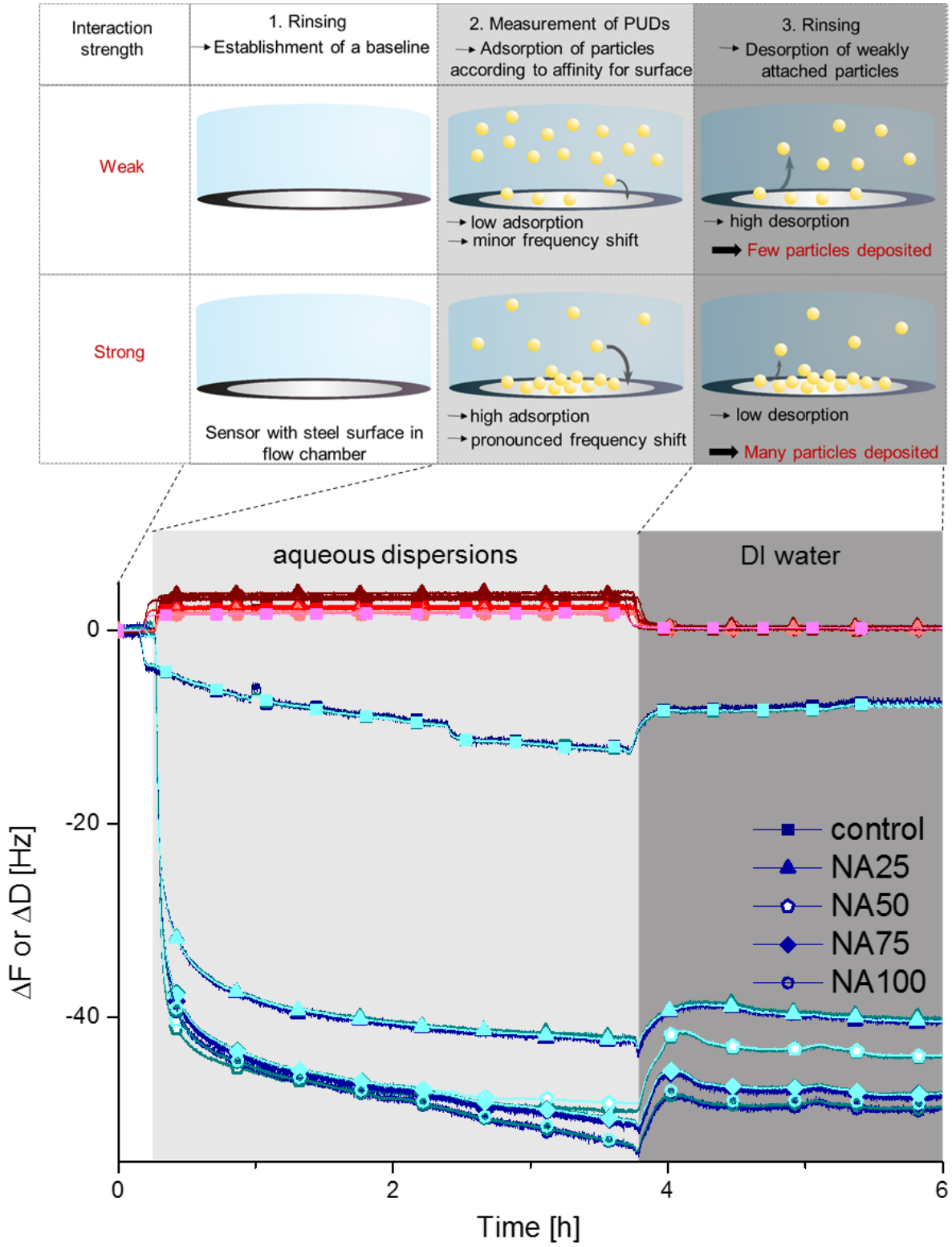

***Figure 4.3.9**: QCMD results of dispersions on SS2343-coated sensors. The samples with NA endcap show a much improved adhesion compared to the control sample. As observed on HAP, P-functionalization greatly improved the affinity for SS2343. This figure is reproduced from the publication*

"Phosphonic Acid-functionalized Polyurethane Dispersions with Improved Adhesion Properties" by Laura Breucker, Katharina Landfester, and Andreas Taden, to be published in 2015 in ACS Applied Matierals & Interfaces*, DOI: 10.1021/acsami.5b06903.*[158] *Reprinted with permission. Copyright 2015 American Chemical Society.*

4.3.4. Method B to obtain P-PUDs

The results presented in this section derive from the above-termed Method B where the NCO-reactive prepolymer is dispersed in alkaline solutions of the endcapping reagents NA or AMPA. The pH of the respective reagent solution is adjusted to 11 for AMPA and to 12 for NA in order to allow for the reaction to take place during the dispersing step. Lastly, dialysis is conducted for desalting.

4.3.4.1. Colloidal stability of the dispersions

As can be seen in ***Table 4.3.10***, before dialysis, the z-average particle size for the AMPA sample was 235 nm with a PDI of 0.223. The z-average particle size for the NA sample was 201 nm with a PDI of 0.167. Compared to the P-PUD preparation using Method A, larger particle sizes and broader size distributions were observed in case of NA, which can be attributed to a significantly increased salt concentration/ionic strength during the homogenization step which weakens the colloidal stabilization by reduced electrostatic repulsion. Furthermore, an influence of the covalent endcapping reaction and side reaction with water leading to chain extension cannot be excluded. The overall increase in molecular weight as well as specific interactions between phosphonic acid groups may additionally hinder particle formation.

After dialysis, the measured z-average particle sizes and distributions were 257 nm with a PDI of 0.253 for NA, and 311 nm with a PDI of 0.182 for AMPA, respectively. The increase in both z-average size and PDI can be attributed to minor coagulation occurring due to the high salt concentration (as was also observed with Method A, see section 5.3.3.1). Despite the fact that the obtained results are inferior to those with the method described previously, we can conclude that this approach still yielded stable nanoparticles.

Table 4.3.10*: DLS measurements before and after dialysis for the P-PUDs based on NA and AMPA following Method B. The increase in particle size and PDI can be attributed to minor coagulation due to high salt concentrations.* *This table is reproduced from the publication "Phosphonic Acid-functionalized Polyurethane Dispersions with Improved Adhesion Properties" by Laura Breucker, Katharina Landfester, and Andreas Taden, to be published in 2015 in* ACS Applied Matierals & Interfaces*, DOI: 10.1021/acsami.5b06903.*[158] *Reprinted with permission. Copyright 2015 American Chemical Society.*

Sample name	Chemical formula of endcap reagent	endcap in...	Stoichiometry n(NCO)/ n(reagent)	before dialysis		after dialysis	
				Particle size	PDI	Particle size	PDI
AMPA	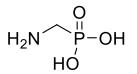 Aminomethyl phosphonic acid (AMPA)	dispersion	1:1	235 nm	0.223	257 nm	0.253
NA	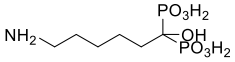 Neridronic Acid (NA)	dispersion	1:1	201 nm	0.167	311 nm	0.182

4.3.4.2. Quantification of the overall P-content of the dispersions

In order to assess the conversion of the endcap reaction for both reagents, samples before and after dialysis were freeze-dried and the P-content was measured using ICP-OES. The results thereof are displayed in ***Figure 4.3.11a***. It can be seen that the conversion for the NA sample is almost three times higher than for the AMPA sample. This may be attributed to a more hydrophobic structure of NA due to its longer alkyl chain. The driving force towards the interface between the aqueous phase and the forming particle is thus higher and the endcap conversion is as well.

4.3.4.3. Quantification of P-groups at the interface

These samples were also characterized using titration experiments to calculate the surface coverage of the particles and the percentage of the attached P-groups localized at the interface (see ***Figure 4.3.11b***). The calculated values are very high with 1.0 P-groups/nm^2 for the AMPA sample and 2.8 P-groups/nm^2 for the NA sample. However, taking into consideration that for the AMPA sample, 83 mol% of attached P-groups are localized at the interface whereas for the NA sample, the value is much smaller with 29 mol%, we drew the same conclusions as in section 4.3.3.3. NA reacts more readily than AMPA, leading to a higher conversion. However, the particle surface is very densely covered with P-groups, forcing a large majority of the attached groups inside the particles.

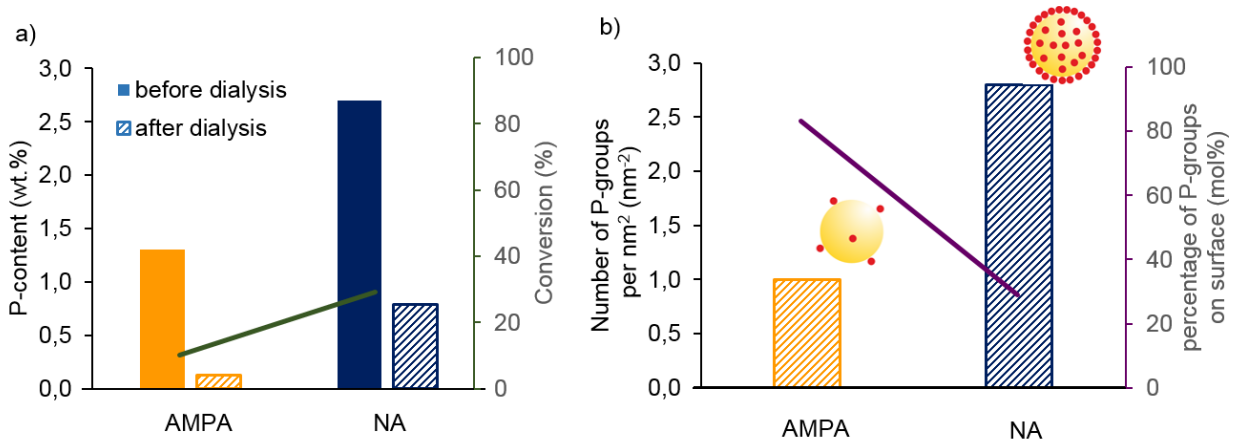

***Figure 4.3.11**: Results of ICP-OES measurements of the P-content of freeze-dried samples and results of PCD measurements of the dispersions. a) The conversion (green line) was determined from the quotient of the P-content before (solid columns) and after dialysis (striped columns) for AMPA (in orange) and NA (in blue). The coupling efficiency is higher for the NA sample which can be attributed to its more hydrophobic structure. b) The surface coverage per unit area (striped columns) and the percentage of P-groups on the surface (purple line) were calculated from titration experiments. The percentage of P-groups on the surface was calculated from the surface coverage and the number of P-groups after dialysis. This figure is reproduced from the publication "Phosphonic Acid-functionalized Polyurethane Dispersions with Improved Adhesion Properties" by Laura Breucker, Katharina Landfester, and Andreas Taden, to be published in 2015 in* ACS Applied Matierals & Interfaces, *DOI: 10.1021/acsami.5b06903.*[158] *Reprinted with permission. Copyright 2015 American Chemical Society.*

4.3.4.4. Effect of the functionalization on film properties

In the same way as for functionalization using Method A, changes in the PU composition can be expected to affect the crystallization behavior of the PTMA segments. As can be seen in ***Figure 4.3.12***, melting transitions can be observed in both phosphonic-acid functionalized samples. The measured enthalpies are again much lower than that of the control of 46 J/g. However, it is interesting to note that the melting enthalpy of the NA sample of 18 J/g is drastically lower than that of the AMPA sample of 35 J/g. Furthermore, whereas melting occurs in a temperature range of 45 °C – 60 °C for the AMPA sample, the melting range of the NA sample is broader and shifted to much lower values (35 °C - 55 °C). The results are in concurrence with the trends presented previously (see section 4.3.3.4): overall, the phosphonic acid groups greatly hinder crystallization, leading to the formation of smaller crystalline structures. But, whereas for the dispersions functionalized with Method A, melting regimes and enthalpies were very similar, we observed here that low concentrations of P-groups (0.13 wt% P detected in the AMPA sample) affect crystallization

much less than higher concentrations (0.79 wt% P detected in the NA sample). Also, interestingly, although the NA25 sample from section 4.3.3.4 contains the same amount of P-groups as the AMPA sample, the crystallization of the bisphosphonate sample is much more affected. We can therefore also conclude that bisphosphonates generally affect crystallization more than single phosphonic acids.

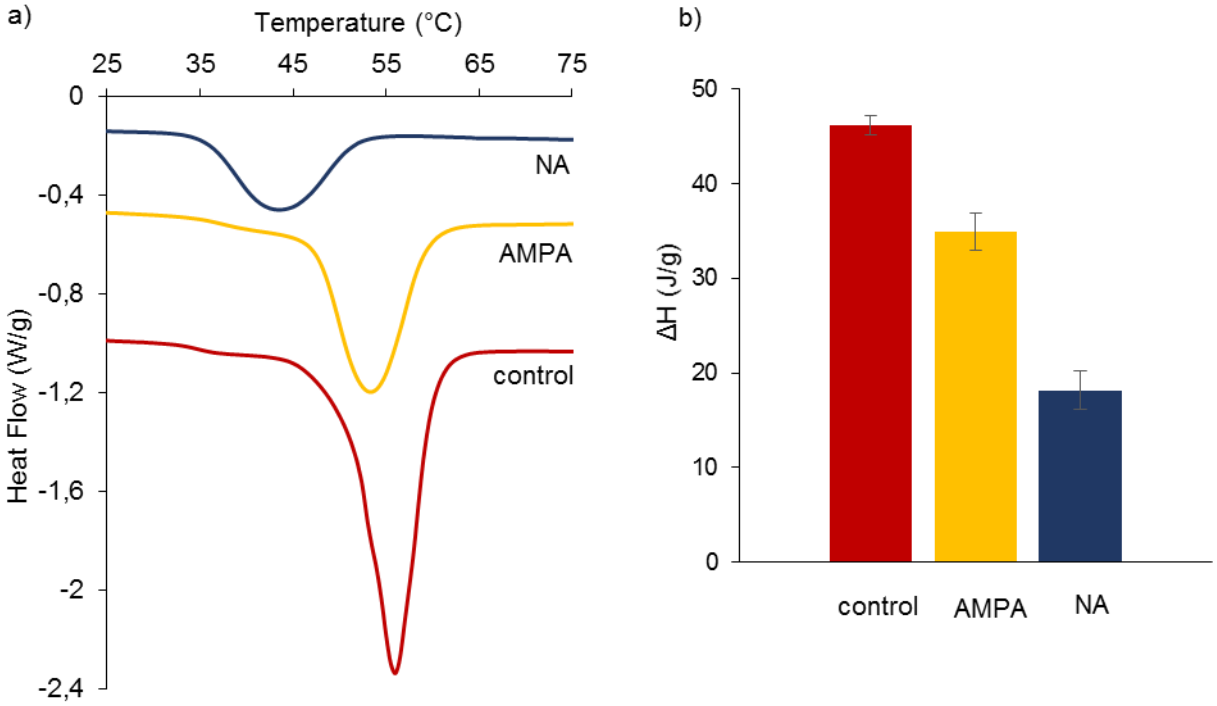

***Figure 4.3.12**: DSC results consisting of a) heat flow curves as a function of temperature and b) melting enthalpies of crystalline domains. Values are averages from three separate measurements and error bars represent the standard deviation. Results indicate a strongly modified crystallization behavior due to phosphonic acid functionalization with an overall decrease in crystallinity and a broader melting range shifted to lower temperatures. This figure is reproduced from the publication "Phosphonic Acid-functionalized Polyurethane Dispersions with Improved Adhesion Properties" by Laura Breucker, Katharina Landfester, and Andreas Taden, to be published in 2015 in* ACS Applied Matierals & Interfaces, *DOI: 10.1021/acsami.5b06903.[158] Reprinted with permission. Copyright 2015 American Chemical Society.*

4.3.4.5. Substrate interactions

In order to assess the effect of the P-functionalization on the adhesive behavior of the dispersions, QCMD measurements on HAP surfaces were conducted and results thereof are displayed in ***Figure 4.3.13***. The graph shows that both P-PUDs show much higher adhesion to HAP than the control sample. Surprisingly, despite their drastically different surface coverage, both P-PUDs seem to show

rather similar adhesive behavior. This may be attributed to a polyelectrolyte effect weakening the interactions between individual P-groups and the interface. In any case, it should be noted that the results of ***Figure 4.3.13***, despite the drastically increased interaction, are inferior to those presented previously (see section 4.3.3.5). For this reason, this method was not further pursued and QCMD measurements on other model substrates (in particular SS2343) were not performed.

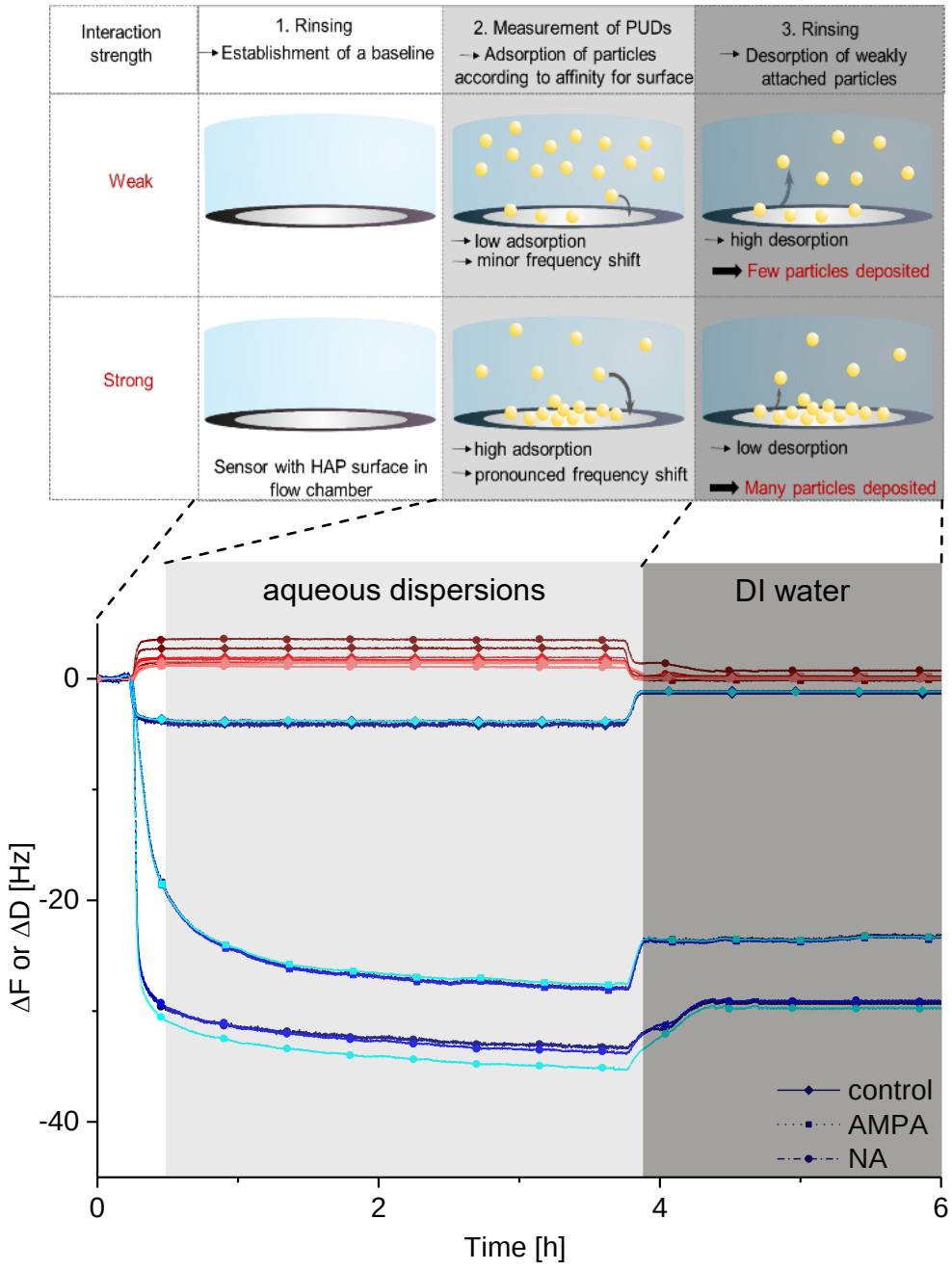

***Figure 4.3.14**: QCMD results of dispersions on HAP-coated sensors. It can be concluded that sample with NA endcap showed the strongest adhesion and that the control sample showed the weakest*

adhesion. Overall, P-functionalization greatly improved the affinity for HAP. However, the results presented here are slightly inferior to those presented with Method A. *This figure is reproduced from the publication "Phosphonic Acid-functionalized Polyurethane Dispersions with Improved Adhesion Properties" by Laura Breucker, Katharina Landfester, and Andreas Taden, to be published in 2015 in* ACS Applied Matierals & Interfaces, *DOI: 10.1021/acsami.5b06903.*[158] *Reprinted with permission. Copyright 2015 American Chemical Society.*

4.3.5. Conclusion

In this section 4.3, we provide two facile routes to phosphonic acid-functionalized polyurethane dispersions with drastically improved adhesion properties. The functionalization is achieved *via* a heterophase endcapping process, *i.e.* the reaction of amino-group carrying (bis)phosphonic acid derivatives with NCO-reactive polyurethane particles in aqueous dispersion. The synthetic approach is not limited to a certain polyurethane composition and circumvents solubility issues of the reaction partners. However, the process is certainly affected by various parameters like pH, ionic strength, reaction time, or stepwise reagent addition. Different reaction conditions and endcapping reagents were evaluated. The first subsection (section 4.3.3) describes the results obtained from the preferred procedure with neridronic acid as encapping reagent and different functionalization degrees and the second subsection (section 4.3.4) describes results obtained using neridronic acid and aminomethyl phosphonic acid. The dispersions were first characterized based upon their particle size and size distribution using light scattering and showed high colloidal stability after dialysis. Dialysis was used to separate any non-attached phosphorus-containing reagents, which constitutes a prerequisite to determining the conversion of the endcap reaction. The latter was shown to depend on the nature of the endcapping reagent. However, it was surprisingly observed that the conversion is almost independent of the stoichiometry for reaction, which points toward an adsorption-dominated process at the interface. This hypothesis is supported with calculations of the surface coverage using titration experiments. It is shown that a maximum surface coverage of 2.4 groups/nm^2 is attained, but only at the expense of forcing the majority of the attached groups inside the particles. Furthermore, the surface coverage and the overall functionalization degree are shown to reflect in the adsorption to hydroxyapatite, utilized as model substrate in quartz crystal microbalance measurements. The experimental data reveal drastically improved adsorption behavior of the P-PUDs, and additionally indicate polymer chain rearrangements and film formation even under wet conditions. We believe this work to be of great value for many applications due to, on the one hand, the great industrial importance of phosphorous-functional dispersions obtained from free radical emulsion polymerization. On the other hand, typical "high performance" polyurethane properties are attainable with our synthetic approach because the latter is not limited to a specific PUD composition. The high degree of synthetic freedom in combination with the

simplicity and control of the functionalization can therefore be seen as a step towards improved waterborne, environmental benign polyurethane coatings and contributes to further close the performance gap compared to classical, solvent-borne systems.

5. Conclusion and Outlook

The present thesis describes the functionalization of polyurethane dispersions in order to provide specific interactions with three model surfaces, namely hair, stainless steel, and hydroxyapatite. Three types of functionalizations are accomplished and the resultant systems are analyzed and described.

For the first project (section 4.1), peptide-functionalized polyurethane dispersions are synthesized using a hydrolyzed protein from wool. On the one hand, this part of the work demonstrates the usefulness of hydrolyzed proteins for the synthesis of peptide-decorated nanoparticles, and it shows on the other hand how those hydrolyzed proteins can be used in order to confer interesting properties to dispersions and films. The peptides are used as sole stabilizing entity for the particles and hence also permit to introduce a pH-triggered coagulation to the system. Furthermore, the peptides strongly influence the polyurethane film properties by affecting the partial crystallization. In order to demonstrate the usefulness of the peptide-decorated polyurethane dispersions for hair care applications, first results concerning the adhesion and film formation on hair substrates are presented. We believe this project to be of great interest for commercial applications (for protection of the hair fiber against heat and radiation, to reconnect split ends, *etc.*, and to allow for a reversible shaping of the hair) and such investigations are currently underway.

For the second project (section 4.2), an alternative, rather more traditional route to peptide-functionalized particles is presented. In this case, a single peptide sequence is used which was screened from a library of peptides for its affinity for stainless steel surfaces. The coupling of the peptide to the dispersions is conducted in a very well-defined manner using a cysteine-maleimide reaction and a detailed analysis of the coupling reaction is provided. An important aspect of the project is the effect of coupling the cationally charged peptide to the anionically stabilized particles and investigations pertaining to the particle stability are presented. Ultimately, the affinity of the hybrid particles for stainless steel surfaces is shown. Consequently, we believe this project to be useful for ecofriendly adhesives for stainless steel, for instance for the construction or automotive industries.

In the last project, phosphonic acid-functionalized PUDs are synthesized using two different functionalization methods and two types of phosphonic acid-containing reagents. The resultant particle compositions are characterized and the particle interface in particular is analyzed. Although phosphonic acids are well-known adhesion promoters for stainless steel and although the particles synthesized here are also shown to be interesting in that regard, an intention in this project was to

also obtain dispersions with a high affinity for hydroxyapatite surfaces. The latter property is proven and we therefore believe this project to be valuable for adhesives or other materials in the fields of orthopedics and dentistry.

Overall, the three projects constituting this thesis show the large degree of variability in the synthesis of polyurethane dispersions for adhesive properties to a wide variety of different substrates. We thereby demonstrate that such an ecofriendly system can be rendered very complex in order to further extend the field of sustainable materials for demanding applications.

6. Experimental Part

This chapter will provide information on the raw materials used in the syntheses (section 6.1) and describe the experimental procedures and techniques used in each project (sections 6.2-6.4).

6.1. Raw materials

Name	Abbreviation	Trade name	Supplier
(3-((3-cholamidopropyl) dimethylammonio)-1-propanesulfonate)	CHAPS		Thermo Fischer
5,5'-dithiobis-(2-nitrobenzoic acid)	DTNB	Ellman's reagent	Sigma-Aldrich
Acetone (anh.)			Roth
Aminomethyl phosphonic acid	AMPA		Solvay P&S
BCA reagents			Roth
Bromophenol blue			Sigma-Aldrich
Catalyst (dimethyl tin neodecanoate)		Fomrez UL-28	Momentive
Defoamer		Foamaster 223	BASF GmbH
Dibutyl amine	DBA		Merck
Dithiothreitol	DTT		Sigma-Aldrich
Ethanol			Sigma-Aldrich
Ethyl acetate (anh.)	EA		Roth
Hydrochloric acid	HCl		Roth
Hydrogen peroxide (30% solution)			Sigma-Aldrich
Hydrolyzed protein from wool		Keratec IFP PE	Croda
Hydroxyethyl maleimide	HEMI		Chongoing Werlchem
Isophorone diisocyanate	IPDI		Sigma-Aldrich
Lithium citrate buffer			Sigma-Aldrich
Molecular sieve 3Å			Roth
N-acetyl-L-cysteine	ACC		Alfa Aesar
Neridronic acid	NA		Solvay P&S
N-Hydroxyethyl maleimide	HEMI		Chongoing Werlchem
Nitric acid			Roth
Poly(dimethyl siloxane)	PDMS	Tegomer H-Si 2311	Evonik Industries
Poly(oxypropylene, oxyethylene) glycol	PPOE-1	K-HN-8200	Hannong Chemicals
Poly(oxypropylene, oxyethylene) glycol	PPOE	Tergitol L-61	Dow Chemical
Polydiallyldimethylammonium chloride	PDADMAC		Roth
Polyester resin	PTMA	Realkyd XTR 20112	Arkema Coatings Resins
Potassium dihydrogen phosphate			Roth
Potassium hydrogen phosphate			Roth

SDS-PAGE buffers and reagents			Thermo Fischer
Sodium acetate	NaOAc		Alfa Aesar
Sodium chloride	NaCl		Roth
Sodium hydroxide solution	NaOH		Roth
Steel-binding peptide			Thermo Fischer
Sulfonated glycol	SPPO	SG	Yedang G&B
tert-butylcatechol			Aldrich
Tetrahydrofuran	THF		Roth
Tris buffer solution			Millipore S.A.S.
Urea			Sigma-Aldrich

6.2. PUDs for unspecific coupling of a hydrolyzed protein

6.2.1. Synthesis of PU prepolymer

A prepolymer with a theoretical M_n of 8 000 g/mol was synthesized. PPOE (25.00 g ; 11.36 mmol), PTMA (70.44 g ; 33.54 mmol), and PDMS (125.0 g ; 56.82 mmol) were heated to 80 °C until molten, then vacuum (P < 0.1 mbar) was applied for 1 h to remove traces of water. N_2 was fed into the flask and the temperature was allowed to drop to 70 °C. IPDI (29.56 g ; 133.1 mmol) was added. Under nitrogen atmosphere and reflux, 0.02 g of catalyst (50 wt% in dried ethyl acetate) were added. After the initial increase in temperature, the reaction was carried out at 80 °C. The NCO content was checked every half hour according to ISO 14896:2009-07 Method A until it had reached the theoretical residual value of 1.05% (2 h).

6.2.2. Partial dibutyl amine endcap

The prepolymer was split into two flasks, containing 125 g each. Dibutyl amine (DBA) was added slowly to one flask in order to react with the residual NCO groups (approximately 4.045 g ; 31.25 mmol). The reaction was followed using FTIR and the DBA-endcapped prepolymer was characterized using GPC.

6.2.3. Fourier transform infrared spectroscopy

Fourier transform infrared (FTIR) spectroscopy measurements were taken using an Alpha FT-IR Spectrometer from Bruker Optik GmbH, Ettlingen Germany. It was operated in Platinum ATR single reflection diamond module. Aliquots of the polymer melt were taken and measured directly.

6.2.4. Gel permeation chromatography

Gel permeation chromatography (GPC) measurements of the macrodiols and of the DBA-endcapped prepolymer were carried out in THF at 40 °C according to DIN 55672-1 using APC XT Columns 450 A, 125 A, and 45 A from the Waters Corporation, Milford, MA, USA. APC RI-detectors were used and molecular weights were determined by using narrowly distributed polystyrene standards from PSS Polymer Standards Service GmbH, Mainz, Germany.

6.2.5. Nuclear magnetic resonance spectroscopy

^{13}C Nuclear magnetic resonance (NMR) spectroscopy measurements were carried out in $CDCl_3$ using a 600 MHz Agilent spectrometer (Agilent Technologies, Santa Clara, CA, USA). 5 000 scans were performed at 25 °C to generate the spectrum.

6.2.6. Dispersing

Both prepolymers were treated identically. For each one, dried ethyl acetate (125 g) was added under vigorous stirring and reflux and the temperature was allowed to drop to 40 °C. From the prepolymer solution, four batches of 35.5 g each were taken. To each solution, one drop of defoamer was added. Three solutions of peptide were prepared containing 0.71 g, 1.06 g, and 1.42 g of peptide (corresponding to 4, 6, and 8 wt% relative to PU prepolymer, respectively) and deionized water was added to each for a total respective mass of 70.0 g. For the negative control, 70.0 g of deionized water were prepared. The prepolymer solutions and the peptide solutions were heated to 40 °C. Dispersions were formed using an UltraTurrax (T25 basic from IKA Labortechnik, Staufen, Germany) operating at 13 000 rpm for 10 min. Each dispersion was then passed four times through a homogenizer (M-110Y Microfluidizer from Microfluidics, Newt.on, USA) containing two chambers of 400 µm and 200 µm diameter and operating at a pressure of 6 bar.

6.2.7. Dialysis

In order to separate the non-attached peptides from the PUDs, dialysis was performed after dispersion for both the reactive and the nonreactive dispersions. A dialysis membrane from cellulose ester with a molecular weight cut off (MWCO) of 100 kDa was obtained from Carl Roth GmbH & Co. KG, Karlsruhe, Germany. Each piece of membrane was filled with 40.0 g of the dispersions (containing 0 wt%, 4 wt%, 6 wt% or 8 wt% peptide) and closed off with clamps. Dialysis baths each containing 4.00 l of deionized water were prepared and dialysis was carried out for one week in

total. The dialysis water was changed after 1.5 h, 3 h, 18 h, 66 h, and 168 h (1 week). Samples of the dialysis water were held back in order to permit quantifying the peptide flushed out.

6.2.8. Sodium dodecyl sulfate polyacrylamide gel electrophoresis

For sodium dodecyl sulfate polyacrylamide gel electrophoresis (SDS-PAGE), 10 µg of the hydrolyzed protein was mixed with 4x NuPAGE LDS Sample Buffer and 10x NuPAGE Sample Reducing Agent and loaded onto a NuPAGE 10% Bis-Tris Protein Gel. The electrophoresis was carried out in NuPAGE MES SDS Running Buffer at 150 V for 1.5 h. As a molecular marker SeeBlue Plus2 Pre-Stained Standard was run in parallel. Proteins were visualized with SimplyBlue SafeStain. Buffers, gel, standard and stain were all obtained from Thermo Fisher Scientific, Waltham, MA, USA.

6.2.9. Isoelectric focusing

The isoelectric focusing (IEF) experiment was conducted in a similar manner as described in the literature.[228] 100 µg peptide was diluted in 500 µl rehydration buffer containing 8 M Urea, 3 mg/ml DTT, 4% (w/v) CHAPS, 0.001% (w/v) Bromophenol blue and 2% (v/v) ampholytes (Servalyt 3-10, SERVA Electrophoresis GmbH, Heidelberg, Germany). The sample was loaded onto an immobilized pH gradient (IPG) strip (SERVA IPG BlueStrip 3-10, 24 cm, SERVA Electrophoresis) by overnight passive in-gel rehydration at 20 °C. The rehydrated strip was focused using an IEF100 isoelectric focusing unit (Hoefer Inc., Holliston, USA) at 20 °C under a layer of Immobiline DryStrip Cover Fluid (GE Healthcare, Solingen, Germany). For improved sample entry, initial voltage was limited to 500 V for 3 h, 1000 V for the next 3 h, and then increased with a gradient up to 5000 V using a total of 50 000 V/h. After IEF the strip was fixed with 20% (v/v) trichloroacetic acid and stained with SimplyBlue SafeStain (Life Technologies, Carlsbad, USA).

6.2.10. Laser diffraction

Laser diffraction (LD) measurements were carried out using a Horiba LA-950 Particle Analyzer (Retsch Technology GmbH, Haan, Germany). Samples from each synthesis (using 4 wt%, 6 wt%, and 8 wt% peptide) prepared with a reactive and a nonreactive dispersion were measured three times every week for one month after synthesis according to ISO 13320. Particle size distribution results are reported as percentages given at the respective mean volume averages.

6.2.11. Bicinchoninic acid assay

To perform the Bicinchoninic acid (BCA) assay, 50 ml samples from each batch of dialysis water (1.5 h, 3 h, 18 h, 42 h, 66 h, 168 h) from each synthesis (0 wt%, 4 wt%, 6 wt%, and 8 wt% peptide) for both the reactive and the nonreactive dispersion were freeze-dried and redissolved in 500 µl of deionized water. The same was done with control samples containing 1.25×10^{-3} wt%, 2.50×10^{-3} wt%, 7.50×10^{-3} wt%, 1.5×10^{-2} wt%, 3.0×10^{-2} wt%, 7.50×10^{-2} wt%, and 1.0×10^{-1} wt% peptide in deionized water. The BCA solution was prepared by adding 50 ml of reagent 1 and 1 ml of reagent 2 from a BCA kit (Carl Roth GmbH & Co. KG, Karlsruhe, Germany). Of each solution to be analyzed, three times 25 µl were taken and poured into a 96-well plate. 200 µl of working reagent were added and the plates were incubated at 40 °C for 45 min. Fluorescence intensity was measured at 590 nm using a Tecan M1000 infinite plate reader (Tecan Group Ltd., Männedorf, Switzerland).

6.2.12. High-pressure liquid chromatography

High-pressure liquid chromatography (HPLC) measurements were conducted in order to elucidate the amino acid composition of the peptides recovered after dialysis. 7.66 mg of each sample after freeze-drying was hydrolyzed in acidic medium and ion exchange chromatography was performed as described in the literature.[34] Peptides were dissolved in 5 ml of lithium citrate buffer pH 2.2 and diluted 1:5 (v/v) prior to the measurement.

6.2.13. Zeta potential analysis

Zeta potential measurements of samples after dialysis were carried out using a Zetasizer Nano ZS (Malvern Instruments Ltd., Malvern, United Kingdom). Only the samples without peptide were measured right after synthesis because it did not remain stable thereafter.

6.2.14. Turbidity-titration

For turbidity-titration experiments, the 8 wt% peptide reactive dispersion after dialysis was diluted to a solid content of 3 % and titrated using 2 M NaOH and HCl solutions. Turbidity measurements were carried out using a 662 photometer from Metrohm Lt., Herisau, Switzerland.

6.2.15. Differential scanning calorimetry

For differential scanning calorimetry (DSC) experiments, films were cast from the reactive and the nonreactive dispersions containing 4 wt%, 6 wt%, and 8 wt% of peptide, and from the reactive

prepolymer before dispersion formation. The films were stored at 70 °C for 1 h, then at 5 °C for 1 h, and at 40 °C for 3 days in order to permit for melting of crystalline domains, crystal nucleation and growt.h, respectively. DSC was conducted with a Universal V4.3A (TA Instruments, Wetzlar, Germany). Experiments were performed under nitrogen atmosphere with 6-7 mg of sample in an open-top aluminum crucible with a heating rate of 10 K/min in a temperature range of -30 °C to 120 °C.

6.2.16. Transmission electron microscopy

For transmission electron microscopy (TEM) sample preparation, a drop of the diluted dispersion containing 8 wt% peptide was applied on a carbon-coated grid. Water was evaporated at RT. TEM images were obtained with a Tecnai F20 (FEI Deutschland GmbH, Frankfurt, Germany) operating at an acceleration voltage of 200 kV.

6.2.17. Scanning electron microscopy

For scanning electron microscopy (SEM) sample preparation, bleached European brown hair was coated with the 8 wt% peptide reactive dispersion by waving the hair through the solution for 3 seconds, subsequent rinsing with water and drying at room temperature. Pieces of coated and uncoated hair were then depicted using a field emission microscope (LEO (Zeiss) 1530 Gemini, Oberkochen, Germany) with an acceleration voltage of 10 kV.

6.3. PUDs for specific coupling of peptides

Similarly to the previous section (6.2), FTIR measurements were carried out to follow the endcap reaction (see section 6.2.3), zeta potential measurements were conducted out to assess the charge of the particles (see 6.2.13), films were cast and tempered, and DSC measurements were carried out (see 6.2.15.). Please refer to the corresponding subsections for information on the sample preparation and on the apparatus used.

6.3.1. Synthesis of PU prepolymer

PPOE (4.00 g ; 2.05 mmol), PPOE-1 (4.00 g ; 2.06 mmol), PTMA (76.35 g ; 26.4 mmol), and SG (4.00 g ; 9.41 mmol) were heated to 80 °C until molten, then vacuum (P < 0.1 mbar) was applied for 1 h to remove traces of water. $N_{2(g)}$ was fed into the flask and the temperature was allowed to drop to 70 °C. IPDI (11.66 g ; 52.43 mmol) was added. Under nitrogen atmosphere and reflux, 0.01 g of catalyst were added. After the initial increase in temperature, the reaction was carried out at 80 °C. The NCO content was checked every half hour using the back titration method according to ISO

14896:2009-07 method A until it had reached the theoretical residual value of 1.05% (2 h). Then, the prepolymer was split into two batches of 50.0 g each. To one batch, HEMI was added (8.82 g ; 62.50 mmol, 33 wt% in dried acetone) in excess to react with the remaining NCO groups (*n*(HEMI):*n*(NCO)= 2.5:1) and the successful endcap was confirmed by FTIR. To the other batch, DBA (3.23 g ; 25.00 mmol) was gradually added to react with the residual NCO groups and the successful endcap was again confirmed by FTIR.

6.3.2. Dispersing

Both batches of prepolymer were treated identically and separately. Dried acetone (50 g each) were added to the prepolymers under vigorous stirring and reflux. Twice 300 g of deionized water were heated to 40 °C. Dispersions were formed using an UltraTurrax operating at 11 000 rpm for 5 min. Then, the dispersions were passed through a homogenizer containing two chambers of 400 nm and 200 nm diameter and operating at a pressure of 6 bar.

6.3.3. Dialysis

Dialysis membranes with a MWCO of 100 kDa were obtained from Carl Roth GmbH & Co. KG, Karlsruhe, Germany and used for all dialyses performed for this project. Dialysis was carried out twice: Firstly, the MI-functionalized dispersion and the control dispersion were dialyzed against deionized water for purification. Accordingly, the dispersions were dialyzed for three days directly after synthesis while changing the dialysis water daily. Afterwards, the dispersions were freeze-dried for solid content measurement and DLS measurements were performed. Secondly, the different MI-PUDs and the control dispersion were dialyzed after coupling in order to remove unattached peptide. In this case, dialysis was performed against P-buffer (0.01 M, pH 7.0) overnight and the dialysis water was changed 3 times over that period of time.

6.3.4. Determination of the amount of maleimide at the interface

The maleimide-functionalized dispersion and the DBA-endcapped control dispersion were diluted to a solid content of 1.00 wt%. 726 µl of a 10 mM ACC solution were added to 1.00 g of MI-PUD and to 1.00 g of the control (for a stoichiometry of *n*(SH):*n*(MI) = 3:1) and left to stir for 24 h. The Ellman's test was performed (see section 6.3.7 for details) immediately after addition and after 24 h to measure the residual ACC concentration.

6.3.5. Partial maleimide de-functionalization

Using the determined amount of reactive maleimide (MI) in the dispersion, 2.38 ml or 3.57 ml of a 10 mM ACC solution ($2.38x10^{-5}$ mol or $3.57x10^{-5}$ mol) were added to 2.00 g of MI-PUD (solid content 9.85 wt%) in order to react with 50% or 75% of MI groups, respectively. The obtained dispersions were correspondingly termed MI-PUD(50) and MI-PUD(25).

6.3.6. Coupling of Cysteine-containing peptide to PUD

For coupling, all three dispersions (MI-PUD, MI-PUD(50), and MI-PUD(100)) were diluted to a solid content of 3.54%. 100 mg ($6.06 x10^{-5}$ mol) of peptide were dissolved in 40.4 ml of phosphate-buffer (0.01 M, pH 7.0) for a concentration of 1.5 mM. To 13.47 ml of peptide solution, 1.575 ml of PUD were added such that *n*(MI):*n*(cysteine)=1:1.5. The mixture was allowed to stir for 24 h to permit for coupling to occur. Aliquots were taken after 1 h, 3 h, 6 h, 8 h, and 24 h to follow the reaction using the Ellman's test.

6.3.7. Ellman's test

A DTNB stock solution was prepared containing 2 mM DTNB and 50 mM NaOAc, along with Tris buffer (1 M, pH 8.0), and ACC solutions for calibration of 2.5 mM, 1 mM, 0.5 mM, 0.25 mM, and 0.1 mM). To perform the test, aliquots of 10 µl were taken from the reaction. 50 µl of DTNB stock solution, 100 µl of Tris buffer, and 840 µl of deionized water were added and the solution was incubated for 5 min at room temperature. Then, three 300 µl fractions were taken and put into a 96-well plate for absorption measurements at 412 nm.

6.3.8. Protein charge calculations

Calculations were carried out using the Protein Calculator v3.4.[194]

6.3.9. Dynamic light scattering

Dynamic light scattering (DLS) measurements were performed using a Zetasizer Nano ZS from Malvern Instruments Ltd., Malvern, United Kingdom. Samples were diluted to a solid content of approximately 0.01 wt%. Results are displayed as z-Average values and the related PDI.

6.3.10. Ultraviolet-visible spectroscopy

Absorption measurements at 412 nm were carried out using a Synergy H1 Multi Detection Reader from Bio-tek Instruments GmbH, Bad Friedrichshall, Germany.

6.3.11. Quartz crystal microbalance with dissipation

For quartz crystal microbalance with dissipation (QCMD) measurements, stainless steel sensors were obtained from LOT-QuantumDesign GmbH, Darmstadt, Germany. Prior to use, sensors were cleaned by UV/ozone treatment for 10 min, subsequent immersion in an aqueous SDS solution (2 wt%) for 30 min, rinsing with deionized water and drying under nitrogen gas. Two QCMD measurements were carried out at 20 °C with a flow rate of 50 µl/min by letting first Phosphate-buffer (0.01 M, pH 7.0) flow over the sensor for 1 h. Then, the dispersions (solid content 0.35 wt%) and the peptide solution (0.45 µmol/ml) in Phosphate-Buffer were allowed to flow over the sensor for 1 h, and lastly, the sensor was rinsed with buffer for 2 h.

6.4. P-functionalization of PUDs

Similarly to the previous sections (6.2 and 6.3), FTIR measurements were carried out to follow the endcap reaction with DBA (see section 6.2.3), films were cast and tempered, and DSC measurements were carried out (see 6.2.15). Furthermore, as described in 6.3.9, DLS was used for all dispersions to measure the particle size. Please refer to the corresponding subsections for information on the sample preparation and on the apparatus used.

6.4.1. Synthesis of PU prepolymer

SG (8.00 g; 18.8 mmol), PPOE (8.00 g; 4.21 mmol), PPOE-1 (8.00 g; 3.77 mmol), and PTMA (149.7 g; 51.7 mmol) were heated to 80 °C, and vacuum (P < 0.1 mbar) was applied for 1 h to remove traces of water. N2 was fed into the flask and the temperature was allowed to drop to 70 °C. IPDI (26.33 g; 118.5 mmol) was added. Under nitrogen atmosphere and reflux, 0.020 g of catalyst (50 wt% in acetone) were added. After the initial increase in temperature, the reaction was carried out at 80 °C. Endgroup analysis was utilized to observe the increase of the number average molecular weight, i.e. the NCO content was checked every half hour according to ISO 14896:2009-07 method A until it had reached the theoretical residual value of 1.68% (2 h).

6.4.2. Endcap with dibutyl amine in solution

Once the polymerization was complete, 200 g of acetone (anh.) were added and the temperature was allowed to drop to 40 °C under reflux. The solution was split into two batches of 200 g each. To the first batch, DBA was gradually added (5.16 g; 40.0 mmol) and the endcap was monitored through FTIR (see section 4.3.3 for details). The endcapped prepolymer was then dispersed in water (300 g, 40 °C) using an UltraTurrax (T25 basic from IKA Labortechnik, Staufen, Germany) operating at 11 000 rpm for 5 min. The dispersion was then passed through a homogenizer (M-110Y Microfluidizer from Microfluidics, Newt.on, USA) containing two chambers of 400 µm and 200 µm diameter and operating at a pressure of 6 bar.

The second batch was dispersed in water as described above and the endcap was then performed in dispersion.

6.4.3. Endcap in dispersion

Two synthetic approaches were conducted which differ in the order of pH adjustment and dispersion formation. For Method A, the reactive dispersion was split into four batches of 50.0 g each. NA was added based on the respective (NCO)/(NA) stoichiometry ratios, i.e. 1:1 (5.54 g; 20.0 mmol), 4:3 (4.16 g; 15.0 mmol), 2:1 (2.77 g; 10.0 mmol), and 4:1 (1.38 g; 5.00 mmol). Afterwards, the pH value was increased to pH 12 using concentrated NaOH solution and the dispersions were left to stir for 30 min. For Method B, pH adjustment was conducted prior to dispersion formation and with NA and AMPA as encapping reagents and using a 1:1 stoichiometry of n(NCO):n(endcap reagent).

6.4.4. Dialysis

All dispersions were dialyzed using a cellulose ester membrane with a molecular weight cut off of 30 kDa (Carl Roth GmbH + Co. KG, Karlsruhe, Germany) after synthesis and for an overall period of 1 week against water of decreasing salt concentration using NaCl in order to desalt and to remove any unattached endcapping reagent.

6.4.5. Inductively-coupled plasma optical emission spectroscopy

Inductively-coupled plasma optical emission spectroscopy (ICP-OES) measurements were conducted using a high pressure asher (HPA-S model from Anton Paar GmbH, Graz, Austria) and an ICP spectrometer (model 720 from Agilent Technologies, Santa Clara, CA, USA). 0.2 g to 0.4 g of freeze-dried sample were prepared and 4 ml HNO_3 and 0.2 ml H_2SO_4 were added. The recipient was closed

off tightly and administered into the asher under nitrogen atmosphere. The protocol starting temperature was 25 °C at a pressure of 100 bar, then the temperature was increased to 80 °C isobarically. Over the course of 120 min, the temperature was increased to 300 °C at a maximum pressure of 130 bar and then kept constant for 30 min. Through venting, the temperature was then decreased to room temperature

6.4.6. Particle charge detection

Particle charge detection (PCD) measurements were carried out using a detector (Mütek GmbH, Germany) in combination with a Titrino Automatic Titrator (Metrohm AG, Switzerland). Samples were diluted to a solid content of 0.1 wt% and 10 ml were titrated with the positively charged poly(diallyldimethyl) ammonium chloride (PDADMAC). Calculations of the number of groups on the surface and the surface coverage were done as described in the literature,[217] based upon the average volume of polyelectrolyte from three titration experiments.

6.4.7. Quartz crystal microbalance with dissipation

For quartz crystal microbalance with dissipation (QCMD) measurements, hydroxyapatite and stainless steel sensors were obtained from LOT-QuantumDesign GmbH, Darmstadt, Germany. Prior to use, HAP sensors were cleaned by UV/ozone treatment for 10 min, subsequent immersion in ethanol for 30 min, rinsing with deionized water and drying under nitrogen gas. Stainless steel sensors were cleaned as described in section 6.3.11. Measurements were carried out using a Q-Sense E4 device (Biolin Scientific, Stockholm, Sweden). Measurements were conducted at 20 °C and a flow rate of 50 µl/min. After establishment of a stable baseline, the dispersions (solid content 3 wt%) were allowed to flow through the system for 3 h 30 min. Subsequent rinsing was carried out for 2 h 30 min.

7. Works Cited

1. Mazza, P. P. A.; Martini, F.; Sala, B.; Magi, M.; Colombini, M. P.; Giachi, G.; Landucci, F.; Lemorini, C.; Modugno, F.; Ribechini, E. *J. Archaeol. Sci.* **2006,** 33, (9), 1310-1318.
2. Landfester, K.; Musyanovych, A., Targeted Polymeric Nanoparticles. In *Antibody Engineering*, Kontermann, R.; Dübel, S., Eds. Springer-Verlag GmbH Berlin Heidelberg, **2010**; pp 417-428.
3. Landfester, K. *Colloid Chem.* **2003,** 227, 75-123.
4. Merrifield, R. B. *J. Am. Chem. Soc.* **1963,** 85, (14), 2149-2154.
5. Gauthier, M. A.; Klok, H. A. *Chem. Commun.* **2008**, (23), 2591-2611.
6. Shu, J. Y.; Panganiban, B.; Xu, T. *Annu. Rev. Phys. Chem.* **2013,** 64, 631-57.
7. Froimowicz, P.; Muñoz-Espi, R.; Landfester, K.; Musyanovych, A.; Crespy, D. *Curr. Org. Chem.* **2013,** 17, (9), 900 - 912.
8. Meier-Westhues, U., *Polyurethanes: Coatings, Adhesives, and Sealants*. Vincentz Network GmbH & Co KG, 2nd ed.; 2007.
9. González, I.; Mestach, D.; Leiza, J. R.; Asua, J. M. *Prog. Org. Coat.* **2008,** 61, (1), 38-44.
10. Monge, S.; Canniccioni, B.; Graillot, A.; Robin, J.-J. *Biomacromolecules* **2011,** 12, (6), 1973-1982.
11. Fu, B. P.; Sun, X. M.; Qian, W. X.; Shen, Y. Q.; Chen, R. R.; Hannig, M. *Biomaterials* **2005,** 26, (25), 5104-5110.
12. Pshley , R.M., *Applied Colloid and Surface Chemistry*. John Wiley & Sons, Ltd: Chichester, **2004**.
13. Visser, J. *Powder Technol.* **1989,** 58, (1), 1-10.
14. Myers, D., *Surfaces, Interfaces, and Colloids: Principles and Applications*. Second ed.; John Wiley & Sons, Ltd: New York, **1999**.
15. Millter, C.A., *Interfacial Phenomena: Equilibrium and Dynamic Effects*. Second ed.; CRC Press Taylor & Francis Group LLC, **2008**; Vol. 139.
16. Butt, H.-J.; Kappl, M.; *Physics and Chemistry of Interfaces*. Second ed.; Wiley-VCH Verlag GmbH & Co. KGaA: Weinheim, **2006**.
17. Hamaker, H. C. *Physica* **1937,** 4, 1058-1072.
18. Eisenschitz, R.; London, F. *Z. Physik* **1930,** 60, (7-8), 491-527.
19. Derjaguin, B. *Acta Physicochim. URSS* **1939,** 10, (3), 333-346.
20. Verwey, E. J. W. *J. Phys. Colloid Chem.* **1947,** 51, (3), 631-636.
21. Ruckenstein, E. *J. Colloid Interface Sci.* **1978,** 66, (3), 531-543.
22. Hamaker, H. C. *Recl. Trav. Chim. Pays-Bas* **1936,** 55, 1015-1026.
23. Vrij, A. *Pure Appl. Chem.* **1976,** 48, (4), 471-483.
24. Napper, D. H. *J. Colloid Interface Sci.* **1977,** 58, (2), 390-407.
25. Vieira, M. J.; Oliveira, R.; Melo, L.; Pinheiro, M. M.; Martins, V. *Colloid Surf. B-Biointerfaces* **1993,** 1, (2), 119-124.
26. Norrish, K. *Discuss. Faraday Soc.* **1954**, (18), 120-134.
27. Tomas, J., *Particles on Surfaces: Detection, Adhesion and Removal*. VSP Utrecht: **2003**; Vol. 8.
28. Hertz, H. *Journal für die reine und angewandte Mathematik* **1882,** 92, 156-171.
29. Derjaguin, B. *Kolloid-Z* **1934,** 69, (2), 155-164.
30. Lifshitz, E. M. *Soviet Physics Jetp-USSR* **1956,** 2, (1), 73-83.
31. Johnson, K. L.; Kendall, K.; Roberts, A. D. *Proc. R. Soc. London Ser.A* **1971,** 324, (1558), 301-&.
32. Derjaguin, B. V.; Muller, V. M.; Toporov, Y. P. *J. Colloid Interface Sci.* **1975,** 53, (2), 314-326.
33. Muller, V. M.; Yushchenko, V. S.; Derjaguin, B. V. *J. Colloid Interface Sci.* **1980,** 77, (1), 91-101.
34. Maugis, D.; Pollock, H. M. *Acta Metall.* **1984,** 32, (9), 1323-1334.
35. Seymour, R. B.; Kauffman, G. B. *J. Chem. Educ.* **1992,** 69, (11), 909.
36. Sonnenschein, M. F.; Koonce, W., Polyurethanes. In *Encyclopedia of Polymer Science and Technology*, John Wiley & Sons, Ltd: New York, **2002**.
37. Uhlig, K., *Polyurethan-Taschenbuch*, Carl Hanser Verlag GmbH & Co. KG: Munich, 3. ed.; **2005**.
38. Association, E. D. a. P. P. Polyurethanes Timeline. http://www.polyurethanes.org/en/what-is-it/timeline (March 15, **2015**),
39. Oertel, G. A., L., *Polyurethane Handbook: Chemistry, Raw Materials, Processing, Application, Properties*. Carl Hanser Verlag GmbH & Co. KG: Munich, 2nd ed.; **1994**.
40. Delebecq, E.; Pascault, J. P.; Boutevin, B.; Ganachaud, F. *Chem. Rev.* **2013,** 113, (1), 80-118.

41. Krol, P. *Prog. Mater. Sci.e* **2007,** 52, (6), 915-1015.
42. Chattopadhyay, D. K.; Raju, K. V. S. N. *Prog. Polym. Sci.* **2007,** 32, (3), 352-418.
43. Bullermann, J.; Friebel, S.; Salthammer, T.; Spohnholz, R. *Prog. Org. Coat.* **2013,** 76, (4), 609-615.
44. Li, Y. Y.; Noordover, B. A. J.; van Benthem, R.; Koning, C. E. *Eur. Polym. J.* **2014,** 52, 12-22.
45. Sonnenschein, M. F.; Lysenko, Z.; Brune, D. A.; Wendt, B. L.; Schrock, A. K. *Polymer* **2005,** 46, (23), 10158-10166.
46. Noble, K. L. *Prog. Org. Coat.* **1997,** 32, (1-4), 131-136.
47. Kim, B. K. *Colloid Polym. Sci.* **1996,** 274, (7), 599-611.
48. Tiarks, F.; Landfester, K.; Antonietti, M. *J. Polym. Sci. Pol. Chem.* **2001,** 39, (14), 2520-2524.
49. Barni, A.; Levi, M. *J. Appl. Polym. Sci.* **2003,** 88, (3), 716-723.
50. Jhon, Y. K.; Cheong, I. W.; Kim, J. H. *Colloid Surf. A-Physicochem. Eng. Asp.* **2001,** 179, (1), 71-78.
51. ardon, H.; Irusta, L.; Fernandez-Berridi, M. J.; Luna, J.; Lansalot, M.; Bourgeat-Lami, E. *J. Appl. Polym. Sci.* **2011,** 120, (4), 2054-2062.
52. Holmberg, K. J., B.; Kronberg, B.; Lindman, B., *Surfactants and Polymers in Aqueous Solution*. John Wiley & Sons Ltd: Chichester, 2nd edition ed.; **2002**.
53. Guyot, A. *Curr. Opin. Colloid Interface Sci.* **1996,** 1, (5), 580-586.
54. Poth, U. S., R.; Schwartz, M., *Acrylatharze*. **2011**.
55. Ramesh, S.; Tharanikkarasu, K.; Mahesh, G. N.; Radhakrishnan, G. *J. Macromol. Sci.-Rev. Macromol. Chem. Phys.* **1998,** C38, (3), 481-509.
56. Kim, B. K.; Lee, J. C. *J. Polym. Sci. A: Polym. Chem.* **1996,** 34, (6), 1095-1104.
57. Mequanint, K.; Sanderson, R. D. *Macromol. Symp.a* **2002,** 178, 117-130.
58. Wynne, J. H.; Fulmer, P. A.; McCluskey, D. M.; Mackey, N. M.; Buchanan, J. P. *ACS Appl. Mater. Interfaces* **2011,** 3, (6), 2005-2011.
59. Nelson, A. M.; Long, T. E. *Macromol. Chem. Phys.* **2014,** 215, (22), 2161-2174.
60. Mishra, V. K.; Patel, K. I. *J. Dispersion Sci. Technol.* **2015,** 36, (3), 351-362.
61. Winnik, M. A. *Curr. Opin. Colloid Interface Sci.* **1997,** 2, (2), 192-199.
62. Vanderhoff, J.W.; Bradford, E. B.; Carringt.Wk. *J. Polym. Sci., Part C: Polym. Symp.* **1973**, (41), 155-174.
63. Adam, N.; Avar, G.; Blankenheim, H.; Friederichs, W.; Giersig, M.; Weigand, E.; Halfmann, M.; Wittbecker, F.-W.; Larimer, D.-R.; Maier, U.; Meyer-Ahrens, S.; Noble, K.-L.; Wussow, H.-G., Polyurethanes. In *Ullmann's Encyclopedia of Industrial Chemistry*, Wiley-VCH Verlag GmbH & Co. KGaA: **2000**.
64. Delpech, M. C.; Coutinho, F. M. B. *Polym. Test.* **2000,** 19, (8), 939-952.
65. Koberstein, J. T.; Galambos, A. F. *Macromolecules* **1992,** 25, (21), 5618-5624.
66. Yanagihara, Y.; Osaka, N.; Murayama, S.; Saito, H. *Polymer* **2013,** 54, (8), 2183-2189.
67. Mishra, A.; Aswal, V. K.; Maiti, P. *J. Phys. Chem. B* **2010,** 114, (16), 5292-5300.
68. Van Bogart, J. W. C.; Gibson, P. E.; Cooper, S. L. *J. Polym. Sci., Polym. Phys. Ed.* **1983,** 21, (1), 65-95.
69. Wang, C. B.; Cooper, S. L. *Macromolecules* **1983,** 16, (5), 775-786.
70. Korley, L. T. J.; Pate, B. D.; Thomas, E. L.; Hammond, P. T. *Polymer* **2006,** 47, (9), 3073-3082.
71. Huh, D. S.; Cooper, S. L. *Polym. Eng. Sci.* **1971,** 11, (5), 369-376
72. Mohammad Mizanur, R.; Han-Do, K. *J. Adhes. Sci. Technol.* **2007,** 21, (1), 81-96
73. Bower, D. I., *An Introduction to Polymer Physics*. Cambridge University Press: **2002**.
74. Jackson, K. A., Nucleation. In *Kinetic Processes*, Wiley-VCH Verlag GmbH & Co. KGaA: **2005**; pp 175-201.
75. Becker, R.; Döring, W. *Ann. Phys.* **1935,** 416, (8), 719-752.
76. Jackson, K. A., Interface Instabilities. In *Kinetic Processes*, Wiley-VCH Verlag GmbH & Co. KGaA: **2005**; pp 143-153.
77. Volmer, M.; Weber, A. *Z. Phys. Chem., Stoechiom. Verwandtschaftsl.* **1926,** 119, (3/4), 277-301.
78. Taden, A.; Landfester, K. *Macromolecules* **2003,** 36, (11), 4037-4041.
79. Reiter, G. *Chem. Soc. Rev.* **2014,** 43, (7), 2055-2065.
80. Degennes, P. G. *C. R. Acad. Sci. Ser. II* **1988,** 307, (19), 1949-1953.
81. Degennes, P. G. *J. Chem. Phys.* **1971,** 55, (2), 572-&.

82. Keddie, J.; Routh, A. F., *Fundamentals of Latex Film Formation: Processes and Properties*. Springer_verlag GmbH Berlin Heidelberg: **2010**.
83. Büchner, J.; Ganster, O.; Klein, G.; Lucas, H.-W.; Matussek, A., Einkomponentige isocyanatvernetzende Zweiphasen-Systeme. **2003**.
84. Bhushan, B., *Biophysics of Human Hair*. 1st ed.; Springer-Verlag GmbH Berlin Heidelberg: **2010**.
85. Popescu, C.; Hocker, H. *Chem. Soc. Rev.* **2007,** 36, (8), 1282-1291.
86. Marshall, R. C.; Orwin, D. F. G.; Gillespie, J. M. *Electron Microscopy Reviews* **1991,** 4, (1), 47-83.
87. Plowman, J. E.; Paton, L. N.; Bryson, W. G. *Exp. Dermatol.* **2007,** 16, (9), 707-714.
88. Feughelman, M. *Text. Res. J.* **1959,** 29, (3), 223-228.
89. Jones, L. N.; Watts, N. R.; Booy, F. P.; Steven, A. C.; Parry, D. A. D. *Asian Australas. J. Anim. Sci.* **2000,** 13, 120-120.
90. Wortmann, F. J., 4 - The structure and properties of wool and hair fibres. In *Handbook of Textile Fibre Structure*, Eichhorn, S. J.; Hearle, J. W. S.; Jaffe, M.; Kikutani, T., Eds. Woodhead Publishing Ltd., Cambridge: **2009**; Vol. 2, pp 108-145.
91. Robbins, C. R., *Chemical and Physical Behaviour of Human Hair*. Springer-Verlag GmbH: New York, **1994**.
92. Littrell, K. C.; Gallas, J. M.; Zajac, G. W.; Thiyagarajan, P. *Photochem. Photobiol.* **2003,** 77, (2), 115-120.
93. Zahn, H. *Chem. Unserer Zeit* **1989,** 23, (5), 141-150.
94. Negri, A. P.; Cornell, H. J.; Rivett, D. E. *Text. Res. J.* **1993,** 63, (2), 109-115.
95. Bradbury, J. H. *Adv. Protein Chem.* **1973,** 27, 111-211.
96. Nishikawa, N.; Tanizawa, Y.; Tanaka, S.; Horiguchi, Y.; Asakura, T. *Polymer* **1998,** 39, (16), 3835-3840.
97. Robbins, C. R. *Chemical and physical behavior of human hair*, Springer-Verlag GmbH Berlin Heidelberb, **2002**, 386-473.
98. Santos Nogueira, A. C.; Joekes, I. *J. Photochem. Photobiol., B* **2004,** 74, (2-3), 109-17.
99. Gamez-Garcia, M., *The cracking of human hair cuticles by cyclical thermal stresses*. Society of Cosmetic Chemists: New York, **1998**.
100. Stro, A.; Mann, D. W. *J. Soc. Cosmet. Chem* **1986,** 37, 159-175.
101. Cannell, D. W. *Clin. Dermatol.* **1988,** 6, (3), 71-82.
102. Pihillips, D.G., W. J. J. 1991.
103. Benaiges, A.; Fernandez, E.; Martinez-Teipel, B.; Armengol, R.; Barba, C.; Coderch, L. *J. Appl. Polym. Sci.* **2013,** 128, (1), 861-868.
104. Somasundaran, P.; Chakraborty, S.; Qiang, Q.; Deo, P.; Wang, J.; Zhang, R. *J. Cosmet. Sci.* **2004,** 55 Suppl, S1-17.
105. Villa, A. L. V.; Aragao, M. R. S.; Dos Santos, E. P.; Mazotto, A. M.; Zingali, R. B.; De Souza, E. P.; Vermelho, A. B. *BMC Biotechnol.* **2013,** 13.
106. Wiesche, E. S. Z.; Körner, A.; Schäfer, K.; Wortmann, F. J. *J. Cosmet. Sci.* **2011,** 62, (2), 237-249.
107. Rance, R. W. *J. Soc. Cosmet. Chem.* **1974,** 25, (6), 297-&.
108. Bruce, D. W., *Inorganic Materials*. John Wiley & Sons, Ltd: Chichester, **1988**.
109. Kay, M. I.; Young, R. A.; Posner, A. S. *Nature* **1964,** 204, (4963), 1050-1052.
110. Vanblitterswijk, C. A.; Grote, J. J.; Kuijpers, W.; Daems, W. T.; Degroot, K. *Biomaterials* **1986,** 7, (2), 137-143.
111. Ten Cate, A. R., *Oral Histology: Development, Structure and Function*. 4th ed.; Mosby (Elsevier Inc.): **1994**.
112. Suchanek, W.; Yoshimura, M. *J. Mater. Res.* **1998,** 13, (1), 94-117.
113. De Groot, K. *Ceram. Int.* **1993,** 19, (5), 363-366.
114. Jones, F. H. *Surf. Sci. Rep.* **2001,** 42, (3-5), 75-205.
115. Eick, J. D.; Gwinnett, A. J.; Pashley, D. H.; Robinson, S. J. *Crit. Rev. Oral Biol. Med.* **1997,** 8, (3), 306-335.
116. Peppas, N. A.; Langer, R. *Science* **1994,** 263, (5154), 1715-20.
117. Nakabayashi, N.; Kojima, K.; Masuhara, E. *J. Biomed. Mater. Res.* **1982,** 16, (3), 265-273.
118. Khatri, C. A.; Stansbury, J. W.; Schultheisz, C. R.; Antonucci, J. M. *Dent. Mater.* **2003,** 19, (7), 584-588.

119. Yoshioka, M.; Yoshida, Y.; Inoue, S.; Lambrechts, P.; Vanherle, G.; Nomura, Y.; Okazaki, M.; Shintani, H.; Van Meerbeek, B. *J. Biomed. Mater. Res.* **2002,** 59, (1), 56-62.
120. Yoshida, Y.; Van Meerbeek, B.; Nakayama, Y.; Snauwaert, J.; Hellemans, L.; Lambrechts, P.; Vanherle, G.; Wakasa, K. *J. Dent. Res.* **2000,** 79, (2), 709-714.
121. Bayle, M. A.; Gregoire, G.; Sharrock, P. *J. Dent.* **2007,** 35, (4), 302-308.
122. Yoshida, Y.; Nagakane, K.; Fukuda, R.; Nakayama, Y.; Okazaki, M.; Shintani, H.; Inoue, S.; Tagawa, Y.; Suzuki, K.; De Munck, J.; Van Meerbeek, B. *J. Dent. Res.* **2004,** 83, (6), 454-458.
123. Van Landuyt, K. L.; Yoshida, Y.; Hirata, I.; Snauwaert, J.; De Munck, J.; Okazaki, M.; Suzuki, K.; Lambrechts, P.; Van Meerbeek, B. *J. Dent. Res.* **2008,** 87, (8), 757-761.
124. Schweitzer, P. A., *Metallic Materials*. Marcel Dekker, Inc.: New York, **2003**; Vol. 19.
125. Brewis, D., *Surface Analysis and Pretreatment of Plastics and Metals.* Appplied Science: London, **1982**; pp 199-226.
126. Garbassi, F.; Occhiello, E. *Polymer Surfaces from Physics to Technology*. John Wiley& Sons, Ltd: New York, **1994**.
127. Pesetskii, S. S.; Jurkowski, B.; Kuzavkov, A. I. *Int. J. Adhes. Adhes.* **1998,** 18, (5), 351-358.
128. Ochoa-Putman, C.; Vaidya, U. *Composites, Part A* **2011**, 42 (8), 906–915.
129. Cognard, J. *C. R. Chim.* **2006,** 9, (1), 13-24.
130. Mequanint, K.; Sanderson, R.; Pasch, H. *J. Appl. Polym. Sci.* **2003,** 88, (4), 900-907.
131. Wang, C.; Chuang, Y.-Y.; Lin, C.-T. *J. Coat. Technol.* **1999,** 71, (892), 61-67.
132. Mequanint, K.; Sanderson, R.; Pasch, H. *Polymer* **2002,** 43, (19), 5341-5346.
133. Yan, J.; Chen, G.; Tang, B.; Tai, J.; Chen, Q., Adhesion Mechanism and Modification Methods of Solvent-free PU Adhesive. In *Frontiers of Green Building, Materials and Civil Engineering, Pts 1-8*, Sun, D.
134. Sung, W. P.; Chen, R., Eds., Trans Tech Publications Ltd: Dürnten: **2011**; Vol. 71-78, pp 2703-2706.
135. Hlady, V.; Buijs, J. *Curr. Opin. Biotechnol.* **1996,** 7, (1), 72-77.
136. Rabe, M.; Verdes, D.; Seeger, S. *Adv. Colloid Interface Sci.* **2011,** 162, (1-2), 87-106.
137. Nakanishi, K.; Sakiyama, T.; Imamura, K. *J. Biosci. Bioeng.* **2001,** 91, (3), 233-244.
138. Perlin, L.; MacNeil, S.; Rimmer, S. *Soft Matter* **2008,** 4, (12), 2331-2349.
139. Hermanson, G. T., *Bioconjugate Techniques*. 2nd ed.; Academic Press (Elsevier Inc.): San Diego, **2008**.
140. Taden, A.; Veith, B.; Breves, R.; Schmidt, I.; Weber, T. Peptides that can be used in coating agents, adhesion promoters or adhesives for oxidic surfaces. **2014**.
141. Herlinger, H.; Müller, P.; Müller-Dolezal, H.; Stoltz, R.; Söll, H., *Houben-Weyl Methods of Organic Chemistry Vol. XIV/2, 4th Edition: Macromolecular Compounds II*. ThiemeGmbH, Maxdorf: **2014**.
142. Schärtl, W., *Light Scattering from Polymer Solutions and Nanoparticle Dispersions*. Springer-Verlag GmbH Berlin Heidelberg: **2007**.
143. Merkus, H., Laser Diffraction. In *Particle Size Measurements*, Springer Netherlands: **2009**; Vol. 17, pp 259-285.
144. Hunter, R. J., *Zeta Potential in Colloid Science: Principles and Applications*. Academic Press (Elsevier Inc.): San Diego, **1981**.
145. Müller, R. H.; Nitzsche, R.; Paulke, B. R., *Zetapotential und Partikelladung in der Laborpraxis: Einführung in die Theorie, praktische Messdurchführung, Dateninterpretation ; Colloidal drug carriers (cdc) 1st expert meeting Berlin 15. - 17. 6 1995 ; mit 24 Tabellen*. Wissenschaftliche Verlagsgesellschaft, Stuttgart: **1996**.
146. Musyanovych, A.; Rossmanith, R.; Tontsch, C.; Landfester, K. *Langmuir* **2007,** 23, (10), 5367-76.
147. Ziegler, A.; Landfester, K.; Musyanovych, A. *Colloid Polym. Sci.* **2009,** 287, (11), 1261-1271.
148. Smith, P. K.; Krohn, R. I.; Hermanson, G. T.; Mallia, A. K.; Gartner, F. H.; Provenzano, M. D.; Fujimoto, E. K.; Goeke, N. M.; Olson, B. J.; Klenk, D. C. *Anal. Biochem.* **1985,** 150, (1), 76-85.
149. Lottspeich, F., *Bioanalytik*. Elsevier, Spektrum Akademischer Verlag: **2006**.
150. Deacon, S. P. E.; Apostolovic, B.; Carbajo, R. J.; Schott, A. K.; Beck, K.; Vicent, M. J.; Pineda-Lucena, A.; Klok, H. A.; Duncan, R. *Biomacromolecules* **2011,** 12, (1), 19-27.
151. Chen, C. P.; Park, Y.; Rice, K. G. *J. Pept. Res.* **2004,** 64, (6), 237-243.
152. Ellman, G. L. *Arch. Biochem. Biophys.* **1958,** 74, (2), 443-450.
153. Hou, X.; Jones, B. T., Inductively Coupled Plasma/Optical Emission Spectrometry. In *Encyclopedia of Analytical Chemistry*, John Wiley & Sons, Ltd: Chichester, **2006**.

154. Dixon, M. C. *Journal of Biomolecular Techniques : JBT* **2008,** 19, (3), 151-158.
155. Sauerbrey, G. *Z. Physik* **1959,** 155, (2), 206-222.
156. Sauerbrey, G. *Archiv der Elektrischen Übertragung* **1964,** 18, (10), 617-624.
157. Gill, P.; Moghadam, T. T.; Ranjbar, B. *Journal of Biomolecular Techniques : JBT* **2010,** 21, (4), 167-193.
158. Höhne, G. H., Wolfgang; Flammersheim, H.-J., *Differential Scanning Calorimetry*. 2 ed.; Springer-Verlag GmbH Berlin Heidelberg: **2003**; p 298.
159. Breucker, L.; Schöttler, S.; Landfester, K.; Taden, A. *Biomacromolecules* **2015**.
160. Yilgor, I.; Yilgor, E. *Polym. Rev.* **2007,** 47, (4), 487-510.
161. Noguchi, K.; Kondo, H.; Ichikawa, Y.; Okuyama, K.; Washiyama, J. *Polymer* **2005,** 46, (24), 10823-10830.
162. van Hest, J. C. M.; Tirrell, D. A. *Chem. Commun.* **2001**, (19), 1897-1904.
163. Hamm, D. J. Process for the production of hydrolyzed vegetable proteins using gaseous hydrochloric acid and the product therefrom. 5180597, 1993.
164. Brandelli, A. *Food Bioprocess Technol.* **2008,** 1, (2), 105-116.
165. Dowling, L. M.; Crewther, W. G.; Inglis, A. S. *The Biochemical Journal* **1986,** 236, (3), 695-703.
166. Cardamone, J. M. *J. Mol. Struct.* **2010,** 969, (1–3), 97-105.
167. Cardamone, J. M.; Nu; #241; ez, A.; Garcia, R. A.; Aldema-Ramos, M. *Res. Lett. Mater. Sci.* **2009,** 2009.
168. Hatada, K.; Ute, K.; Oka, K.-I.; Pappas, S. P. *J. Polym. Sci., Part A-1: Polym. Chem.* **1990,** 28, (11), 3019-3027.
169. Gaudin, F.; Sintes-Zydowicz, N. *Colloids Surf., A* **2011,** 384, (1–3), 698-712.
170. Rochery, M.; Vroman, I.; Lam, T. M. *J. Macromol. Sci., Part A: Pure Appl. Chem.* **2000,** 37, (3), 259-275.
171. Finch, C. A. *Polym. Int.* **1996,** 40, (2), 151-151.
172. Chen, F.; Hehl, J.; Su, Y.; Mattheis, C.; Greiner, A.; Agarwal, S. *Polym. Int.* **2013,** 62, (12), 1750-1757.
173. Bouyer, E.; Mekhloufi, G.; Rosilio, V.; Grossiord, J. L.; Agnely, F. *Int. J. Pharm.* **2012,** 436, (1-2), 359-378.
174. Hoffmann, H.; Reger, M. *Adv. Colloid Interface Sci.* **2014,** 205, 94-104.
175. Landfester, K., Miniemulsions for Nanoparticle Synthesis. In *Colloid Chemistry II*, Antonietti, M., Ed. Springer-Verlag GmbH Berlin Heidelberg: **2003**; Vol. 227, pp 75-123.
176. Baslé, E.; Joubert, N.; Pucheault, M. *Chem. Biol.* **2010,** 17, (3), 213-227.
177. Boutureira, O.; Bernardes, G. J. L. *Chem. Rev.* **2015,** 115, (5), 2174-2195.
178. Roddick-Lanzilotta A.; Kelly, R. C., S.; Challoner, N. *Int. J. Appl. Sci.* **2004**, 3-9.
179. Gauthier, M. A.; Klok, H.-A. *Polym. Chem.* **2010,** 1, (9), 1352-1373.
180. Heredia, K. L.; Bontempo, D.; Ly, T.; Byers, J. T.; Halstenberg, S.; Maynard, H. D. *J. Am. Chem. Soc.* **2005,** 127, (48), 16955-16960.
181. Wilke, P.; Börner, H. G. *ACS Macro Letters* **2012,** 1, (7), 871-875.
182. Ji, S. X.; Zhu, Z. X.; Hoye, T. R.; Macosko, C. W. *Macromol. Chem. Phys.* **2009,** 210, (10), 823-831.
183. Kidoaki, S.; Matsuda, T. *Langmuir* **1999,** 15, (22), 7639-7646.
184. Landfester, K.; Musyanovych, A.; Mailänder, V. *J. Polym. Sci. Part A-1: Polym. Chem.* **2010,** 48, (3), 493-515.
185. Vernikouskaya, I.; Fekete, N.; Bannwarth, M.; Erle, A.; Rojewski, M.; Landfester, K.; Schmidtke-Schrezenmeier, G.; Schrezenmeier, H.; Rasche, V. *Contrast Media Mol. Imaging* **2014,** 9, (2), 109-121.
186. Alexandrino, E. M.; Ritz, S.; Marsico, F.; Baier, G.; Mailander, V.; Landfester, K.; Wurm, F. R. *J. Mater. Chem. B* **2014,** 2, (10), 1298-1306.
187. Lee, B. P.; Messersmith, P. B.; Israelachvili, J. N.; Waite, J. H. *Annu. Rev. Mater. Res.* **2011,** 41, 99-132.
188. Hentschel, J.; Bleek, K.; Ernst, O.; Lutz, J. F.; Borner, H. G. *Macromolecules* **2008,** 41, (4), 1073-1075.
189. Kochendoerfer, G. G.; Chen, S. Y.; Mao, F.; Cressman, S.; Traviglia, S.; Shao, H. Y.; Hunter, C. L.; Low, D. W.; Cagle, E. N.; Carnevali, M.; Gueriguian, V.; Keogh, P. J.; Porter, H.; Stratton, S. M.; Wiedeke, M. C.; Wilken, J.; Tang, J.; Levy, J. J.; Miranda, L. P.; Crnogorac, M. M.; Kalbag, S.;

Botti, P.; Schindler-Horvat, J.; Savatski, L.; Adamson, J. W.; Kung, A.; Kent, S. B. H.; Bradburne, J. A. *Science* **2003,** 299, (5608), 884-887.
190. Cazalis, C. S.; Haller, C. A.; Sease-Cargo, L.; Chaikof, E. L. *Bioconjugate Chem.* **2004,** 15, (5), 1005-1009.
191. Veronese, F. M. *Biomaterials* **2001,** 22, (5), 405-417.
192. Van den Berg, K. J.; Van der Ven, L. G. J.; Van den Haak, H. J. W. *Progr. Org. Coat.* **2008,** 61, (2-4), 110-118.
193. Jose, J.; Meyer, T. F. *Microbiol. Mol. Biol. Rev.* **2007,** 71, (4), 600-+.
194. Jose, J. *Appl. Microbiol. Biotechnol.* **2006,** 69, (6), 607-614.
195. ProteinCalculatorv3.4. http://protcalc.sourceforge.net/
196. Decher, G., Layer-by-Layer Assembly. In *Multilayer Thin Films: Sequential Assembly of Nanocomposite Materials*, 2nd ed.; Gero Decher, J. B. S., Ed. Wiley VCH Verlag GmbH & Co. KGaA: **2012**.
197. Kotov, N. A.; Dekany, I.; Fendler, J. H. *J. Phys. Chem.* **1995,** 99, (35), 13065-13069.
198. Breucker, L.; Landfester, K.; Taden, A. *ACS Appl. Mater. Int.* **2015**.
199. Decher, G., Layer-by-Layer Assembly. In *Multilayer Thin Films: Sequential Assembly of Nanocomposite Materials*, 2nd ed.; Gero Decher, J. B. S., Ed. Wiley VCH Verlag GmbH & Co. KGaA: **2012**.
200. Kotov, N. A.; Dekany, I.; Fendler, J. H. *J. Phys. Chem.* **1995,** 99, (35), 13065-13069.
201. Hemp, S. T.; Zhang, M.; Allen, M. H.; Cheng, S.; Moore, R. B.; Long, T. E. *Macromol. Chem. Phys.* **2013,** 214, (18), 2099-2107.
202. Weber, J.; Kreuer, K.-D.; Maier, J.; Thomas, A. *Adv. Mater.* **2008,** 20, (13), 2595-2598.
203. Yuan, J.; Mecerreyes, D.; Antonietti, M. *Prog. Polym. Sci.* **2013,** 38, (7), 1009-1036.
204. Zhang, S.; Zou, J.; Zhang, F.; Elsabahy, M.; Felder, S. E.; Zhu, J.; Pochan, D. J.; Wooley, K. L. *J. Am. Chem. Soc.* **2012,** 134, (44), 18467-18474.
205. Steinbach, T.; Wurm, F. R. *Angew. Chem., Int. Ed. Engl.* **2015,** 54, (21), 6098-108.
206. van der Veen, I.; de Boer, J. *Chemosphere* **2012,** 88, (10), 1119-53.
207. Chattopadhyay, D. K.; Webster, D. C. *Progr. Polym. Sci.* **2009,** 34, (10), 1068-1133.
208. Kühnle, H.; Börner, H. G. *Angew. Chem., Int. Ed.* **2009,** 48, (35), 6431-6434.
209. Pellach, M.; Atsmon-Raz, Y.; Simonovsky, E.; Gottlieb, H.; Jacoby, G.; Beck, R.; Adler-Abramovich, L.; Miller, Y.; Gazit, E. *ACS Nano* **2015,** 9, (4), 4085-4095.
210. Monge S., D., G., *Phosphorus-Based Polymers: From Synthesis To Applications*. Royal Society of Chemistry: Oxfordshire, **2014**; pp 151-270.
211. David, G.; Negrell-Guirao, C.; Iftene, F.; Boutevin, B.; Chougrani, K. *Polym. Chem.* **2012,** 3, (2), 265-274.
212. Brown, W. T.; Bardman, J. K., Polymer particles having select pendant groups and composition prepared therefrom. **2007**.
213. Johnson, M. M.; Swartz, A. J.; Williams, D. E., Liquid-applied sound damping. **2009**.
214. Rolf, D.; Alexander, H.; Gregor, L.; Gyopar, R. M.; Bernhard, S.; Cheng-Le, Z., Aqueous polymer dispersion containing an emulsifier with phosphate groups. **1999**.
215. Staller, C. D.; Schumacher, K. H. D.; Schlarb, B. D.; Centner, A. D.; Hartz, O., Use of polymer dispersions containing an emulsifier with phosphate groups as adhesive. **2010**.
216. Horzum, N.; Mari, M.; Wagner, M.; Fortunato, G.; Popa, A.-M.; Demir, M. M.; Landfester, K.; Crespy, D.; Munoz-Espi, R. *RSC Advances* **2015,** 5, (47), 37340-37345.
217. Sauer, R.; Froimowicz, P.; Scholler, K.; Cramer, J. M.; Ritz, S.; Mailander, V.; Landfester, K. *Chemistry* **2012,** 18, (17), 5201-12.
218. Zeller, A.; Musyanovych, A.; Kappl, M.; Ethirajan, A.; Dass, M.; Markova, D.; Klapper, M.; Landfester, K. *Acs Appl. Mater. Interf.* **2010,** 2, (8), 2421-2428.
219. Kirschbaum, S.; Landfester, K.; Taden, A. *Macromolecules* **2015,** 48, (12), 3811-3816.
220. Kirschbaum, S.; Landfester, K.; Taden, A. *Angew. Chem.,Int. Ed.* **2015,** 54, (19), 5789-5792.
221. Jaudouin, O.; Robin, J.-J.; Lopez-Cuesta, J.-M.; Perrin, D.; Imbert, C. *Polym. Int.* **2012,** 61, (4), 495-510.
222. Chen, H.; Luo, Y.; Chai, C.; Wang, J.; Li, J.; Xia, M. *J. Appl. Polym. Sci.* **2008,** 110, (5), 3107-3115.
223. Gu, L.; luo, Y. *Ind. Eng. Chem. Res.* **2015,** 54, (9), 2431-2438.
224. Celebi, F.; Aras, L.; Gunduz, G.; Akhmedov, I. M. *J. Coat. Technol.* **2003,** 75, (944), 65-71.

225. Mequanint, K.; Sanderson, R. *J. Appl. Polym. Sci.* **2003,** 88, (4), 893-899.
226. Chougrani, K.; Boutevin, B.; David, G.; Seabrook, S.; Loubat, C. *J. Polym. Sci., Part A: Polym. Chem.*
227. Nancollas, G. H.; Tang, R.; Phipps, R. J.; Henneman, Z.; Gulde, S.; Wu, W.; Mangood, A.; Russell, R. G. G.; Ebetino, F. H. *Bone* **2006,** 38, (5), 617-627.
228. Saari, A. L.; Hyvonen, H.; Lahtinen, M.; Ylisirnio, M.; Turhanen, P.; Kolehmainen, E.; Peraniemi, S.; Vepsalainen, J. *Molecules* **2012,** 17, (9), 10928-45.
229. Hermann, P.; Lukes, I. *J. Chem. Soc., Dalton Trans.* **1995**, (16), 2605-2610.
230. Jiang, D. D.; Yao, Q.; McKinney, M. A.; Wilkie, C. A. *Polym. Degrad. Stabil.* **1999,** 63, (3), 423-434.
231. Weller, D.; Medina-Oliva, A.; Claus, H.; Gietzen, S.; Mohr, K.; Reuter, A.; Schäffel, D.; Schöttler, S.; Koynov, K.; Bros, M.; Grabbe, S.; Fischer, K.; Schmidt, M. *Macromolecules* **2013,** 46, (21), 8519-8527.

8. Abbreviations and Symbols

This chapter provides a list of all of the abbreviations and the symbols used in the thesis.

8.1 Abbreviations

Abbreviation	Full name
AA	Amino acid
ACC	N-acetyl-L-cysteine
Ala	Alanine
AMPA	Aminomethyl phosphonic acid
Arg	Arginine
Asp	Aspartic acid
BCA	Bicinchoninic acid
Ca	Calcium
DBA	Dibutyl amine
DLS	Dynamic light scattering
DLVO	Derjaguin, London, Verwey and Overbeek
DMPA	Dimethylolpropionic acid
DMT model	Derjaguin, Muller, Toporov model
DSC	Differential scanning calorimetry
DTNB	5,5'-dithiobis-(2-nitrobenzoic acid)
EA	Ethyl acetate
EO	Ethylene oxide
EU	European Union
Glu	Glutamic acid
Gly	Glycine
GPC	Gel permeation chromatography
H_{12}MDI	4,4'-methylenebis(cyclohexylisocyanate)
HAP	Hydroxyapatite
HDI	Hexamethylene diisocyanate
HEMI	Hydroxyethyl maleimide
His	Histidine
HPLC	Liquid chromatography
ICP-OES	Inductively coupled plasma optical emission spectroscopy
IEF	Isoelectric focusing
IF	Intermediate filament
IFP	Intermediate filament protein
Ile	Isoleucine

IP	Isoelectric point
IPDI	Isophorone diisocyanate
IR	Infrared
JKR model	Johnson, Kendall, Roberts model
KAP	Keratin associated proteins
KP	Keratin protein
LD	Laser diffraction
Leu	Leucine
Lys	Lysine
MDI	4,4'-methylenebis(phenylisocyanate)
Met	Methionine
Mg	Magnesium
MI	Maleimide
MI-PUD	Maleimide-functionalized PUD
MI-PUD(25)	Maleimide-functionalized PUD with 25 mol% residual MI
MI-PUD(50)	Maleimide-functionalized PUD with 50 mol% residual MI
M_n	Number average molecular weight
MNB	5-Mercapto-2-nitrobenzoate
mol%	Mole percent
MP model	Maugis and Pollock model
MWCO	Molecular weight cut off
NA	Neridronic acid
NA100	NA-functionalized PUD with a stoichiometry of 1:1 (n(NCO):n(NA))
NA25	NA-functionalized PUD with a stoichiometry of 4:1 (n(NCO):n(NA))
NA50	NA-functionalized PUD with a stoichiometry of 2:1 (n(NCO):n(NA))
NCO	Isocyanate
PCD	Particle charge detection
PDADMAC	Polydiallyldimethylammonium chloride
PDI	Polydispersity index
PDMS	Poly(dimethylsiloxane)
PEG	Polyethylene glycol
PES-Na	Sodium polyethylene sulphate
P-group	Phosphonate group
Phe	Phenylalanine
PO	Propylene oxide
PPOE	Poly(oxypropylene, oxyethylene) glycol
PPOE-1	Poly(oxypropylene, oxyethylene) glycol
P-PUDs	PUDs comporting phosphonate groups
P-reagent	Phosphonate-functionalized reagents

Pro	Proline
PTMA	poly(tetramethylene adipate)
PU	Polyurethane
PUD	Polyurethane dispersion
QCMD	Quartz crystal microbalance with dissipation
SDS-PAGE	Sodium dodecyl sulfate-polyacrylamide gel electrophoresis
SEM	Scanning electron microscopy
Ser	Serine
SG	Sulfonated glycol
SS	Stainless steel
S-S	Disulfide link
TDI	Toluene diisocyanate
TEM	Transmission electron microscopy
THF	Tetrahydrofuran
Thr	Threonine
Tyr	Tyrosine
UV	Ultraviolet
Val	Valine
VOC	Volatile organic compound
wt%	Weight percent
ZP	Zeta potential

8.2 Symbols

Greek	Meaning
a	Static polarizability of a given atom
γ	Surface tension
γ^{AB}	Lewis acid-base surface tension
γ^{LW}	Lifshitz-van der Waals surface tension
ε	Permittivity of a given medium
λ	Wavelength
λ_D	Debye length
λ_{int}	Interaction parameter
ν	Poisson's ratio
ν_0	Frequency of the electron in the ground state
ϕ	Electrostatic potential
ϕ_0	Electrostatic surface potential

Latin/Roman	Meaning
A	Hamaker constant
a	Radius of deformation of a substrate
$Å$	Ångström
d	Radius of the indenter
e	Charge of the electron
E	Young's modulus
E_{el}	Electrostatic force of interaction
H	Distance of separation
h	Planck's constant
H_0	Equilibrium distance of separation
k_B	Boltzmann constant
l	Distance of separation between two charges
l_B	Bjerrum length
N_i^2	Density of atoms per volume
n_0	Density of counterions
n_P	Density of atoms in a particle
n_S	Density of atoms in a substrate
P	Compressive load
R	Radius of a spherical particle
T	Temperature
V_{BRsp}	Born repulsion energy of interaction in the sphere-plate model
V_{wsp}	Van der Waals energy of interaction in the sphere-plate model
V_{wss}	Van der Waals energy of interaction in the sphere-sphere model
z_0	Separation distance between two materials

9. Scientific Contributions

The following publications, patents, posters, or oral presentations are based on this thesis or on parts thereof.

Publications

- Breucker, L.; Schöttler, S.; Landfester, K.; Taden, A.: Polyurethane Dispersions with Peptide Corona: Facile Synthesis of Stimuli-Responsive Dispersions and Films, *Biomacromolecules* **2015**
- Breucker, L.; Landfester, K.; Taden, A.: Phosphonic Acid-functionalized Polyurethane Dispersions with Improved Adhesion Properties, *ACS Applied Materials & Interfaces* **2015**
- Breucker, L.; Meißler, M.; Börner, H.; Landfester, K.; Taden, A.: Peptide-functionalizaiton of Polyurethane Dispersions for Adhesion to Stainless Steel, *in preparation*

Patents

- Taden, A.; Breucker, L.; Landfester, K.: "Aqueous peptide-stabilized polyurethane dispersions," EP14188808, **2014**
- Taden, A.; Lnadfester, K.; Breves, R.; Breucker, L.; Kastner, C.; Veith, B.: "Aqueous peptide-functionalized polyurethane dispersions," EP15156504, **2015**

Conferences

- Poster "Adhesion of Peptide-functionalized Particles to Steel," Ostwald-Kolloquium "Particles @ Interfaces", September 17-19, 2014, Mainz, Germany
- Poster "Peptide-decorated Polyurethane Dispersions: Controlling Stability in Dispersion and Crystallinity in the Film," Nature Inspires Chemistry Engineers Conference, October 15-17, 2014, Nice, France
- Oral presentation "Functionalization of Polyurethane Dispersions for Adhesion to Hydroxylapatite," European Polymer Congress 2015, June 21-26, 2015, Dresden, Germany
- Oral presentation "Functionalization of Polyurethane Particles for Controlled Interactions with Different Substrates," ACS National Meeting & Exposition, August 16-20, 2015, Boston, USA

Danksagung

Curriculum Vitae

Laura Breucker

Studium und Beruf

Seit Sept 2012	Promotion am **MPI für Polymerforschung**, Mainz in Kooperation mit der Henkel AG & Co. KGaA in Düsseldorf
	im AK von Prof. Dr. Katharina Landester
	Titel der Doktorarbeit: Funktionalisierung von Polyurethandispersionen für gezielte Wechselwirkungen mit verschiedenen Substraten
2009-2012	**Ecole Normale Supérieure**, Paris, Studienfach Chemie
Jun 2012:	Erlangen des Masters, Fachrichtung Polymerchemie
Feb-Jun 2012:	Masterarbeit am MPI für Polymerforschung, Mainz
	im AK von Prof. Dr. Katharina Landfester
Feb-Jun 2011:	Praktikum am MPI für Neurologische Forschung, Köln
	im AK von Prof. Dr. Mathias Hoehn
Apr 2010:	Praktikum an der Ecole Supérieure de Physique et de Chimie Industrielles
	im AK von Prof. Dr. Ludwik Leibler
2007-2009	**Universität Pierre & Marie Curie, Paris VI**
Jun 2010:	Erlangen des Bachelors, Studienfach Chemie
Aug 2008:	Praktikum bei der UCL Umwelt Control Labor GmbH, Lünen

Schulausbildung

2004 – 2007	**Harriton Senior High School** of Rosemont / PA, USA
Jun 2007:	Erlangen des International Baccalaureat
1999 – 2004	**Theodor-Heuss-Gymnasium**, Waltrop
	Bilingualer Zweig deutsch-französisch